

## ABSTRACT

Title of Dissertation: DEVELOPMENT OF MAGNETORHEOLOGICAL  
FLUID ELASTOMERIC DAMPERS  
FOR HELICOPTER STABILITY AUGMENTATION

Wei Hu, Doctor of Philosophy, 2005

Dissertation directed by: Professor Norman M. Wereley  
Department of Aerospace Engineering

Conventional lag dampers use passive materials, such as elastomers, to dissipate energy and provide stiffness, but their damping and stiffness levels diminish markedly as amplitude of damper motion increases. Magnetorheological (MR) fluids based dampers have controllable damping with little or no stiffness. In order to combine the advantages of both elastomeric materials and MR fluids, semi-active magnetorheological fluid elastomeric (MRFE) lag dampers are developed in this thesis. In such a damper configuration, magnetic valves are incorporated into the chamber enclosed by elastomeric layers. Preliminary MRFE damper design analysis was conducted using quasi-steady Bingham-plastic MR flow mode analysis, and MRFE damper performance was evaluated analytically. To investigate the feasibility of using a combination of magnetorheological (MR)

fluids and elastomeric materials for augmentation of lag mode damping in helicopters, a semi-active linear stroke MRFE lag damper was developed as a retrofit to an existing elastomeric helicopter lag damper. Consistent with sinusoidal loading conditions for a helicopter lag damper, single frequency (lag/rev) and dual frequency (lag/rev and 1/rev) sinusoidal loadings were applied to the MRFE damper. Complex modulus and equivalent damping were used to compare the characteristics of the MRFE damper with the passive elastomeric damper. The experimental damping characteristics of the MRFE damper were consistent with the analytical results obtained from the Bingham plastic analysis of the MR valve. Based on measurements, the Field-OFF MRFE characteristics are similar to the passive elastomeric damping, and controllable damping as a function of different flight conditions is also feasible as the applied current is varied in the MR valve.

A second key objective of the present research is to develop an analytical model to describe the nonlinear behavior demonstrated by an MRFE damper. Since the damping behavior of both elastomers and MR fluids is dominated by friction mechanisms, a rate-dependent elasto-slide element is developed to describe the friction characteristics. An MR model developed from a single elasto-slide element successfully emulated the yield behavior of the MR damper, and this model captured nonlinear amplitude and frequency dependent behavior of MR dampers using constant model parameters. Meanwhile, using a distributed elasto-slide structure, an elastomeric model was developed to describe the stiffness and damping behavior of the elastomer as the amplitude of excitation increases. The fidelity of this five parameters time domain model is demonstrated by good correlation between modeling and experimental results for both the

complex modulus and steady-state hysteresis cycles. Since an MRFE damper was shown to be a linear combination of the elastomeric and MR component, a time domain MRFE damper model was constructed based on the linear combination of the MR and elastomer models to describe the nonlinear behavior of the MRFE damper. Good correlation between the model and experimental data demonstrates the feasibility of the MRFE model for future MRFE damper applications.

DEVELOPMENT OF MAGNETORHEOLOGICAL  
FLUID ELASTOMERIC DAMPERS  
FOR HELICOPTER STABILITY AUGMENTATION

by

Wei Hu

Dissertation submitted to the Faculty of the Graduate School of the  
University of Maryland, College Park in partial fulfillment  
of the requirements for the degree of  
Doctor of Philosophy  
2005

Advisory Committee:

Professor Norman M. Wereley, Chair/Advisor  
Professor Amr Baz, Dean's Representative  
Professor Inderjit Chopra  
Professor Sung Lee  
Professor Darryll Pines

© Copyright by

Wei Hu

2005

# DEDICATION

To my mother and sister who always support me unconditionally

To my love, wish this is the best present for her

To my father:

If tomorrow starts without you, and you are not there to see.  
If the sun should rise and find my eyes all filled with tears for you, I  
wish so much I wouldn't cry.

While thinking of the many things, I know how much I love you as  
much as you love me!

It seemed almost impossible that you were leaving me.  
I thought of all the yesterdays, the good ones and the bad.  
I thought of all the love we shared, and all the fun we had.  
If I could be there yesterday, just even for a while, I'd say goodbye  
and kiss you and maybe see you smile.

But then I fully realized that this could never be, my heart was  
filled with sorrow...

Your life on earth is past, but there life starts anew.

At last you're free.

So won't you come and take my hand, and share my happiness with  
me for my graduation?

So when tomorrow starts without you, never think we're far apart.

For every time I think of you, you are right here, in my heart.

## ACKNOWLEDGEMENTS

I would like to express my deep and sincere gratitude to my advisor, Professor Norman Wereley, for all the direction he has given me throughout the course of this research. His wide knowledge and his logical way of thinking have been of great value for me. His understanding, encouragement and personal guidance have provided a good basis for the present thesis. His complete faith in me and friendship have made my graduate experience most pleasurable and enriching.

I wish to express my warm and sincere thanks to Professor Amr Baz, Professor Inderjit Chopra, Professor Sung Lee and Professor Darryll Pines for agreeing to serve on my dissertation committee. Having taken courses with each of these professors, I can honestly say that they are some of the best instructors I have had in my academic career. Their ideals and concepts have had a remarkable influence on my entire career in the field of smart materials and structures research. Many thanks to Dr. Peter C. Chen from Techno-Sciences Inc. for his invaluable technical support and constructive comments.

During this work I have collaborated with many colleagues for whom I have great regard, and I wish to extend my warmest thanks to all those who have helped me with my work in the Department of Aerospace Engineering at the University of Maryland. A special word of thanks to Dr. Gang Wang, Dr. Jinsong Bao, Dr. Y.T. Choi, Dr. J.H. Yoo, Dr. V.T. Nagaraj, Rebecca Snyder Grilli, Shaju John, William B. FaceyIII, Nicholas Rosenfeld, and Anirban Chaudhuri for their valuable insights and suggestions related to my research. Thanks as well to Dr. V.K. Pavlin and Mike Perna for their technical support.

I owe my loving thanks to my parents. They have lost a lot due to my research abroad. Without their encouragement and understanding it would have been impossible for me to finish this work. My special gratitude is due to my sister and her family for their loving support. May my dissertation be a best present for my father, and may he rest in peace.

This research was supported by the National Rotorcraft Technology Center under the Rotorcraft Center of Excellence program (Dr. Yung Yu as technical monitor). Research instrumentation support from the U.S. Army Research Office contract 37718-EG-RI is also acknowledged (Dr. Gary Anderson as technical monitor). Also, I would like to thank Hutchinson Aerospace (Mr. Christian Casse and Mr. Louis Chemouni) for providing the elastomeric specimens and the linear stroke elastomeric lag dampers used in this study. Financial support provided by the Vertical Flight Foundation Scholarship

is also gratefully acknowledged.

# TABLE OF CONTENTS

|   |           |
|---|-----------|
| <b>List of Tables</b>   | <b>x</b>  |
| <b>List of Figures</b>  | <b>xi</b> |
| <b>1 Introduction</b>   | <b>1</b>  |
| 1.1 Objective . . . . .   | 1         |
| 1.2 Background and Motivation . . . . .                               | 2         |
| 1.3 Literature Review . . . . .                                       | 8         |
| 1.3.1 Semi-active Lag Damping . . . . .                               | 8         |
| 1.3.2 MR Fluids and MR Damper Modeling . . . . .                      | 11        |
| 1.3.3 Elastomeric Modeling . . . . .                                  | 14        |
| 1.4 Scope of Current Research . . . . .                               | 20        |
| <b>2 Characterization and Modeling of a Magnetorheological Damper</b> | <b>29</b> |
| 2.1 Experimental Characterization . . . . .                           | 32        |
| 2.2 Evaluation of a Rate-dependent Elasto-slide Model . . . . .       | 37        |
| 2.2.1 Rate-dependent slide . . . . .                                  | 37        |
| 2.2.2 Elasto-slide model . . . . .                                    | 39        |
| 2.2.3 Identify model parameters using hysteresis data . . . . .       | 42        |

|          |  |            |
|----------|--|------------|
| 2.3      | Model Validation . . . . .                                     | 45         |
| 2.3.1    | Numerical fulfillment of the model . . . . .                   | 45         |
| 2.3.2    | Experimental validation . . . . .                              | 47         |
| 2.4      | Conclusion . . . . .   | 49         |
| <b>3</b> | <b>Characterization and Modeling for Elastomeric Materials</b> | <b>69</b>  |
| 3.1      | Experimental Setup . . . . .                                   | 76         |
| 3.2      | Elastomer Characterization . . . . .                           | 80         |
| 3.3      | Distributed Rate-dependent Elasto-slide Model . . . . .        | 82         |
| 3.4      | Determination of Model Parameters . . . . .                    | 88         |
| 3.5      | Model Applications . . . . .                                   | 92         |
| 3.5.1    | Single Frequency Modeling Results . . . . .                    | 92         |
| 3.5.2    | Dual Frequency Modeling Results . . . . .                      | 94         |
| 3.5.3    | 1-DOF Dynamic Response Analysis . . . . .                      | 96         |
| 3.6      | Conclusions . . . . .  | 97         |
| <b>4</b> | <b>MRFE Damper Design and Analysis</b>                         | <b>119</b> |
| 4.1      | MR Flow Mode Analysis . . . . .                                | 120        |
| 4.2      | MR Valve Design . . . . .                                      | 126        |
| 4.2.1    | Determine MR Valve and Performance . . . . .                   | 126        |
| 4.2.2    | Magnetic Circuit Design . . . . .                              | 129        |
| 4.3      | MRFE Damping Performance Prediction . . . . .                  | 131        |
| 4.4      | Conclusion . . . . .   | 133        |
| <b>5</b> | <b>Characterization and Modeling for MRFE Damper</b>           | <b>138</b> |
| 5.1      | Damper Setup and Testing . . . . .                             | 140        |
| 5.2      | MRFE Damper Characterization . . . . .                         | 143        |

|          |   |            |
|----------|---|------------|
| 5.2.1    | Linearization of Damper Characteristics . . . . .   | 143        |
| 5.2.2    | Single and Dual Frequency Characteristics . . . . . | 145        |
| 5.2.3    | Equivalent Damping of the MRFE Damper . . . . .     | 147        |
| 5.3      | MRFE Damper Modeling . . . . .                      | 152        |
| 5.3.1    | Determine Model Parameters . . . . .                | 154        |
| 5.3.2    | Modeling Results . . . . .                          | 156        |
| 5.4      | Conclusions . . . . .                               | 157        |
| <b>6</b> | <b>Summary and Conclusions</b>                      | <b>180</b> |
| 6.1      | MR Damper Modeling . . . . .                        | 182        |
| 6.2      | Elastomer Modeling . . . . .                        | 183        |
| 6.3      | MRFE Damper Design and Analysis . . . . .           | 184        |
| 6.4      | MRFE Damper Development and Modeling . . . . .      | 185        |
| 6.5      | Future Work . . . . .                               | 186        |
| 6.5.1    | Future MR and Elastomeric Model . . . . .           | 186        |
| 6.5.2    | Future Development of the MRFE Damper . . . . .     | 187        |
|          | <b>Bibliography</b>                                 | <b>191</b> |

# LIST OF TABLES

|     |   |     |
|-----|---|-----|
| 2.1 | Dual Frequency Test Matrix . . . . .                | 52  |
| 2.2 | Model Parameters . . . . .                          | 59  |
| 3.1 | Model Parameters for Elastomeric Specimen . . . . . | 107 |
| 3.2 | Model Parameters for Elastomeric Damper . . . . .   | 108 |
| 5.1 | Dual Frequency Test Matrix . . . . .                | 160 |
| 5.2 | Model Parameters . . . . .                          | 172 |

# LIST OF FIGURES

|      |   |    |
|------|---|----|
| 1.1  | Possible MRFE Damper Configurations . . . . .   | 27 |
| 1.2  | Preliminary MRFE Damper Test Setup . . . . .  | 28 |
| 2.1  | Schematics of an MR Damper . . . . .  | 51 |
| 2.2  | Test Setup for MR Damper . . . . .  | 51 |
| 2.3  | Hysteresis Cycles for MR Damper . . . . .   | 53 |
| 2.4  | Linear Damping Characterization of the MR damper . . . . .                                    | 54 |
| 2.5  | Rate Dependent Elasto-slide Model . . . . .   | 55 |
| 2.6  | Quasi-Static Force-Velocity Relationship Predicted by MR Mod-<br>els . . . . .                | 56 |
| 2.7  | Hysteresis Behavior of an Elasto-slide Model . . . . .  | 56 |
| 2.8  | Determined Initial Loading Curve . . . . .  | 57 |
| 2.9  | Model Parameters (Yield Force and Preyield Stiffness) as a Func-<br>tion of Current . . . . . | 58 |
| 2.10 | Quasi-steady Behavior of the Model . . . . .  | 60 |
| 2.11 | Model Fit at 5Hz and 0A . . . . .   | 61 |
| 2.12 | Model Fit at 5Hz and 0.3A . . . . .   | 62 |
| 2.13 | Model Fit at 2.5Hz and 0.1A . . . . .   | 63 |
| 2.14 | Model Fit at 2.5Hz and 0.3A . . . . .   | 64 |

|      |  |     |
|------|--|-----|
| 2.15 | Model Fit at 7.5Hz and 0A . . . . .  | 65  |
| 2.16 | Model Fit at 7.5Hz and 0.2A . . . . .  | 66  |
| 2.17 | Dual Frequency Modeling at 5.0Hz and 2.5Hz . . . . .   | 67  |
| 2.18 | Dual Frequency Modeling at 5.0Hz and 7.5Hz . . . . .   | 68  |
|      |  |     |
| 3.1  | Elastomeric Specimen Test Setup . . . . .  | 100 |
| 3.2  | Schematic of the Elastomeric Double Lap Shear Specimen (Di-<br>mensions in mm) . . . . .     | 100 |
| 3.3  | Elastomeric Lag Damper Test Setup . . . . .  | 101 |
| 3.4  | Cross Section of Concentric Bearing Elastomeric Lag Damper (Di-<br>mensions in mm) . . . . . | 101 |
| 3.5  | Linear Characterization of an Elastomeric Specimen . . . . .                                 | 102 |
| 3.6  | Linear Characterization of the Elastomeric Damper . . . . .                                  | 103 |
| 3.7  | Distributed Elasto-Slide Model . . . . .   | 104 |
| 3.8  | Hysteresis Modeling for Elastomeric Specimen . . . . .                                       | 105 |
| 3.9  | Determination of the Initial Loading Curve for Elastomeric Spec-<br>imen . . . . .           | 106 |
| 3.10 | Elasto-slide Distribution for Elastomeric Specimen . . . . .                                 | 106 |
| 3.11 | Single Frequency Hysteresis Modeling for Elastomeric Specimen .                              | 109 |
| 3.12 | Variation of Complex Modulus with Dynamic Amplitude for Elas-<br>tomeric Specimen . . . . .  | 110 |
| 3.13 | Single Frequency Hysteresis Modeling for Elastomeric Damper . .                              | 111 |
| 3.14 | Dual Frequency Hysteresis Modeling for Elastomeric Specimen . .                              | 112 |
| 3.15 | Dual Frequency Hysteresis Modeling for Elastomeric Specimen .                                | 113 |
| 3.16 | Dual Frequency Hysteresis Modeling for Elastomeric Specimen .                                | 114 |
| 3.17 | Dual Frequency Hysteresis Modeling for Elastomeric Specimen .                                | 115 |

|      |   |     |
|------|---|-----|
| 3.18 | Modeling Results for Dual Frequency with Slowly Varying Amplitude . . . . .                     | 116 |
| 3.19 | Dynamic Oscillator . . . . .  | 117 |
| 3.20 | Transient Response with Displacement Perturbation and Nominal System Damping Ratio 5% . . . . . | 118 |
| 3.21 | Transient Response with Displacement Perturbation and Zero System Damping . . . . .             | 118 |
| 4.1  | Flow-mode MR Valve Mechanism . . . . .  | 135 |
| 4.2  | Typical Velocity Profile . . . . .  | 135 |
| 4.3  | Analytical Quasi-Steady MR Valve Behavior . . . . .   | 136 |
| 4.4  | MRFE Equivalent Damping Prediction . . . . .  | 137 |
| 5.1  | Schematic of MRFE Damper . . . . .  | 159 |
| 5.2  | MRFE Damper Experimental Setup . . . . .  | 159 |
| 5.3  | Typical Hysteresis Cycles of the Baseline Damper for Varying Displacements . . . . .            | 161 |
| 5.4  | Linear Characterization of the Baseline Damper . . . . .  | 162 |
| 5.5  | Hysteresis of the MRFE Damper . . . . .   | 163 |
| 5.6  | Linear Characterization of MRFE Damper at Single Frequency . . . . .                            | 164 |
| 5.7  | Linear Characterization of MRFE Damper at Different Frequencies . . . . .                       | 165 |
| 5.8  | Dual Frequency Characterization . . . . .   | 166 |
| 5.9  | Dual Frequency Hysteresis . . . . .   | 167 |
| 5.10 | Empirical Relationship between Yield Stress and Current . . . . .                               | 168 |
| 5.11 | Empirical Relationship between Yield Force and Current . . . . .                                | 168 |
| 5.12 | MRFE Equivalent Damping Prediction . . . . .  | 169 |

|      |   |     |
|------|---|-----|
| 5.13 | Dual Frequency Equivalent Damping . . . . .   | 169 |
| 5.14 | Semi-active MR Damping Power Characteristics . . . . .  | 170 |
| 5.15 | MRFE Model Structure . . . . .  | 171 |
| 5.16 | Field Dependent N and K . . . . .   | 173 |
| 5.17 | Force-Displacement Hysteresis Modeling at 2.5 Hz, Four Amplitude Cases: 0.25, 0.50, 0.75 and 1 mm . . . . . | 174 |
| 5.18 | Force-Displacement Hysteresis Modeling at 5.0 Hz, Four Amplitude Cases: 0.25, 0.50, 0.75 and 1 mm . . . . . | 175 |
| 5.19 | Force-Displacement Hysteresis Modeling at 7.5 Hz, Four Amplitude Cases: 0.25, 0.50, 0.75 and 1 mm . . . . . | 176 |
| 5.20 | Field-OFF (0.0 A) Dual Frequency Modeling . . . . .   | 177 |
| 5.21 | Field-ON (0.4 A) Dual Frequency Modeling . . . . .  | 178 |
| 5.22 | Dual Frequency Modeling: $A_{tag}=0.25$ mm, $A_1=0.75$ mm . . . . .   | 179 |

# Chapter 1

## Introduction

### 1.1 Objective

Aeromechanical instabilities due to the coupling of the lightly damped blade lag motion with other motions are serious concerns in helicopter rotor systems, and lead-lag dampers are widely used to mitigate these instabilities. However, as more advanced helicopter rotor systems emerge, such as soft-in-plane hingeless or bearingless rotors, elastomeric snubbers/dampers on these advanced rotors exhibit a large reduction of lag damping as the amplitude of the blade motion increases, leading to excessive size and weight of dampers in order to accommodate all operating conditions. Meanwhile, current snubber/damper designs account for a large fraction of the rotor cost [1]. In addition, despite continued improvement in material performance, some articulated rotors require more damping than current elastomers can achieve and this is particularly true for rotors that were originally designed to use hydraulic lead-lag dampers [2]. The greatest amount of lag mode damping at the lowest cost (both initial and maintenance) is desirable. Semi-active lead-lag dampers employing field control-

lable fluids such as magnetorheological (MR) fluids have been proposed [3], and substantial damping augmentation has been observed in model-scaled dampers between on-off conditions. However, neither full scale semi-active dampers have been developed, nor has the behavior of an adaptable lead-lag damper activated by a continuously controllable field been evaluated.

The objective of this dissertation is firstly to develop MR fluid elastomeric dampers (MRFE) and evaluate their controllable damping performance under loading conditions encountered by a helicopter lag damper, and secondly to develop an MRFE damper model to describe MRFE damper behavior.

## 1.2 Background and Motivation

Aeromechanical stability of helicopters is a nonlinear phenomenon involving complex interactions of aerodynamic, inertial and elastic forces. The state of the art on rotorcraft aeromechanical stability is addressed in a review [4]. Due to stress and weight considerations, advanced helicopter rotors are soft-in-plane, and are susceptible to aeromechanical instabilities, such as air and ground resonance. Classical ground resonance, caused by the coupling of blade lag motion and landing gear modes, is mitigated in conventional articulated rotors using mechanical lag dampers. Air resonance, which is a coupling of rotor blade modes with fuselage modes for an airborne vehicle, is mitigated via elastomeric dampers, and is strongly dependent on flight condition. However, lag damper effectiveness is reduced for advanced rotors because of small displacements near the blade root. The reduced effectiveness of existing lag mode dampers, coupled with high maintenance cost and weight/drag of mechanical dampers, and

high cost of elastomeric dampers, make alternative rotor stability augmentation schemes attractive. Therefore, except that the blade root is strong and heavy enough to accommodate the in-plane loads [5], passive and active damping strategies are indispensable for soft-in-plane rotors and should be explored to exploit the full potential of damping augmentation strategies in the rotor.

One example of lag damping augmentation strategies is applied on the Comanche's five-bladed bearingless main rotor [6]. The Boeing-Sikorsky RAH-66 Comanche is configured as an advanced five-bladed bearingless main rotor. As is characteristic of many soft-in-plane main rotor aircraft, the Comanche exhibited a lightly damped roll response or a regressing lag mode oscillation when undergoing a sustained high-G maneuver. This air resonance phenomenon was caused by the coalescence of the body roll-regressing flap mode with the rotor regressing lag mode and was interpreted by the pilot as a ringing in the roll response at the regressing lag mode frequency. The Comanche main rotor employed a passive snubber-damper at the root end of the blade to provide auxiliary damping to the first lag mode. Since the Comanche demonstrated adequate levels of air resonance stability in most flying states and significant ground resonance stability margins, using a improved damper to add lead-lag damping was not a cost-effective option. Instead, the fly-by-wire Automatic Flight Control System (AFCS) on the Comanche provided the option of active augmentation of air resonance stability. Using body pitch and roll rate signals to calculate swashplate control inputs that enhanced rotor stability, the air resonance controller significantly augmented the air resonance damping especially at high thrust conditions and meanwhile satisfied all of the stability and handling quality requirements. Active control methods to augment aeromechanical stability are also applied on

other helicopters. A Stability Augmentation System (SAS) was developed for ground and air resonance, and was claimed to be highly efficient and robust on a Super Puma Mk2 helicopter [7]. Other active control technology using Individual Blade Control (IBC) control system was mentioned in Refs. [8] and [9]. These efforts show the effectiveness of active feedback with the potential benefit being a lighter system solution for the lead-lag dampers. However, in the active damping control strategy, a sophisticated digital flight control system is needed and additional power input is required to actuate swashplate or blade flap actuators. In addition, although a limited number of studies have shown considerable promise for active control on aeromechanical stability, the active damping augmentation strategy is not yet mature and will not be fielded in the short term. Other alternative approaches to provide lag damping instead of using hydraulic or elastomeric dampers have been under development, such as the tuned vibration absorbers [10] and the piezoelectric lag damper [11]. The absorbers can be embedded inside the blade leading edge weight structure, and the piezoelectric materials can be attached to a rotor flexure of a hingeless rotor. Thus, both configurations can be claimed to provide an aerodynamically cleaner rotor hub. These approaches are feasible from a practical point of view only if they are simple and durable enough to compete with lead-lag dampers. While research has been ongoing to design damperless main rotor configurations, at this time, development of semi-active lag dampers is still a more straightforward mechanical solution to enhance aeromechanical stability.

Conventional lag dampers use passive materials, such as elastomers, to dissipate energy, but their damping and stiffness levels diminish markedly as amplitude of damper motion increases. In forward flight conditions, the blade lead-lag

motion in helicopters occurs at two frequencies - the lead-lag or first in-plane rotor blade bending modal frequency ( $\text{lag/rev}$ ) and the rotor operational frequency ( $1/\text{rev}$ ). Large in-plane bending motions at  $1/\text{rev}$  will reduce the damping capacity at  $\text{lag/rev}$  substantially, thus, introducing the potential for undesirable limit cycle oscillations [12]. Moreover, as mentioned in damping requirements for the Comanche [6], damping augmentation is only required over certain flight regimes where there is a potential for instabilities to occur, and a passive damper providing sufficient damping over the expected amplitude range could produce unfavorably large periodic loads on the rotor hub as well as a bulkier damper. Additionally, the mechanical properties of different dampers should be matched to minimize the impact of varying damper mechanical properties on rotor tracking conditions [3]. Clearly, an adaptable or semi-active damper would be of considerable value if it had the following capabilities: 1) to produce sufficient damping at key flight conditions while simultaneously reducing periodic hub loads at other flight conditions, 2) to compensate for damping losses at the  $\text{lag/rev}$  frequency for high amplitude single frequency excitations, 3) to compensate for the reduction in damping at  $\text{lag/rev}$  because of  $1/\text{rev}$  excitation of the lag mode, 4) to compensate for differences among individual dampers employed in a rotor hub.

A promising option is to employ controllable or smart fluids. Magnetorheological (MR) fluids are a soft ferromagnetic powder (typically, 30 micron carbonyl iron) suspended in a silicone oil, and each particle has a natural magnetic dipole. The physical mechanism of the MR fluid is one of magnetic polarization. When a magnetic field is applied across the volume of fluid, the magnetic dipoles orient themselves with respect to the applied magnetic field and form chains. It

is these chains that induce the yield stress: a local shear stress must be applied that is greater than the yield stress before the chains break and flow is induced. The yield stress can be as high as 100 kPa for commercial MR fluids [13], and the substantial field-induced yield stresses exhibited by MR fluids make possible many applications, such as rotary brakes or dampers. Applications of MR fluids in fluid-based dampers have been examined [14–16]. Compared with passive and active dampers, MR dampers can provide continuously variable damping force with little energy input effort. Many MR dampers for shock and vibration isolation mounts have been designed and tested, and their controllable damping capabilities are well established [17–20].

Typically, elastomeric lag dampers are concentric bearing type or multiple laminations of metallic and elastomeric rings. By introducing an adaptable material, such as MR fluids, as a working fluid inside the lamination stack forming the elastomeric bearing, and an electromagnet to activate the MR fluid, the apparent viscosity can be greatly increased. Deformation of the elastomer results in relative motion between the damper body and an enclosed MR valve. An advantage of such an approach is that there is no dynamic rod seal since the elastomeric members are used to create a fluid chamber, so that the possibility of leaks due to the erosion of dynamic seals is eliminated. Second, while the stiffness in the elastomer is available as a necessary rotor hub design parameter and the damping is provided by the combination of the elastomer and MR fluids, the magnetorheological fluid and elastomeric (MRFE) hybrid lag damper can actively and selectively augment damping over critical frequency ranges and increase stability of a helicopter rotor. In addition, the passive damping, in both elastomeric and MR damping elements, provides fail-safe damping in the event

that control of the field dependent MR damping is lost.

The MRFE damper can be developed in different configurations. Schematic structures of the proposed prototype concentric bearing type MRFE damper are shown in Figure 1.1(a) and (b). The linear stroke damper consists of elastomeric layers and an MR fluid reservoir enclosed by the elastomer layer. The relative motion between the damper rod and the damper body leads to a shear deformation of the elastomer along the damper body length, and also forces the MR fluid to flow through the field activated gaps in the piston. Thus, the output force of the damper is a field dependent damping force provided by the MR component in addition to a passive spring and damping force provided by the elastomeric layer. Schematic diagrams of the proposed prototype MRFE snubber damper is shown in Figure 1.1(c). The primary elements that comprise this MRFE snubber are the lag bearing, torsion bearing, paddle with MR valves, damper cover (for attachment to the torque tube) and circular flange (to attach to the flexbeam). The lag bearing consists of plates interspersed with elastomeric layers, or a multiple lamination of metallic and elastomeric layers. The MR fluid would fill the cavity (nearly elliptical with flat sides) inside the lag bearing. The paddle will move through the MR fluid reservoir inside the lag bearing as the stack of metal-elastomer layers shear relative to each other due to lag motion. The MR valve on the paddle will allow flow through the valves in the absence of field, but in the presence of magnetic field, the MR valves will impede flow through the valves. By varying the magnetic field, the MR damping component can be greatly modified.

Since an MRFE damper includes damping effect from elastomers and MR fluids, appropriate analytical models for the elastomer and MR material are

necessary to describe the behavior of an MRFE damper. The behavior of these materials, however, is very complex. Constitutive behaviors and characteristics of both elastomers and MR fluids are nonlinear and dependent on the amplitude and frequency of loading motion. Especially, the behavior of an elastomer is also affected by temperature and preloading conditions. These properties make characterization, modeling, and design of MRFE dampers a very difficult task. The need for a precise damper model cannot be over-emphasized as the damper strongly influences the dynamics and aeromechanical stability characteristics of the helicopter rotor, such that attempts to predict these without accurate damper characterization are of limited value. This provided the motivation to develop an accurate MRFE lag damper constitutive model that can adequately represent its behavior over the range of operating conditions. Since the MRFE model should be easily and conveniently integrated into a rotor dynamic analysis including trim and perturbation analysis, the damper model to be developed should be a phenomenological or mechanical time domain model rather than in terms of microstructural or atomic processes.

## **1.3 Literature Review**

### **1.3.1 Semi-active Lag Damping**

The study on applying semi-active damping to helicopter rotor systems dates back to the 1990s when the Comanche helicopter was reported to be encountering a significant air resonance due to the nonlinearity of the elastomeric damper [21]. This led to two key research topics on helicopter lag dampers. One was elastomeric damper modeling, which could be used to study the effect of the elas-

tomeric dampers on aeromechanical instabilities and these research efforts will be reviewed later. The other research work emphasized measures to improve the performance of the lead-lag dampers. A significant solution was the development of a fluid elastomeric hybrid damper (Fluidlastic) [22,23]. To counter the disadvantage of elastomeric dampers, this fluid elastomeric damper uses proven bonded elastomer technology in conjunction with inert silicon based viscous damping fluids to expand dynamic range. However, all these dampers are passive dampers, and their damper properties will change due to ambient temperature changes and self-heating resulting in uncertainties in lag damping enhancement [24]. Thus, following the emergence of the MR technology, some academic researchers, especially the research group led by N.M. Wereley at University of Maryland and the research group led by K.W. Wang at Penn State, began a feasibility study on the semi-active lead-lag dampers using MR technology. The first MR lag damper study was conducted by Kamath, Wereley and Jolly (Ref. [3]). They developed a Froude-scaled MR fluid damper by incorporating a permanent magnet inside the chamber body of the baseline Froude-scaled Fluidlastic damper. Their study demonstrated the feasibility of using MR dampers for lag mode damping applications wherein a substantial increase in damping can be achieved by applying a magnetic field. The feasibility of a combination of MR fluids and elastomeric materials was studied by an emulation of a magnetorheological fluid and elastic (MRFE) composite damper [25]. The experimental study of this emulation validated a considerable damping control range provided by the flow mode valve in the linear stoke MR component of the damper. While the damping was provided by the combination of the elastomer and MR fluid, this preliminary MRFE damper can actively augment damping

over critical frequency ranges and enhance the stability of helicopter rotors.

Despite the fact that a number of algorithms have been developed for controlling smart fluid devices since the 1990s [26–28], lag damping control schemes using MR dampers for helicopter stability augmentation are not much explored. Marathe *et al* [29] firstly investigated the effect of two different control schemes on rotor stabilities by integrating an MR damper model with a rotor aeromechanical model. Two different control schemes were the On-Off scheme and Feedback Linearization scheme, and they were compared for lag transient response in ground resonance and their ability to reduce periodic damper loads in forward flight. Based on analysis using a shear mode MR damper model, the MR damper of a size comparable to an elastomeric damper can provide sufficient damping for ground resonance stabilization and can significantly reduce periodic damper loads with a judicious choice of operation scheme. The On-Off scheme is straightforward and easy to implement but is not optimal for reducing hub loads. Feedback control is more versatile but required more complexity due to sensors and feedback control system. When the feedback linearization scheme was utilized, Gandhi *et al* [30] explored the effects of MR fluid damper model uncertainties on helicopter rotor system stability. For specified uncertainty bounds, a robust control can be synthesized to eliminate instabilities by using a much larger value of prescribed damping ratio. Zhao *et al* [31] developed a different linearization feedback control strategy to integrate the MR damper into a classic linear ground resonance analysis assuming an isotropic rotor hub (all dampers and blades similar) or an anisotropic rotor hub (for example, lag damper dissimilarity due to damage), and they assessed the capability of the MR damper to stabilize a rotor system which exhibited unstable ground resonance behavior

as a result of lag damper degradation or damage. The analysis developed in this study demonstrated that an MR damper, in conjunction with semi-active feedback control using sliding mode or feedback linearization strategies, can stabilize an unstable rotor except for the case where 100% damping was lost on one blade. The ground resonance analysis of helicopter using MR lag dampers are also found in the study conducted by Wang *et al* [32]. Overall, as shown in these analysis, MR dampers offer an opportunity to enhance stability augmentation strategies over passive elastomeric dampers, and should be considered in advanced rotor design.

### 1.3.2 MR Fluids and MR Damper Modeling

MR fluids are semi-active materials with a controllable yield stress in the presence of magnetic field. The most common constitutive model to describe the MR fluid behavior in fully developed flow is the idealized Bingham plastic model [33]. The Bingham plastic model implies that the material remains rigid below a critical field-dependent yield stress and exhibits nearly Newtonian behavior after the shear stress exceeds the yield stress. While this assumption works well for high strain rates where the onset of flow has occurred, it does not accurately describe the fluid behavior for small strain rates below the yield point where there is elastic deformation. Since most MR dampers operate in dynamic or transient response, the exact description of material characteristics in the pre-yield region becomes important since the entire hysteresis cycle needs to be predicted such that the behavior of MR dampers in damping control applications can be evaluated. To be consistent with quasi-steady modeling using MR fluids, the Bingham-plastic constitutive model [34–37] was used to describe

the MR damper behavior under oscillatory sinusoidal loading conditions. Similar to the fluid constitutive model, even though the Bingham plastic model is mathematically simple and gives a good description of postyield behavior of an MR damper, the damper force predicted by the model exhibits a step jump discontinuity in the transition region from preyield to postyield. Thus, Bingham plastic model cannot account for the practical behavior of the progressive and continuous yield behavior that is observed in the test data. To mitigate the drawback of the Bingham plastic model, a biviscous model was introduced by Williams and Stanway *et al* [38,39]. The biviscous model is characterized by two distinct viscosities in accord with the preyield and postyield regions, and the preyield viscosity is much greater than the postyield viscosity. Since the biviscous model cannot describe a smooth transition from preyield to postyield, Lionel *et al* [40] developed an Eyring-plastic model to provide improvement over the Bingham plastic model and the biviscous model. In the Eyring model, an arc hyperbolic sine function was used to introduce a smooth transition through the preyield and postyield region which is much closer to the practical situation. However, both biviscous and Eyring models are not capable of describing the preyield stiffness effects or compression loop, and the force-velocity hysteresis behavior cannot be described by these models.

To capture the preyield force-velocity hysteresis, various phenomenological modeling methods were developed. Using a combination of several piecewise continuous models, the hysteretic biviscous model [36,41] can well describe the hysteresis behavior of MR dampers. Alternatively, some modeling efforts use suitable mathematical functions to phenomenally describe the hysteresis behavior demonstrated by MR dampers. The nonlinear hysteretic Bingham model

with simplicity in form [18] was proposed to describe the low speed hysteresis characteristics of an MR isolator, and this model was shown successfully in control applications. Kamath and Wereley [3, 42] developed a nonlinear piecewise smooth viscoelastic-plastic model using a nonlinear shape function to describe a smooth transition between preyield viscoelastic and postyield viscous state. A polynomial model proposed by Choi *et al* [43] employed polynomial to fit the force-velocity hysteresis loop, and it predicted fairly well the nonlinear hysteresis behavior of the MR damper. Also focusing on predicting the behavior of electrological dampers (similar to MR dampers), Gamota and Filisko [44] proposed an extension of the Bingham model, which is given by a Bingham model in series of a standard linear solid model. All of these models can accurately capture the postyield and preyield behavior of MR dampers. However, these models only phenomenologically describe the hysteresis using some shape functions and do not reflect the physical yield mechanism in the MR damper. As a result, this type of modeling strategy leads to amplitude and frequency dependent model parameters. While the damper model is implemented, damper loading amplitude and frequency have to be known as *a priori* which is unfavorable in predicting the response under complex loading conditions.

An exception for hysteretic modeling is the Bouc-Wen model [45]. To accurately describe a variety of hysteretic phenomena exhibited in structural systems under dynamic loading, a hereditary restoring function between loading,  $x$ , and response,  $z$ , was introduced in the Bouc-Wen model. In differential form, the model force is determined by

$$\begin{aligned} \dot{z} &= -\alpha|\dot{x}|z^n - \beta\dot{x}|z^n| + A\dot{x}, & \text{for } n \text{ odd} \\ \dot{z} &= -\alpha|\dot{x}|z^{n-1}|z| - \beta\dot{x}z^n + A\dot{x}, & \text{for } n \text{ even} \end{aligned} \tag{1.1}$$

or in an integral form

$$\frac{dz}{dx} = A \pm (\alpha \pm \beta)z^n \quad (1.2)$$

A variety of hysteretic responses can be constructed by adjusting the values of the constants of  $A$ ,  $\alpha$ ,  $\beta$  and  $n$ . The Bouc-Wen model has proven successful in analytical modeling of a hysteretic system under random excitation. Based on the Bouc-Wen model, a generalized hysteresis model was proposed by Spencer *et al* [46]. The model parameters were determined to best fit the response data due to step loading, constant voltage/random displacement and random displacement/random voltage, so the hysteretic behavior of the damper under step and random loading was predicted very well using this modified fourteen parameter Bouc-Wen model. However, the physical interpretation of the Bouc-Wen model parameters is tenuous at best, and the model structure is quite complicated. In contrast, the hydro-mechanical model developed by Hong *et al* [47] is also a nonlinear differential equation. The hydro-mechanical model consists of physically motivated hydromechanical lumped parameters to represent fluid inertia, damping, yield force and compliances associated with MR dampers, and preyield hysteresis force behavior is well represented by the lumped mechanical parameters.

Both the Bouc-Wen model and the hydromechanical model are able to capture the field dependent hysteresis behavior of MR dampers, but the capability of both models to describe the amplitude dependent behavior were not shown.

### 1.3.3 Elastomeric Modeling

An elastomeric damper has proven to be efficient for damping augmentation in helicopter rotors due to their simple design, low weight and high reliability.

However, filled elastomeric dampers exhibit significant nonlinearities, especially the amplitude dependent and weakly frequency dependent behavior [48]. The large reduction of damping as the amplitude of loading motion increases leads to excessive size and weight of dampers in order to accommodate all operating conditions. It was also found that the highly damped elastomeric dampers demonstrated low loss factors at low amplitudes resulting in unacceptable limit cycle oscillations [24]. Therefore, a precise analytical model is necessary to describe these nonlinear behaviors of an elastomeric damper and determine the dynamic characteristics when the damper is implemented in a helicopter.

Since the complex modulus method is successful in characterizing viscoelastic materials under harmonic excitation, early modeling efforts focused on linearization using complex moduli at a given frequency, where the storage modulus is a measure of the energy stored, and the loss modulus is measure of the energy dissipated, over one period of oscillation. This model can be represented as a spring and a dashpot in parallel (Kelvin chain). The complex modulus is a linearization method in the frequency domain which replaces the nonlinear hysteresis loop with an equivalent ellipse, and is only applicable to steady harmonic forced response analysis. For nonlinear elastomeric materials, the complex moduli are also amplitude dependent. Some researchers extended the basic Kelvin chain to a more complicated mechanism-based modeling approach to describe the nonlinear behavior of elastomers. Felker *et al* [12] developed a nonlinear complex modulus model based on one single Kelvin chain, in which the spring force was a nonlinear function of the displacement, and the damping force was a nonlinear function of displacement and velocity. This model was used to describe the amplitude dependent moduli and to study dual frequency damper motions. In

order to display basic behavioral characteristics, such as creep and relaxation, a viscoelastic solid can be represented as a spring in series with Kelvin elements (if one Kelvin element is used, it is called a Zener model [49]). Gandhi and Chopra [50] developed a nonlinear viscoelastic solid model in which a nonlinear leading spring was used in series with a single linear Kelvin chain. Using this model, the variation of the analytical complex moduli with different amplitudes matched closely with experimental data. The parameters in all of these models were identified using amplitude-dependent complex modulus data, and they cannot capture nonlinear stress time histories of elastomers. Kunz [51] similarly used a nonlinear Kelvin chain to capture the nonlinear hysteresis behavior of an elastomeric damper. In this model, the stiffness was expressed as a fourth order polynomial function of displacement, and the damping was described by a second order polynomial function of velocity. Though it can predict the harmonic damper force rather well, this approach is only applicable for a particular amplitude and frequency. In the model developed by Tarzanin *et al* [52], the total damper force was represented by a nonlinear spring force and a nonlinear Coulomb friction damping force. This model was based on single frequency data and was used to match the value of energy dissipation per cycle. However, a sudden jump in predicted damper force was shown when velocity changed sign, which was unrealistic. Panda *et al* [24] replaced the Coulomb friction damping element with a variable friction damping element whose force was calculated based on the peak displacement of excitation when the velocity was zero. This model correlated well with experimental hysteresis data, but the effectiveness of this model over a range of amplitudes and frequencies has not been demonstrated in the literature. In a recent study, Krishnan [53] developed a model

which consisted of a linear Kelvin chain and a parallel cubic spring element. Snyder [37] improved this model by adding an elasto-slide element. Both models were developed to capture nonlinear elastomeric damper hysteresis cycles, but the model parameters were still amplitude and frequency dependent.

On the other hand, some elastomeric models were developed using internal variable or nonlinear integral equations. Strganac [55] used a stress shift function to formulate a nonlinear time domain model for elastomers, but the nonlinear integral formulation in the model was difficult to implement in traditional aeromechanical analysis. Lesieutre and Bianchini [56] developed the anelastic displacement field (ADF) method to describe the frequency-dependent behavior of linear materials. It was based on the notion of scalar internal variables or augmenting thermodynamic fields (ATF) [57] that described the interaction of the displacement field with irreversible processes occurring at the materials level. In the ADF approach, the effects of the thermodynamic processes were focused on the displacement field which consists of both elastic and anelastic parts. The anelastic part may be further subdivided to consider the effects of multiple relaxation processes. Although there is no explicit physical interpretation when multi-anelastic elements are involved, one single ADF model is mechanically analogous to the Zener model. In order to capture the characteristic nonlinear behavior of elastomeric materials, Govindswamy *et al* [58] developed a nonlinear ADF model, in which the linear ADF parameters were replaced with nonlinear terms. The model captured the variations of the complex modulus with amplitude, and performed as well in matching the strain-stress hysteresis. Furthermore, other functional forms for the ADF parameters were introduced in order to improve hysteresis loop predictions. Brackbill *et al* [59] improved the nonlinear ADF

model by adding rate independent nonlinearity, in which friction-damping and linear-spring elements in parallel with the baseline nonlinear ADF model were used to provide additional amplitude dependent relaxation behavior. As many as sixteen parameters were used to construct the model. Although the complex moduli were fitted well along amplitude and frequency ranges, nonlinear stress time histories could still be improved. Moreover, the parameter determination process was complicated by the fact that some parameters were chosen by empirical observation. In a recent study, Ramrakhyani *et al* [60] developed an ADF based model containing nonlinear fractional derivatives and frictional elements. This model used eight parameters instead of sixteen parameters to capture the amplitude-dependent and mild frequency-dependent modulus. However, it did not improve prediction of the hysteresis loop, and the determination of model parameters remains complicated.

Generally, most existing modeling efforts are based on the viscoelastic assumption for elastomeric characteristics. However, an elastomeric damper usually demonstrates tribo-elastic behavior [48] such that those damper models using linear or nonlinear Kelvin chain combinations cannot adequately capture the elastomeric behavior. Either the model parameters are amplitude dependent or the model poorly describes the hysteretic behaviors of an elastomeric damper. Although in some modeling efforts Coulomb or friction damping was used to describe the rate-independent damping behavior significantly demonstrated by the elastomer, a single or even finite number of Coulomb dampers are not sufficient to adequately model damper force in response to sinusoidal excitation over a range of amplitude and frequency. The disadvantage for these modeling efforts is that the excitation amplitude must be known *a priori* to use these models

effectively.

Thus, an efficient and accurate model for an elastomeric model will be developed based on a physical understanding of the damping mechanisms within the damper material. Physically, the amplitude dependent behavior demonstrated by the elastomer is mostly based on the interaction between fillers and rubber compound inside the filled elastomeric materials [61]. Before large deformation of a filled elastomeric damper, an intact filler structure displays a large stiffness and small loss factor for small amplitudes. As the amplitude increases, the filler structure breaks resulting in a stiffness reduction. However, the breaking of filler structures, which is similar to frictional behavior, increases the loss factor. As the amplitude increases further and the frictional effect is fully released, both stiffness and loss factor drop to lower levels, which then are maintained relatively constant by the remaining polymer chains.

Motivated by the above physical mechanisms, a number of researchers have attempted combinations of springs and frictional slides to represent the filler and rubber compound in filled rubbers or elastomers. As early as 1930, Timoshenko [62] suggested that the general hysteretic system consist of a large number of ideal elasto-plastic elements with different yield levels. Iwan [63,64] further developed a distributed-element model to study the steady-state dynamic response of a hysteretic system. Instead of specifying a distribution function numerically to agree with experimental data, a constant band-limited statistical function was used to define yield properties of the slide elements in this model. This model proved successful in predicting steady-state frequency response of a hysteretic system using method of linearization. However, the excitation amplitude must be known as *a priori* while this model is applied in the analysis, which is only

applicable in steady-state response prediction. The theory of triboelasticity [65] also stated that the behavior of a filled elastomer can be represented by a large or infinite number of alternate springs and frictional slides in series, and each slide has a constant yield force and each spring has a constant stiffness. Coveney et al [48] developed a three-parameters standard triboelastic solid (STS) based on theory of triboelasticity and further developed a four-parameter rate-dependent triboelastic (RT) model. These models gave a satisfactory representation of material behavior. However, since the yield force is fixed along different slides, these models shows less flexibility to represent the amplitude dependent behavior for different filled-level materials.

## 1.4 Scope of Current Research

Semi-active Magnetorheological Fluid-Elastic (MRFE) lag damper technology is developed in this study to overcome the amplitude dependent damping loss issues associated with passive elastomeric lag dampers and to provide adaptable lag damping for varying lag damping requirements at different flight conditions. The layout of this thesis is based on the process of the development of the MRFE damper. Firstly, the material components of the MRFE damper, i.e. MR fluids and elastomers, are studied individually. Characterization and modeling efforts for the MR fluid based damper and elastomeric damper are summarized, and new modeling methodologies are developed for an MR valve and an elastomeric damper, respectively. Using a quasi-steady MR fluid flow analysis, the overall MRFE system architecture, actuator design, analysis, and component integration aspects of the MRFE damper are described. This is followed by a discus-

sion of damper prototyping and testing and experimental evaluation. Finally, an MRFE damper model is constructed based on the MR and elastomeric modeling approaches, and it is used to describe the damper behavior.

In preparation for the development of an MRFE damper, a substantial feasibility study was undertaken in order to provide the controllability analysis and evaluate the compatibility of the elastomer with the MR fluid over a similar range of displacement loading. A preliminary MRFE damper test setup was constructed as shown in Figure 1.2, and two distinct damping components were mounted in the test fixture: 1) an elastomeric damping component, and 2) a magneto-rheological damping component. The elastomeric damping component was a double lap shear specimen of high loss factor filled elastomer, and the second component consisted of two linear stroke MR dampers. In this parallel configuration, the damping contributions from each damping component were found to be additive, so that the MR and elastomeric damper can be characterized independently. To obtain a general MRFE damper behavior including extreme working conditions, a broad displacement loading was used and ranged from 0.5mm to 5 mm (ranging from 2.5 % to 50 % shear strain) and suitable frequency range for helicopter systems. This experimental feasibility study demonstrated that a substantial damping control range was provided by the MR component of the damper. While the stiffness in the elastomer is still available as a design parameter, the semi-active MR damping can augment the passive elastomeric damping. In addition, the passive damping contributed by the elastomeric and MR damping component provides fail-safe damping capability in the event that the field dependent MR damping is lost. The details of the feasibility study can be found in Ref. [25].

To describe the nonlinear behavior demonstrated by both MR and elastomeric components, analytical models for MR and elastomeric dampers are developed separately based on the experimental results of the preliminary MRFE damper setup. First, a new modeling approach was developed for the MR damper to describe the damper hysteretic behavior over a broad amplitude and applied current range, and the modeling results were correlated with experimental data using comprehensive loading conditions. In this model, a rate-dependent elasto-slide was used to physically describe the effects of preyield stiffness, preyield slip and postyield viscous damping demonstrated by the field activated MR flow. Rate-dependence of the slide was determined via numerical analysis by a robust initial differential algorithm. In parallel with a linear viscous fluid damping and a weak accumulator stiffness, the rate-dependent elasto-slide model captures most physical properties of an MR damper. Model parameters were determined by extracting the virtual loading curve from the force-displacement and force-velocity hysteresis. In order to validate the model, extensive MR damper tests including single frequency and dual frequency tests were conducted on a material test machine. Uniquely, this model describes the amplitude and frequency dependent behavior of an MR damper using parameters that are independent of the displacement excitation amplitude. Second, in order to evaluate the dynamic behavior of the elastomer, a new elastomer modeling effort using five constant parameters is to be described on the basis of a detailed characterization of an elastomeric specimen. This physically motivated model consists of a non-uniform distribution of rate-dependent elasto-slide elements and a parallel linear spring. The elasto-slide element is used to emulate filler structure behavior, and the linear spring represents the remaining polymer stiff-

ness. Extensive tests including single frequency and dual frequency tests were conducted on an elastomeric specimen and a full scale linear stroke elastomeric lag damper using a material testing machine, and complex modulus method was used to characterize the elastomeric specimen and damper. The model parameters were determined using a virtual initial loading curve identified from single frequency force-displacement hysteresis cycles. Efficient numerical algorithms were developed to apply the elastomer model to modeling of force due to sinusoidal displacement inputs, as well as dynamic analysis. This model was applied in predicting forced response while the specimen was under slowly varying cyclic loading conditions. To analytically study the influence of a nonlinear elastomeric damper on the stability performance for a dynamic system, the elastomer model was incorporated into a one single degree of freedom dynamic system and the transient response was compared with the results using corresponding viscous damping. The non-uniform distributed rate-dependent elastomer model is applicable in complex loading conditions without any prior information, and the flexibility in determining distribution function provides a potential to improve the model and to apply the model to elastomers with different filler materials.

At this point of the research, a model for MR damper and a model for the elastomeric damper were validated. The next step was to combine them as two damper components to achieve fail-safe and controllable damping.

Using well established modeling and design procedures [35] developed and experimentally validated, a concentric bearing type MRFE damper is built by incorporating an existing MR damper into the inner chamber available in the baseline damper. The MRFE damper will be characterized in the laboratory using a single frequency and dual sinusoidal excitation. A fixture setup is de-

signed to hold the MRFE damper on a material testing machine such that the uniaxial motion of the loading actuator results in a shear deformation of the elastomer and a uniaxial MR valve translation through an MR fluid reservoir. Complex modulus and equivalent damping are used to characterize the MRFE damper. Performance predictions using quasi-steady nonlinear Bingham-plastic fluid flow analysis and elastomeric characteristic data are conducted as a basis for developing a comprehensive MRFE damper design code. On the other hand, MRFE damper design strategies are developed based on MR flow mode analysis. In addition, a snubber type MRFE lag damper for bearingless helicopter rotor was developed based on a baseline Comanche fluid-elastic damper. The detailed snubber design and experimental results can be found in Ref. [66].

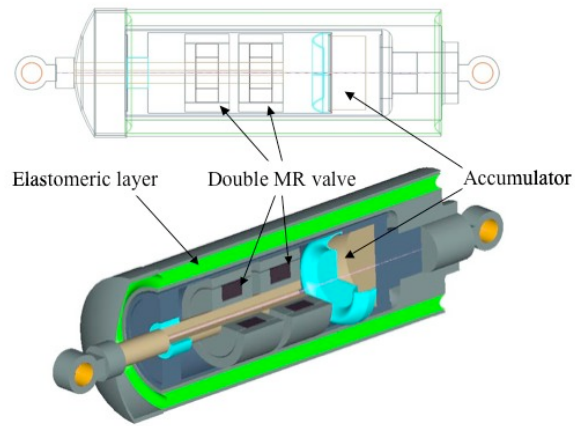
Based on the modeling approaches of the MR valve and elastomeric material, an MRFE time domain model is developed to describe the nonlinear behavior of the MRFE damper, especially the single and dual frequency hysteretic behavior. In this model, a distributed elasto-slide element is used to describe the behavior of the filled elastomer, and a field dependent elasto-slide is used to represent the behavior of the MR valve. Model parameters are determined by extracting the basic characteristics from the virtual initial loading curve. The unique advantage of the MRFE damper model developed in this study is that it can capture amplitude and frequency dependent behavior demonstrated by the MRFE damper and can be applied in any complex loading conditions, without resorting to either amplitude dependent or frequency dependent model parameters.

This dissertation is organized as follows to present the details of design and fabrication, dynamic tests, modeling process of the semi-active MRFE lead-lag dampers and conclusions of the current research.

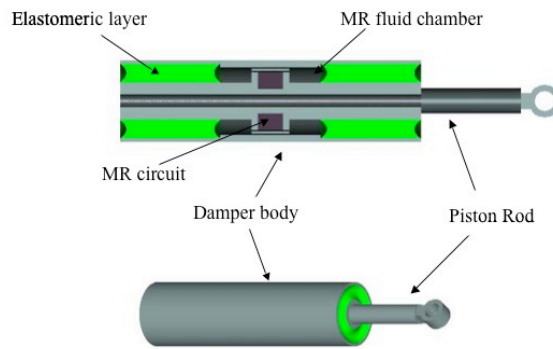
- Chapter 2: As a key element of the MRFE damper, basic characterization of the MR damper is described. To capture nonlinear behavior of the MR component, a new MR damper modeling approach is developed. A commercial truck seat damper is used as a benchmark damper to evaluate the MR model, and single frequency and dual frequency tests are conducted on the MR damper. The determination of model parameters using single frequency test results is described, and the fidelity of the modeling method is validated using both single and dual frequency test data.
- Chapter 3: Elastomer as the second key component of the MRFE damper is characterized and analyzed. To describe the nonlinear viscoelastic behavior of elastomers, a new time domain model for filled elastomers or elastomeric dampers is derived. Hysteresis behavior of an elastomeric specimen and a concentric bearing elastomeric lag damper under sinusoidal loadings is investigated. The determination of model parameters using single frequency test results is described for both elastomeric specimen and damper. The elastomeric model is validated by the correlation results under single and dual frequency loading conditions.
- Chapter 4: Based on quasi-steady MR damper analysis, the important design parameters of the MRFE damper are deduced. Equivalent damping characteristics of the MRFE damper under simulated sinusoidal lag motion is analyzed and validated using experimental test data. The important features to be modified to improve damper performance are also described.
- Chapter 5: The development of a concentric bearing type MRFE damper is described. The MRFE damper is characterized, and damping performance

of the MRFE damper is evaluated. A MRFE damper model is developed based on the MR and elastomer modeling approaches. Damper behavior predicted by the MRFE model is correlated with experimental results.

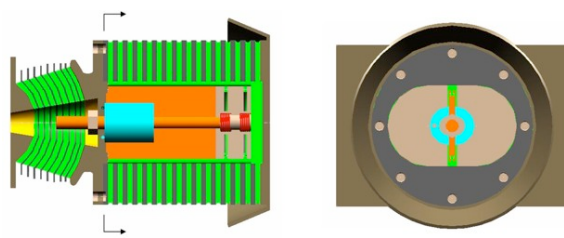
- Chapter 6: Conclusions of the present work are summarized and some recommendations for future work are discussed.



(a) MRFE Damper Configuration I



(b) MRFE Damper Configuration II



(c) MRFE Damper Configuration III

Figure 1.1: Possible MRFE Damper Configurations

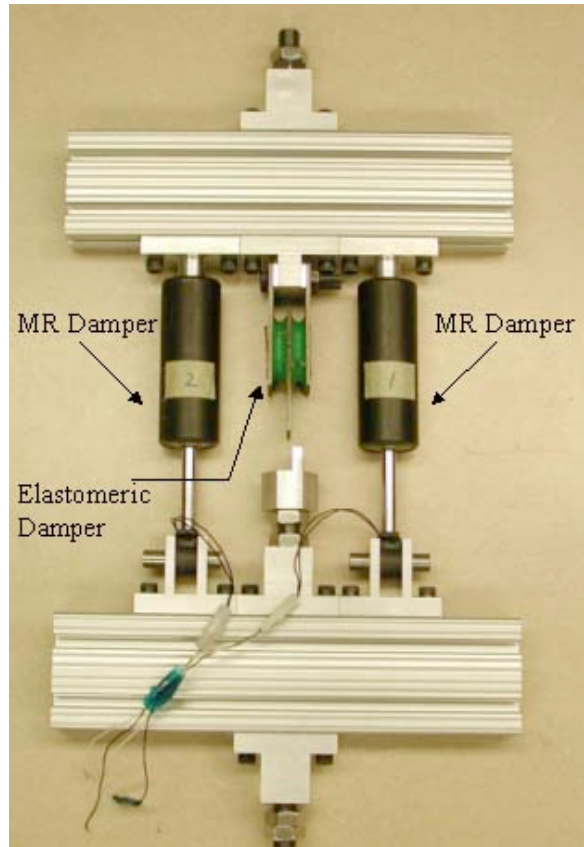


Figure 1.2: Preliminary MRFE Damper Test Setup

## Chapter 2

# Characterization and Modeling of a Magnetorheological Damper

Magnetorheological (MR) fluids are materials that change their rheological behavior in the presence of an applied magnetic field. The substantial field-induced yield stresses exhibited by MR fluids can change their apparent viscosity very rapidly with the application of magnetic field, and MR fluids can be easily activated using standard circuit board DC power sources. Although the quasi-steady behavior of the MR valve or damper can be described by a simple Poiseuille flow analysis as in Refs. [35, 72, 73], the hysteresis behavior demonstrated by the MR valve under a sinusoidal loading cannot be sufficiently captured by the analysis. Since the MR valve in the MRFE damper may operate in dynamic or transient loading conditions, prediction of dynamic behaviors are important to evaluate the performance of the MR valve.

Quasi-steady modeling using the Bingham-plastic constitutive model for MR fluids [33, 35] was extended to describe the behavior of the MR damper under oscillatory sinusoidal loading conditions [36, 37]. The nonlinear Bingham model can be represented by a viscous damping and a Coulomb friction element in

parallel, but it cannot describe the practical behavior of the progressive and continuous preyield behavior that is observed in the test data of MR dampers. On the other hand, the biviscous model [38, 39] and the Eyring-plastic model [40] utilize piecewise or continuous functions to represent preyield and postyield viscosity, but both biviscous and Eyring models cannot be used to describe the force-velocity hysteresis behavior due to preyield stiffness.

Generally, phenomenological modeling methods have been used to capture the preyield force-velocity hysteresis. The hysteretic biviscous model developed by Pang et al [36, 41] is a combination of several piecewise continuous functions, and the force-velocity hysteresis can be reconstructed using these functions. Choi et al [18] developed a single hysteretic function to describe the low speed hysteresis characteristics of an MR isolator, and this model was shown successfully in control applications. In addition, a polynomial model proposed by Choi *et al* [43] employed a polynomial to fit the force-velocity hysteresis loop. All of these models employ mathematical functions, instead of mechanical elements, to capture the force-velocity hysteresis. Alternatively, Kamath and Wereley [3] developed a mechanisms based nonlinear piecewise smooth viscoelastic-plastic model. This model consists of a viscoelastic element for preyield behavior and a viscous element for postyield behavior, between which a nonlinear shape function describes the smooth transition between preyield viscoelastic and postyield viscous behaviors. As an extension of the Bingham plastic model, Gamota and Filisko [44] proposed a model given by a Bingham model in series with a standard linear solid model. All of these models can describe the postyield and preyield behavior of MR dampers. However, these models only phenomenologically describe the hysteresis using some shape functions and do not reflect the physical

yield mechanism in the MR damper. As a result, this type of modeling leads to amplitude and frequency dependent model parameters. In order to implement the damper model, the excitation amplitude and frequency have to be known *a priori*, which is inconvenient when predicting the response under complex loading conditions.

An exception for hysteretic modeling is the Bouc-Wen model [45]. The Bouc-Wen model has proven to be successful in numerical modeling of a hysteretic system under random excitation. Based on the Bouc-Wen model, a generalized hysteresis model was proposed by Spencer et al [46]. The model parameters were determined to best fit the data including step response, constant voltage/random displacement and random displacement/random voltage, so the hysteretic behavior of the damper under step and random loading was predicted very well using this modified fourteen parameter Bouc-Wen model. However, the detailed relationship between model parameters and excitation amplitude and frequency was not shown. Also, the physical interpretation of the Bouc-Wen model parameters is tenuous at best, and the model structure is quite complicated. Thus, a simple and physically-motivated model is required to capture the nonlinear behavior of the MR damper using parameters that are independent of the excitation amplitude.

Based on the Bingham-plastic model, a physically motivated rate-dependent elasto-slide model is developed in this chapter to study the quasi-steady and dynamic behavior of the MR-fluid based damper. Instead of an ideal Bingham relationship between damping force and velocity, this time-domain model uses a rate-dependent slide in parallel with a viscous damping mechanism to emulate practical yield behavior of MR fluids and uses a stiff spring in series with the

slide to reflect the preyield stiffness. A method of identifying model parameters is introduced using MR damper single frequency hysteresis data. The model parameters are determined using virtual initial loading curves identified from the force-displacement and force-velocity hysteretic diagrams. A relationship between current controllable parameters and the corresponding current input is approximated during the process of parameter identification at different currents.

## 2.1 Experimental Characterization

In order to determine model parameters and evaluate the fidelity of the proposed rate-dependent elasto-slide model, dynamic tests with steady-state sinusoidal loading were conducted on two identical MR linear stroke dampers. A schematic of the nominal MR damper is shown in Figure 2.1. The hydraulic cylinder houses the damper piston, in which is mounted a magnetic circuit. At the base and inside the hydraulic cylinder is a nitrogen accumulator. The accumulator is used to compensate for changing rod volume in the hydraulic cylinder, as well as thermal expansion of the MR fluid, and to prevent cavitation on the low pressure side of the piston in the MR damper. The MR fluid in the damper flows through an annular gap in the piston head, where it can be activated by a current applied to the magnetic circuit.

The configuration of the test setup is shown in Figure 2.2. A DC power supply was used to provide current control during testing. The normal range of the applied current is between 0A and 1.5A, and the maximum applied voltage is 10V DC. An HP 8904A multi-function synthesizer was used to generate and sum the sinusoidal signals for dual frequency tests. The frequency range was

chosen appropriate for a helicopter rotor system at  $\Omega_{pri} = 7.5\text{Hz}$ , the baseline 1/rev frequency,  $\Omega_{lag} = 5\text{Hz}$ , the lag/rev frequency, and  $\Omega_{com} = 2.5\text{Hz}$ , a lower harmonic of lag/rev and 1/rev frequencies. An MTS 24.466kN (5000lbs) servo-hydraulic testing machine was used to apply the desired damper shaft sinusoidal displacement. A displacement LVDT sensor was used for displacement measurement and a load cell for measuring the force. The machine can be operated in two ranges for both displacement 127mm and 12.7mm (5in and 0.5in) and force 24.466kN and 2.4466kN (5000lbs and 500lbs). Fixtures and grips were designed to hold the damper in place. Single and dual frequency tests were conducted on the MTS machine at room temperature (25°C).

The steady-state dynamic tests for both MR dampers consist of single frequency and dual frequency tests. For single frequency tests, the shaft of the damper was excited using sinusoidal displacement at amplitudes from 0.25mm to 4mm and at three different frequencies of  $\Omega_{pri}$ ,  $\Omega_{lag}$  and  $\Omega_{com}$  respectively. At each excitation amplitude, the applied currents were in the range of 0-0.3A in increments of 0.1A. The single frequency force-displacement and force-velocity data were used to determine the model parameters and evaluate the fidelity of the model. For dual frequency tests, two dual frequency combination, 2.5Hz/5Hz and 5Hz/7.5Hz, were used to evaluate the adaptability of the model in multi-frequency loading conditions. The dual frequency experimental matrix is shown in Table 2.1.

During each test, the sampling frequency was chosen as 2048Hz, which is far above the required Nyquist frequency. Nominally, ten to twenty cycles of force and displacement data were measured for each test case. To reduce the noise of the sinusoidal displacement signal, a Fourier series was used to reconstruct

the input displacement. The reconstructed displacement signal was then differentiated to obtain the velocity data. The Fourier series expansion of the input displacement is

$$x(t) = \frac{x_0}{2} + \sum_{k=1}^{\infty} [X_{c,k} \cos(k\omega t) + X_{s,k} \sin(k\omega t)] \quad (2.1)$$

where

$$\begin{aligned} X_{c,k} &= \frac{\omega}{\pi} \int_0^{\frac{2\pi}{\omega}} x(t) \cos(k\omega t) dt \\ X_{s,k} &= \frac{\omega}{\pi} \int_0^{\frac{2\pi}{\omega}} x(t) \sin(k\omega t) dt \end{aligned} \quad (2.2)$$

For single frequency testing, any bias and higher harmonics were filtered, so that only the frequency of interest remained where  $\omega = \Omega_{pri}$ ,  $\Omega_{lag}$ , and  $\Omega_{com}$  respectively. The displacement is reconstructed using only the first harmonic as:

$$x(t) = X_c \cos(\omega t) + X_s \sin(\omega t) \quad (2.3)$$

For dual frequency testing, the HP 8904A multi-function synthesizer was used to generate and sum the sinusoidal signals for both frequencies. The general equation for the input dual displacement signal is written as

$$x(t) = A_{lag} \sin(\Omega_{lag} t) + A_{com} \sin(\Omega_{com} t) \quad (2.4)$$

and

$$x(t) = A_{lag} \sin(\Omega_{lag} t) + A_{pri} \sin(\Omega_{pri} t) \quad (2.5)$$

The signal is periodic with a frequency corresponding to the highest common factor of both harmonics, i.e., 2.5Hz. The displacement signal was filtered using  $\omega = 2.5\text{Hz}$  as the base frequency. The first three harmonics were needed to reconstruct the dual frequency displacement signal. Since the MR damper produces nonlinear damping force, the measured force was not filtered. However, to

reduce the offset in the measured force due to the presence of the accumulator, the measured bias force was subtracted using the bias term in the Fourier series of the force.

Typical force-displacement hysteresis data are shown in Figure 2.3(a), where the force-displacement diagram was obtained using a sinusoidal displacement excitation at  $\Omega_{lag} = 5\text{Hz}$  with an amplitude of 3.5mm. Four different currents of 0, 0.1, 0.2 and 0.3A were applied to the MR damper. From the force vs. displacement cycles, damping is proportional to the area enclosed by a force-displacement hysteresis cycle, which is the energy dissipated by the MR damper. The typical effect of the applied current shown in the hysteresis cycles is the increment of the steep area close to the zero velocity (shown at the maximum displacement) such that the enclosed hysteresis area is enlarged. This implies that the damping effect of the MR damper is obtained by the friction effect or yield process of the MR fluid in the flow valve inside the damper. Similarly, the force-velocity diagram of the MR damper shown in Figure 2.3(b) demonstrates a Bingham or yield behavior, and the force-velocity hysteretic behavior results from a preyield stiffness or compression effect.

In order to demonstrate the damping augmentation effect quantitatively, a standard linearization technique, equivalent viscous damping, is applied to the nonlinear MR damper data while under sinusoidal loading

$$x = X_0 \sin(\Omega t + \phi) \quad (2.6)$$

The analytical damping force,  $F(t)$ , is assumed proportional to the damper shaft velocity,  $\dot{x}(t)$ , as

$$F(t) = C_{eq}\dot{x}(t) \quad (2.7)$$

With experimental damper force data,  $f$ , the equivalent viscous damping,  $C_{eq}$ ,

is computed by equating the energy dissipated over a cycle,  $E$ , at frequency,  $\Omega$ , using

$$E = \oint f(t)dx = \int_0^{\frac{2\pi}{\Omega}} f(t)\dot{x}(t)dt \quad (2.8)$$

and equating the dissipated energy of the damper to that of an equivalent viscous damper:

$$C_{eq} = \frac{E}{\pi\Omega X_0^2} \quad (2.9)$$

where,  $X_0$  is the amplitude of the displacement excitation. Thus, the damping characteristic of the MR damper at different amplitudes and currents can be demonstrated using equivalent viscous damping as shown in Figure 2.4. Clearly, the equivalent viscous damping of the MR damper is a nonlinear function of excitation amplitude, which is different from one would expect for linear viscous damping. However, the significant advantage of the MR damper is that the equivalent damping can be varied over a wide range as the applied current is varied.

The equivalent viscous damping is a linear characterization method that can be used to determine the damping capacity of the MR damper, but it cannot be used to predict the nonlinear forced response of the MR damper. Therefore, a rate-dependent elasto-slide damper model is developed in order to capture the nonlinear damper behavior, and the model performance is evaluated by comparison between experimental and predicted damper response under varied loading conditions.

## 2.2 Evaluation of a Rate-dependent Elasto-slide Model

The proposed rate-dependent elasto-slide model (RDES) is shown in Figure 2.5, which is composed of a rate-dependent elasto-slide element to describe the yield behavior of MR dampers, a parallel postyield viscous damping and a parallel soft spring to reflect the stiffness effect of the accumulator. The composition of the model is similar to the Bouc-Wen model, but instead the Bouc-Wen element is replaced with a physically motivated elasto-slide mechanism. It will be shown that this simple elasto-slide element is appropriate for the yield behavior of MR fluid based dampers, and that the rate-dependent elasto-slide model captures most nonlinear characteristics of MR dampers.

While the MR fluid is characterized by the Bingham plastic model, a force-velocity relationship is derived on the basis of a flow mode damper. Since this ideal relationship does not include the effect of practical fluid bleed in the damper, the Bingham damper model cannot describe the transition behavior from preyield to postyield. Thus, extended from the Bingham model mechanisms, the rate-dependent elasto-slide element is physically interpreted. The numerical fulfillment of the model is discussed. A suitable slide function is found to avoid a stiff numerical problem. The identification procedure for the model parameters is also given in this section.

### 2.2.1 Rate-dependent slide

The quasi-steady behavior of MR dampers is well understood by the analysis using MR fluid constitutive model and damper geometry [35, 67, 72]. For a

flow mode damper with a steady shaft velocity, the damping force is developed because of the pressure drop through the annular gap within the cylindrical MR damper body. According to the quasi-steady flow analysis [35], the ideal relationship between damper force,  $F$ , and shaft velocity,  $v$ , is derived as

$$F = \frac{C_0}{(1 - \bar{\delta})^2 \left(1 + \frac{\bar{\delta}}{2}\right)} v \quad (2.10)$$

where,  $C_0$  is the Newtonian damping coefficient for the field-off MR damper, and  $\bar{\delta}$  is the nondimensional plug thickness, which is a function of yield force and shaft velocity. From Eq. 2.10, the ideal quasi-steady force-velocity plots are shown as dotted lines in Figure 2.6. Analytically, before the damper force reaches a certain yield force, the MR fluid in the valve of the damper cannot flow. Thus, there is an abrupt jump in force from preyield solid to postyield Newtonian flow at small velocities, and the yield force is a function of the applied field. It was shown in [25] that Eq. 2.10 can be approximated by a linear summation of a field controlled yield force and a postyield Newtonian force,

$$F = F_y + C_0 v \quad (2.11)$$

This is the Bingham plastic damper model. Since the approximation works best in the high speed post-yield region, the Bingham plastic model inherently cannot predict damper force accurately especially over the transition region from preyield to postyield.

The macro behavior of the damper predicted by both quasi-steady analysis and the Bingham-plastic damper model presents a rigid preyield region which is exactly the behavior of a Coulomb slide. However, the piston bleed or blow-by of fluids between the piston and cylinder in a practical MR damper results in a preyield slip between preyield and postyield phase in the force-velocity

curve. Thus, to render the Coulomb slide more applicable, a rate-dependent slide model can be used to describe the nonlinear damping behavior in the preyield or low velocity region. Taking numerical feasibility into consideration, a fractional power function of velocity is feasible to simulate both preyield and postyield behavior of the force-velocity curve, i.e.

$$N^* = N \left( \frac{v}{v_r} \right)^{\frac{1}{p}} \quad (2.12)$$

where,  $N$  is the field dependent yield force,  $p$  is a positive odd integer, and  $v_r$  is a constant reference velocity at which the slide transitions from the pre-yield region to the post-yield region. The force-velocity relationship described by the rate-dependent slide model combined with a post-yield viscous damping is shown as solid lines in Figure 2.6. Compared with the nonlinear Bingham-plastic model, the rate-dependent slide demonstrates significant improvement in describing the force-velocity relation over a broad velocity and yield stress range.

### 2.2.2 Elasto-slide model

In the above analysis, the MR fluid in the pre-yield condition is assumed rigid. However, due to the compressibility of the fluid, the MR fluid in the preyield regime behaves like an elastic solid such that the MR damper exhibits a strong force-velocity hysteresis at low velocity. Thus, the preyield stiffness must be considered in a physically motivated damper model. In the RDES model, the series combination of a stiff spring and the slide will be proven reasonable to reflect the preyield behavior of the MR fluid, and the coupling between the spring and the rate-dependent slide can be solved by efficient mathematical algorithms.

In order to demonstrate the efficiency of the elasto-slide model in describing

yield behavior of MR fluids, a Coulomb slide instead of the rate-dependent slide is used in series with a linear leading spring. The stiffness of the leading spring is denoted by  $k$ , and the maximum controllable yield force of the Coulomb or slip slide is  $N$ . Apparently, when the spring stiffness becomes large, the elasto-slide model behaves exactly the same as the nonlinear Bingham plastic model. When cycled between fixed deflection limits, the elasto-slide model has a force-deflection diagram similar to that shown in Figure 2.7. Upon initial loading, the spring force increases linearly with the applied displacement until it reaches the maximum slide yield force, i.e.

$$\begin{aligned} f &= kx, \dot{x} > 0, 0 \leq x \leq \frac{N}{k} \\ f &= N, \dot{x} > 0, x \geq \frac{N}{k} \end{aligned} \quad (2.13)$$

If the direction of loading is reversed after the MR fluid has yielded, the force-deflection relation will become

$$\begin{aligned} f &= N - k(A - x), \dot{x} < 0, A - 2\frac{N}{k} \leq x \leq A \\ f &= -N, \dot{x} < 0, x \leq A - 2\frac{N}{k} \end{aligned} \quad (2.14)$$

where  $A$  is the amplitude of the displacement excitation. An expression similar to Eq. 2.14 is obtained when the excitation reaches the minimum deflection and is reversed again so that  $\dot{x} > 0$ . This process continues until the excitation is stopped. The simulated force-displacement hysteresis by the elasto-slide model at two different amplitudes are shown in Figure 2.7, and the arrows on the solid line show the loading direction of the model. Compared with the experimental force-displacement hysteresis of the MR damper, the elasto-slide model captures the major characteristics of the MR fluids yield behavior under sinusoidal excitation except that the hysteresis around the maximum velocity cannot be described

by the Coulomb slide. The Coulomb slide is an approximation of real MR fluid yield behavior, and the amplitude of the excitation must be known as *a priori*. However, this problem can be easily solved if the Coulomb slide is replaced with a rate dependent slide.

Physically, the series combination of a spring and a rate-dependent slide can analytically describe the yield behavior of the MR fluid in the valve. Before an MR damper is subjected to excitation, the MR fluid in the flow gap consists of chain structures due to an applied magnetic field. Thus, it behaves like a elastic solid instead of a fluid. While the damper piston is excited by an initial displacement excitation, the spring force due to the elastic MR solid increases with displacement. At the same time, the movement of the piston induces the partial break-down of the chain structures and the piston bleed reduce the spring force. In this phase, the MR fluid flows like a plug. After all of the chain structures are broken, the MR fluid is totally yielded and the imagined spring is not extended any more such that the damper demonstrates a viscous damping behavior. As the loading is reversed, the direction of the MR flow is also reversed and a similar yield process is repeated.

In addition to the rate-dependent elasto-slide element, a viscous damping element is added in parallel in the RDES model since the postyield behavior of the MR damper is similar to a viscous damper. Meanwhile, a soft parallel spring is introduced to account for the effect of the stiffness of the accumulator in the damper. Thus, as shown in Figure 2.5, the MR damper can be represented by the mechanism-based rate-dependent elasto-slide model. The parameters in the model, including  $N$ ,  $v_r$  and  $p$  for the rate-dependent slide,  $k$  for the leading elasto-spring,  $c$  for viscous damping, and  $k_0$  for the accumulator stiffness, need

to be identified.

### 2.2.3 Identify model parameters using hysteresis data

As stated in the comparison of the elasto-slide model to the Bingham plastic model, the model parameters could be determined from the MR fluid and damper geometry data. On the other hand, when these data are not available, the model parameters can be identified to fit the predicted or modeled response to the experimentally measured response from either quasi-steady or dynamic tests. In this study, we take a system identification perspective, so that we use force-displacement and force-velocity hysteresis cycles obtained from the MR damper under single frequency sinusoidal loadings to identify the model parameters.

The analysis of the Coulomb elasto-slide showed that the initial loading curve from preyield to postyield phase can provide estimates of the yield force  $N$  and the preyield stiffness  $k$ . Therefore, the first step to determine the model parameters is to build a virtual initial loading curve from steady-state hysteresis cycle diagrams. Since the maximum force corresponds to the maximum displacement or zero velocity for a Coulomb friction slide, the virtual initial loading curve can be obtained from the force-displacement hysteresis by locating the damper force at zero velocity for each sinusoidal loading amplitude as shown in Figure 2.8(a). Thus, the effect of the viscous damping force is eliminated. The loading curve is easily optimized by an exponent function as

$$F_{dis} = N \left( 1 - e^{-\frac{k}{N}x} \right) + k_0x \quad (2.15)$$

from which the stiffness  $k + k_0$  is the slope of the loading curve at zero displacement,  $k_0$  is the slope of the postyield region of the loading curve, and  $N$

is the yield force. Since the slope of the loading curve at small displacements is sensitive to the hysteresis curve at smallest amplitude, the determination of the preyield stiffness,  $k$ , was also referred to the force-displacement slope around maximum displacement. Since the Coulomb behavior is an idealization of the RDES model, the virtual initial loading curve determined from the above method is revised by judiciously adjusting yield force in reference to the force-velocity hysteresis to include the effect of the rate-dependent slide and the post-yield viscous damping.

To determine parameters in the rate-dependent elasto-slide, i.e.  $v_r$  and  $p$ , and the postyield viscous damping,  $c$ , a force-velocity loading curve is constructed from experimental force-velocity hysteresis diagrams. As shown in Figure 2.8(b), the damper force at zero displacement is used to obtain the virtual loading curve since ideally the effect of the stiffness is excluded at zero displacement. Without the stiffness, it is known from the RDES model structure that the force-velocity relationship of the damper can be described by

$$F_{vol} = N \left( \frac{v}{v_r} \right)^{\frac{1}{p}} + cv \quad (2.16)$$

Thus, by optimizing the loading curve using this function and the determined yield force,  $v_r$ ,  $p$  and  $c$  can be identified. However, determination of  $p$  is a trade-off process. Physically, the index  $p$  should be large enough so that the postyield damping will not over-predicted, but a larger index will lead to a stiffer system mathematically. Consideration must be taken carefully into account in the choice of  $p$ .

A group of single frequency hysteresis cycles at different excitation amplitudes (0.25-4.0mm) is used to determine the model parameters at a fixed frequency and applied current. The model parameters were determined independently at three

different frequencies, 2.5Hz, 5Hz and 7.5Hz, and at four different currents, 0.0A, 0.1A, 0.2A and 0.3A. Since the damping mechanism for an MR damper is mainly due to the yield process of the MR fluid, the model parameters demonstrate weak dependence on three frequencies. In a moderate frequency range, the model parameters are fixed by an averaging process. The dependence of the parameters on the applied current was also studied. Two major parameters,  $N$  and  $k$ , are a function of current as shown in Figure 2.9. The modeling results for two MR damper demonstrate the same trend as applied current changes from 0A to 0.3A. The yield force increases sharply with the applied current since the magnetic field is not saturated yet. This result is consistent with the result in Ref. [77]. Comparatively, the preyield stiffness varies much slowly with applied current. As the applied current increases, the preyield stiffness converges to a constant value. Since the other four parameters,  $k_0$ ,  $v_r$ ,  $p$  and  $c$ , are not sensitive to the variation of the current, these parameters are fixed at an average value.

The resulting modeling parameters are given in Table 2.2. Note that the field-off yield force is not zero, and it can be interpreted by the effect of the residual magnetization in the MR valve and the friction of the damper assembly. Since the rate-dependent elasto-slide model is a physically motivated model, the determination of model parameters, especially for  $N$ ,  $k$ ,  $c$  and  $k_0$ , is a process to capture the relationship between damper mechanism and damper behavior. Either quasi-steady or dynamic test data can be used to evaluate the model parameters. The method for parameter determination used in this study is only an option, and it does not require fitting the hysteresis response of the model to the experimentally measured response.

## 2.3 Model Validation

Since the rate-dependent elasto-slide model is a time domain model, it can be used for both quasi-steady and dynamic analysis. In this section, the numerical implementation of the model is developed, and the quasi-steady and dynamic modeling results are validated by the experimental data.

### 2.3.1 Numerical fulfillment of the model

Numerically, in the rate-dependent elasto-slide model, the internal displacement  $x_0$  of the rate-dependent slide is a coupling variable between the elastic stiffness and the slide. For a rate-dependent elasto-slide element as shown in Figure 2.5, as displacement loading,  $x$ , is applied, the resistant force of the elasto-slide element is given by

$$F = k(x - x_0) = N \left( \frac{\dot{x}_0}{v_r} \right)^{\frac{1}{p}} \quad (2.17)$$

The coupling displacement,  $x_0$ , is given by

$$\frac{\dot{x}_0}{v_r} = \left[ \frac{k}{N} (x - x_0) \right]^p \quad (2.18)$$

This is a typical well-posed initial-value problem, and numerical solution for this differential equation can be obtained given an initial condition. The simplest way to guarantee a stable solution for stiff initial-value problems is to adopt a predictor-corrector approach with the corrector iterated to convergence (PECE) [79]. In this application, the numerical algorithm for Eq. 2.18 is based on the Adams-Bashforth four-step method as predictor and one iteration of the Adams-Moulton three-step method as corrector, with the starting values obtained from the Runge-Kutta method of order four [79]. In accordance with the ratio of

yield force and stiffness  $\frac{k}{N}$  in current MR damper and an appropriate choice of  $p$ , a stable and fast solution can be given by the Adams-Bashforth-Moulton method using limited time steps. Including the postyield viscous damping and accumulator stiffness, the total MR damper model force is given by

$$F^{MR} = k(x - x_0) + c\dot{x} + k_0x \quad (2.19)$$

In addition, the model response can be solved using MATLAB ODE solver. Since the internal velocity,  $\dot{x}_0$ , is the function of internal displacement,  $x_0$ , and loading displacement,  $x$ , as shown in Eq. 2.18, the internal displacement can be solved using ODE23 and this first-order state-space equation, and the model force is further developed by Eq. 2.19. Similarly, while the MR damper is incorporated in a mass-spring system with damping, the motion of equation of the system is transferred to the first-order state-space form and the system free vibration and forced response can be obtained using ODE solver. For instance, a 1-DOF mass-spring system with an MR damper can be expressed in state space form as

$$\begin{aligned} \dot{x} &= \dot{x} \\ \ddot{x} &= \frac{F(t)}{M} - \frac{K}{M}x - \frac{1}{M} [k(x - x_0) + c\dot{x} + k_0x] \\ \dot{x}_0 &= \left[ \frac{k}{N}(x - x_0) \right]^p v_r \end{aligned} \quad (2.20)$$

where,  $M$  and  $K$  are the mass and spring of the system respectively, and  $F(t)$  is a forced loading on the system. Thus, given a initial condition, the system response will be easily solved. Using the same ODE solver, the RDES model can also be applied in the MATLAB Simulink program such that control simulations using MR damper can be easily realized.

### 2.3.2 Experimental validation

Since the RDES model is a time-domain model, the quasi-steady and steady-state hysteretic modeling results are used to validate the model. For quasi-steady study, the model response is calculated while the damper model is applied by displacement loading with a constant velocity. Figure 2.10 shows the analytical damper force under varied velocities and applied currents in comparison with the experimental data. The experimental data is provided by the Lord's damper performance data sheet, in which the offset force due to the accumulator is excluded. As shown in the figure, the damper force due to a steady shaft velocity predicted by the RDES model demonstrates similar field-dependent characteristics demonstrated by the experimental result.

It is more important to understand the damper behavior while the damper is applied by sinusoidal loadings since the damper is mainly used in a dynamic system to dissipate energy. Single frequency and dual frequency experimental results are used to evaluate the fidelity of the rate-dependent elasto-slide model. For single frequency data, modeling and experimental results are compared using both force-displacement and force-velocity hysteresis cycles. Figure 2.11 and 2.12 show the force-displacement and force-velocity hysteresis at 5Hz. The applied current is 0A and 0.3A respectively. Clearly, the modeling results correlate very well with the experimental results, and especially the proposed model captures the amplitude-dependent damping behavior of the MR damper. The main reason for irregular curve at upper-left and lower-right corner of the experimental force-displacement diagram is due to the loose fit of the insert pin connection between the MR damper and the fixture connected to the material testing machine. Similarly, the single frequency modeling results at 2.5Hz are shown in

Figure 2.13 and Figure 2.14, and the modeling results at 7.5Hz are shown in Figure 2.15 and Figure 2.16. Both figures show that the rate-dependent elasto-slide model can predict the damper response very well in a moderate frequency range.

For dual frequency data, the force-displacement diagram is used to evaluate the MR damper model. The modeling and experimental results at various combinations of dual frequency amplitudes and currents are shown in Figure 2.17 and Figure 2.18. The modeling results for combination of 2.5Hz and 5Hz are shown in Figure 2.17, where  $A_{lag}$  is the amplitude of the sinusoidal signal at 5Hz and  $A_{com}$  is the amplitude at 2.5Hz. There are six combinations of amplitudes for  $A_{lag}$  and  $A_{com}$ , and the results at two different currents demonstrate controllability of the MR damper. The dual frequency data at 7.5Hz and 5Hz are shown in Figure 2.18. The correlation results in both figures show that the rate-dependent elasto-slide model performs quite well in predicting the dual frequency behavior at a broad amplitude and frequency range.

The fidelity of the rate-dependent elasto-slide model over a broad amplitude and moderate frequency range is justified by the good correlation with experimental single and dual frequency test data. Since the proposed model is a time domain model, it also can be used to predict damper behavior under quasi-steady or complex dynamic loading conditions. Especially, while the exact relation between model parameters and the applied current is known, the damper model is capable of predicting the behavior of the MR damper for a continuously controlled magnetic field.

## 2.4 Conclusion

A rate-dependent elasto-slide (RDES) model for a linear stroke MR damper was developed. The MR damping mechanism was developed using the Bingham model of MR fluids and the parallel plate assumption. The relationship between model parameters and damper mechanisms was studied. The model parameters were determined using identified virtual loading curves from force-displacement and force-velocity hysteresis data. A stable numerical method was chosen to predict the model response under various loading conditions. The predicted forced response correlated very well with the single and dual frequency experimental results. Significantly, the nonlinear amplitude dependent behavior of the MR damper was described by this six constant parameters model. The RDES model can be used in a variety of applications such as initial or forced response analysis of the system using MR dampers and a wide range of proposed control strategies dealing with the MR damper. The modeling result is well matched with the experimental data. Significantly, this modeling approach captures nonlinear amplitude and frequency dependent behavior of MR dampers using constant model parameters which can be determined by the properties of the MR fluids and damper geometry data.

Apparently, the MR damper behavior is dominated by damping effect contributed by a preyield elasto-slide mechanism and a postyield viscous damping. As a counterpart, a filled elastomer is a typical visco-elastic material, and can provide fail-safe stiffness and damping. Similar friction behavior due to the intersection of the cross link in the material leads to the damping effect of the elastomer. In the modeling approach for the MR behavior, the elasto-slide element is used to capture the friction effect due to the yield behavior of the

MR fluids, and thus the elasto-slide concept can also be used in the elastomeric modeling effort which will be described in the next chapter.

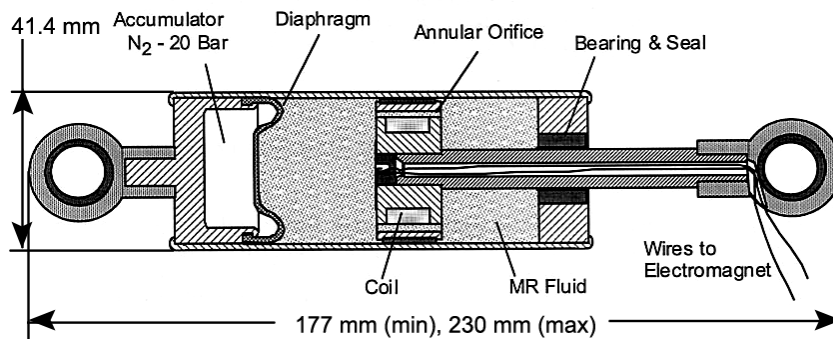


Figure 2.1: Schematics of an MR Damper

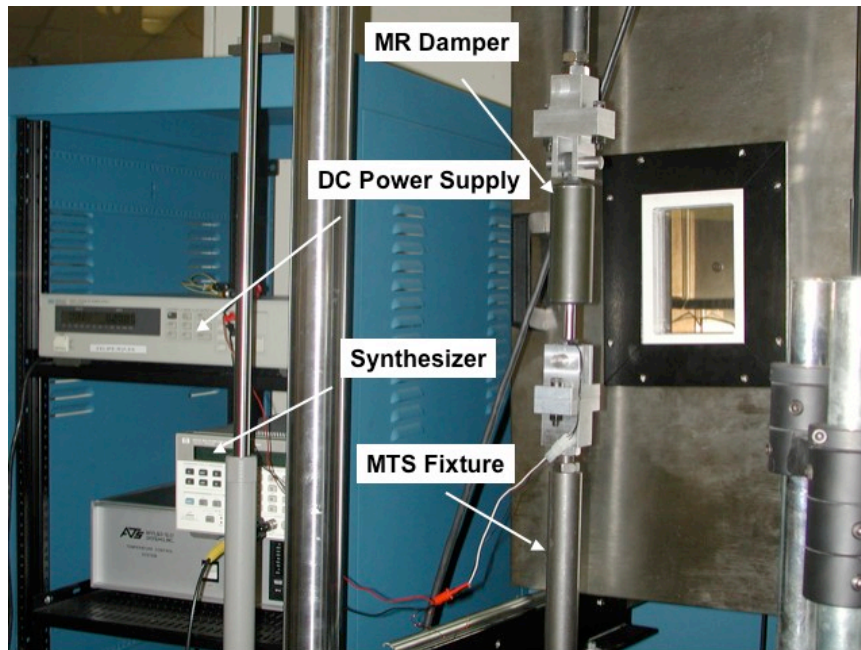
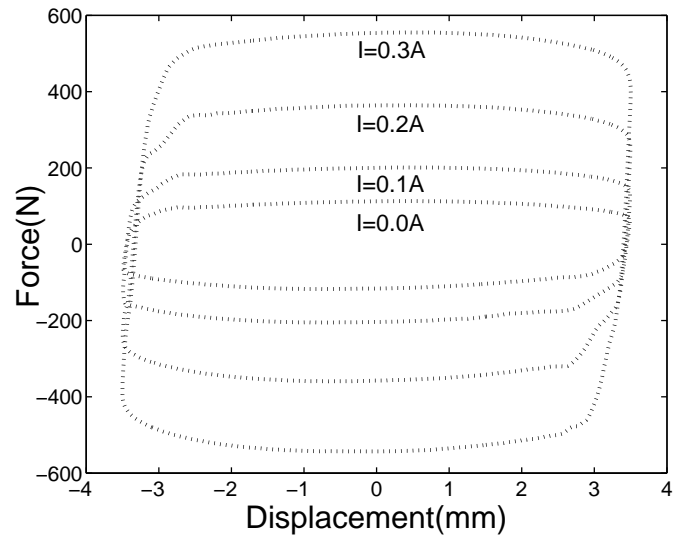


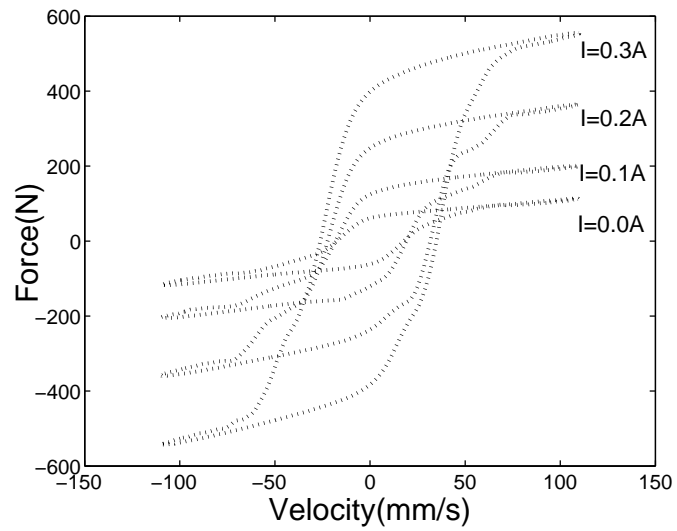
Figure 2.2: Test Setup for MR Damper

Table 2.1: Dual Frequency Test Matrix

|           |       |     |       |       |            |
|-----------|-------|-----|-------|-------|------------|
| 2.5Hz\5Hz | 0.5mm | 1mm | 1.5mm | 2.5mm | Current(A) |
| 0.5mm     | x     | x   | x     | x     | 0-0.3A     |
| 1.0mm     | x     | x   | x     | x     | 0-0.3A     |
| 1.5mm     | x     | x   | x     | x     | 0-0.2A     |
| 7.5Hz\5Hz | 0.5mm |     | 1.5mm | 2.5mm | Current(A) |
| 0.5mm     | x     |     | x     | x     | 0-0.2A     |
| 1.0mm     | x     |     | x     | x     | 0-0.2A     |



(a) Force-Displacement Diagram



(b) Force-Velocity Diagram

Figure 2.3: Hysteresis Cycles for MR Damper

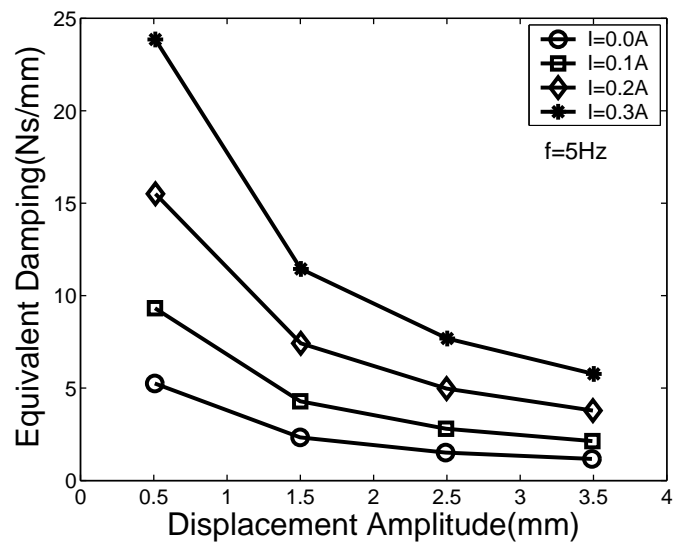


Figure 2.4: Linear Damping Characterization of the MR damper

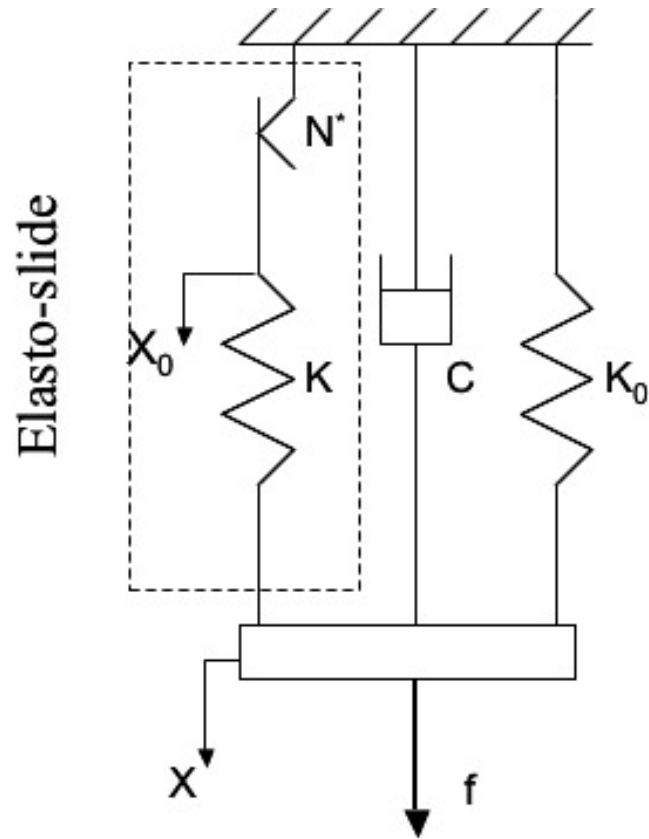


Figure 2.5: Rate Dependent Elasto-slide Model

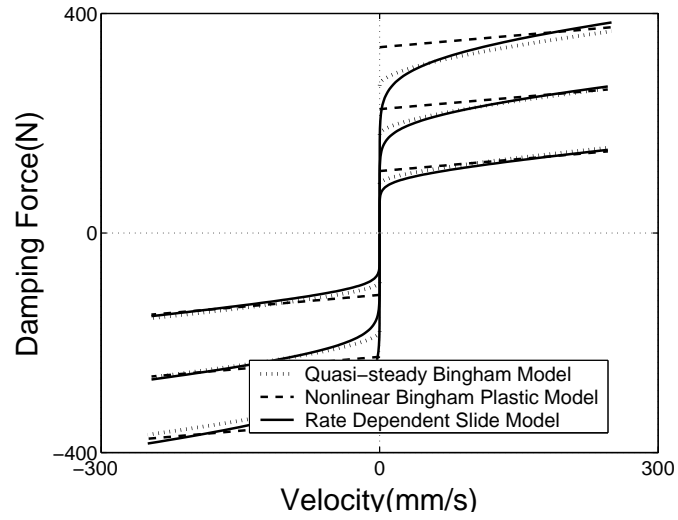


Figure 2.6: Quasi-Static Force-Velocity Relationship Predicted by MR Models

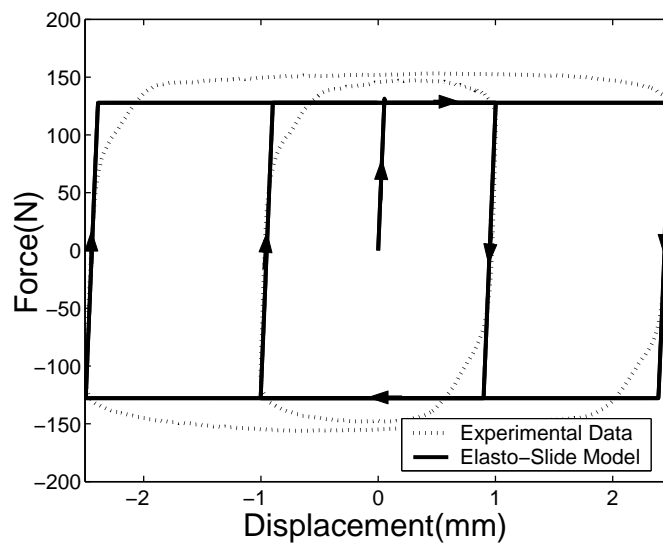
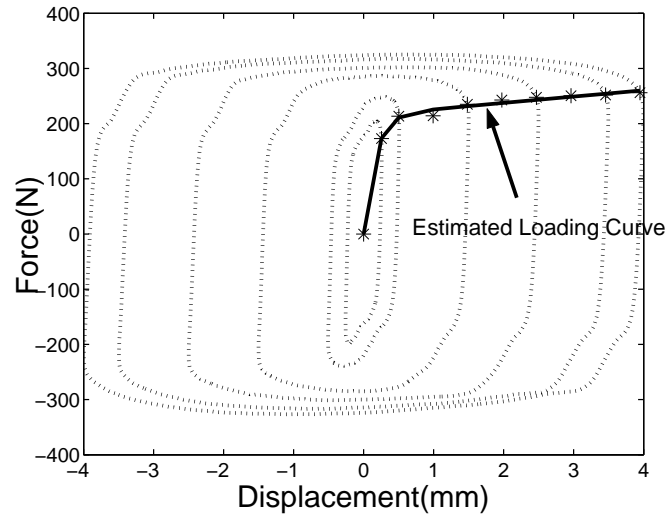
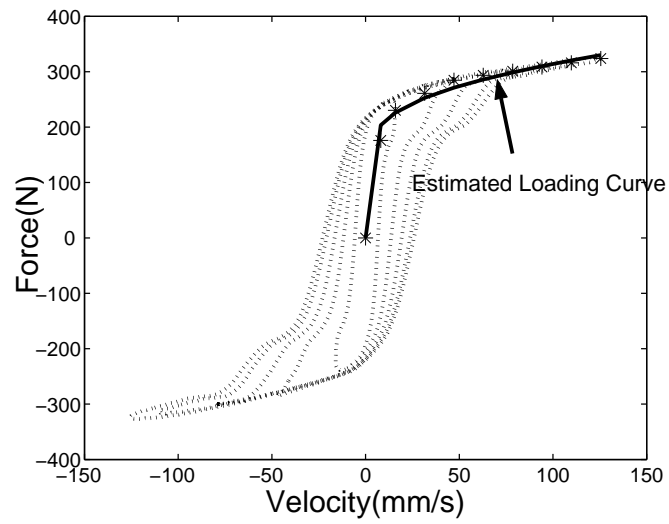


Figure 2.7: Hysteresis Behavior of an Elasto-slide Model

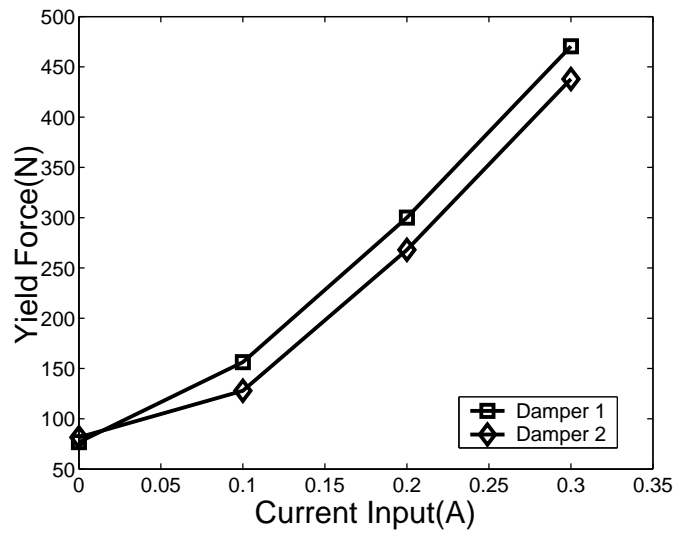


(a) Force-Displacement Diagram

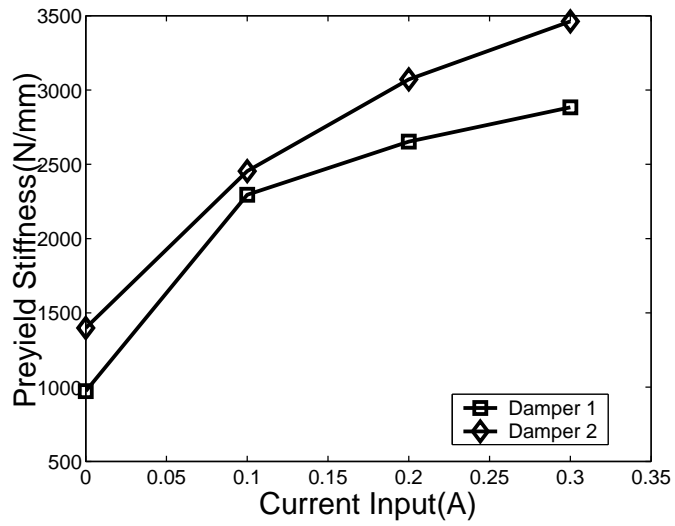


(b) Force-Velocity Diagram

Figure 2.8: Determined Initial Loading Curve



(a) Yield Force



(b) Preyield Stiffness

Figure 2.9: Model Parameters (Yield Force and Preyield Stiffness) as a Function of Current

Table 2.2: Model Parameters

| Parameter    | Value   | Current(A) |
|--------------|---------|------------|
| N(Newton)    | 76.75   | 0          |
|              | 470.48  | 0.3        |
| k(N/mm)      | 973.13  | 0          |
|              | 2883.35 | 0.3        |
| $c$ (N*s/mm) | 0.25    |            |
| $k_0$ (N/mm) | 3       |            |
| $v_r$ (mm/s) | 50      |            |
| n            | 7       |            |

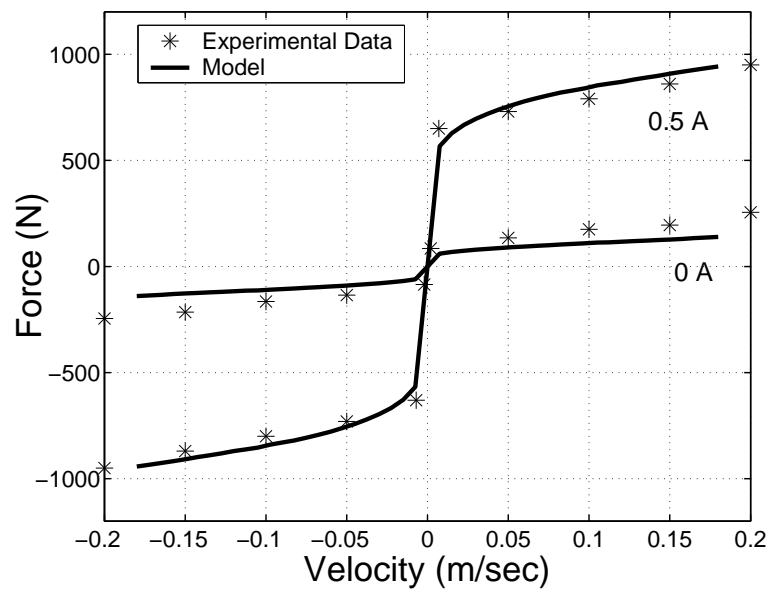
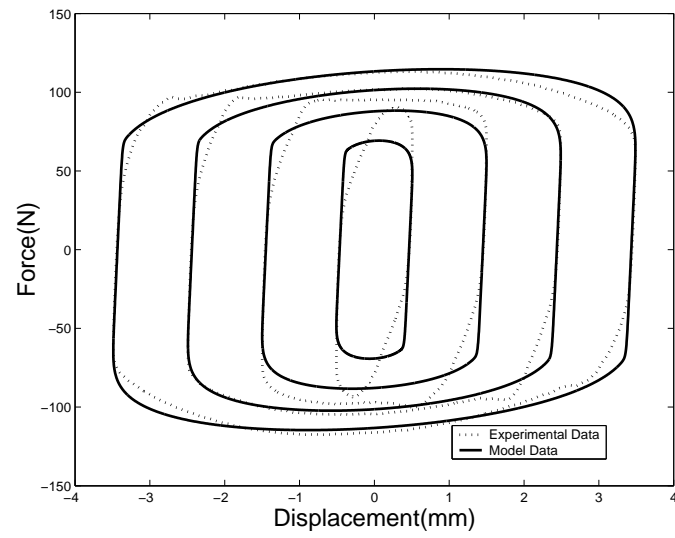
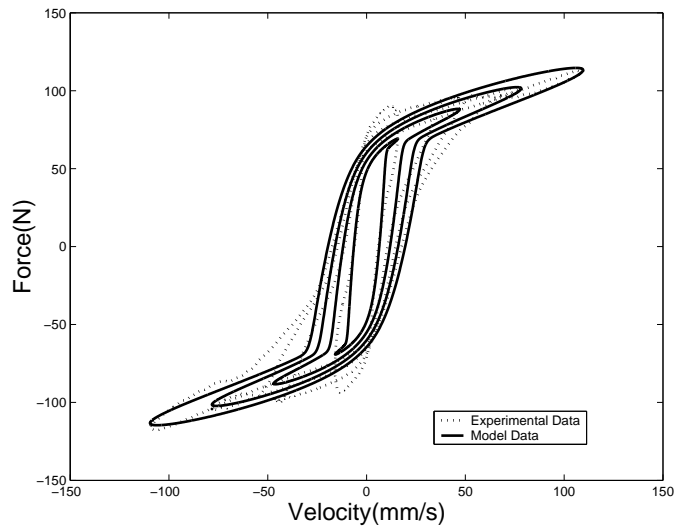


Figure 2.10: Quasi-steady Behavior of the Model

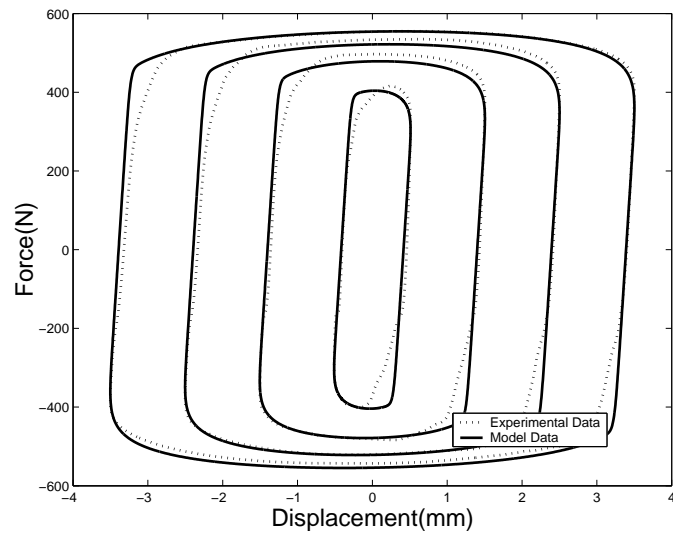


(a) Force-Displacement Diagram

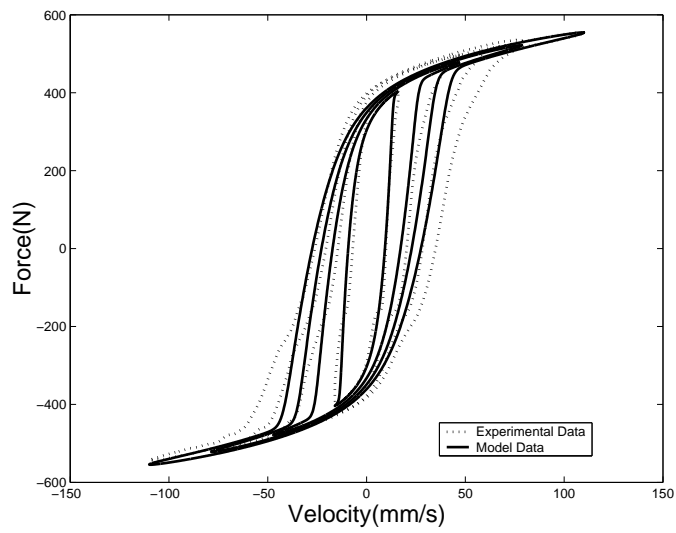


(b) Force-Velocity Diagram

Figure 2.11: Model Fit at 5Hz and 0A

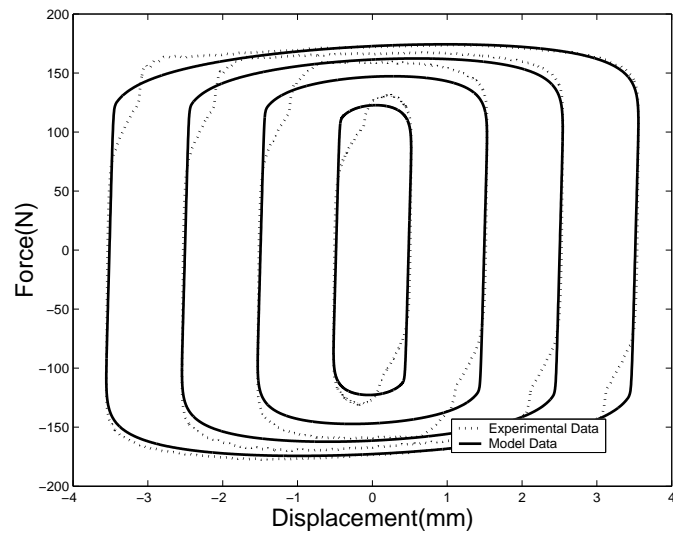


(a) Force-Displacement Diagram

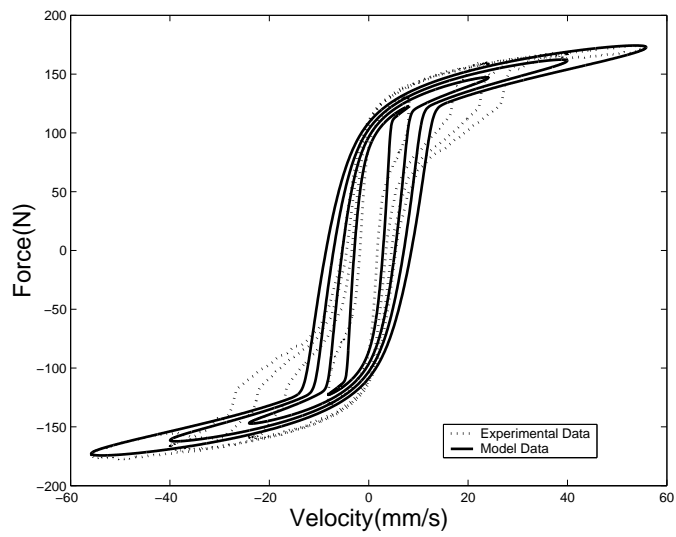


(b) Force-Velocity Diagram

Figure 2.12: Model Fit at 5Hz and 0.3A

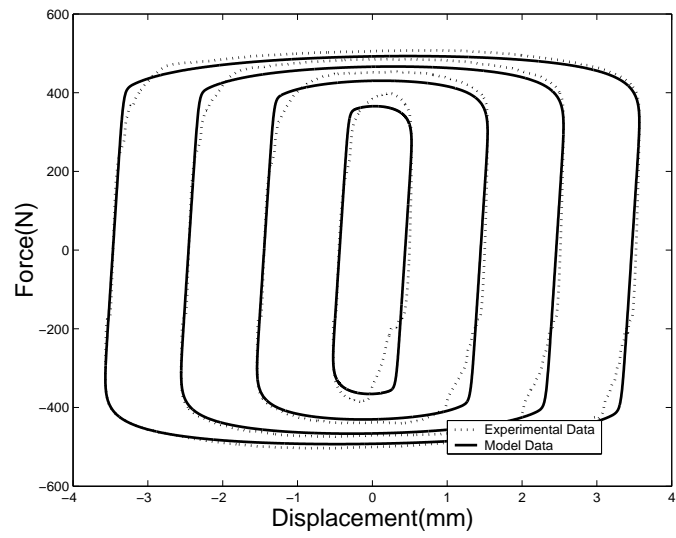


(a) Force-Displacement Diagram

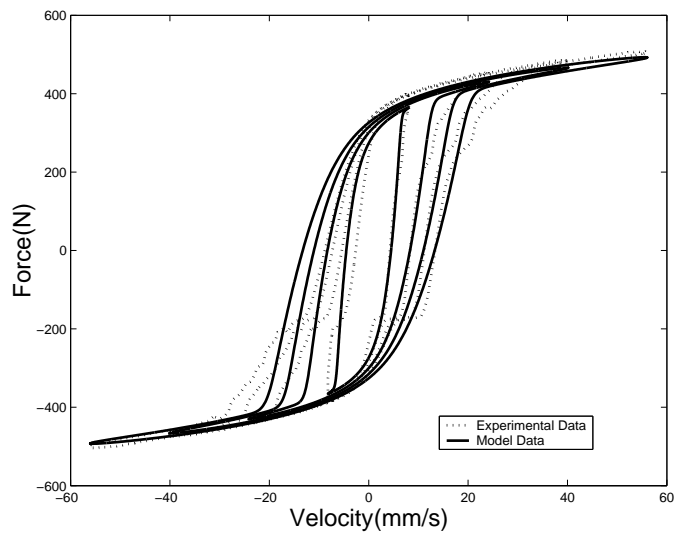


(b) Force-Velocity Diagram

Figure 2.13: Model Fit at 2.5Hz and 0.1A

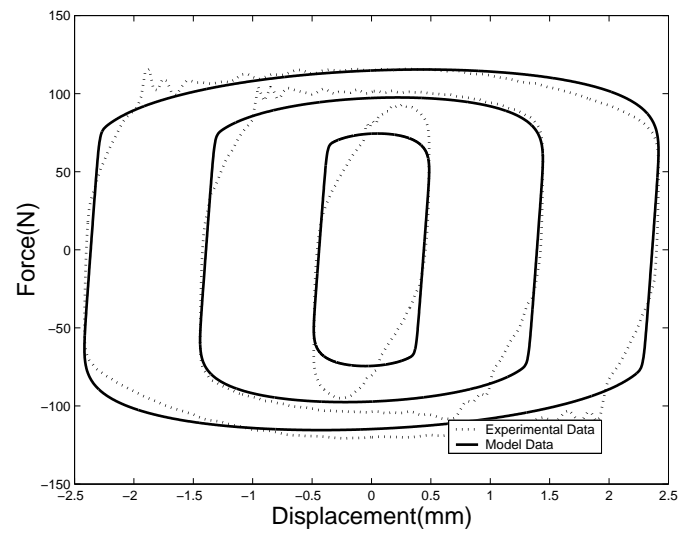


(a) Force-Displacement Diagram

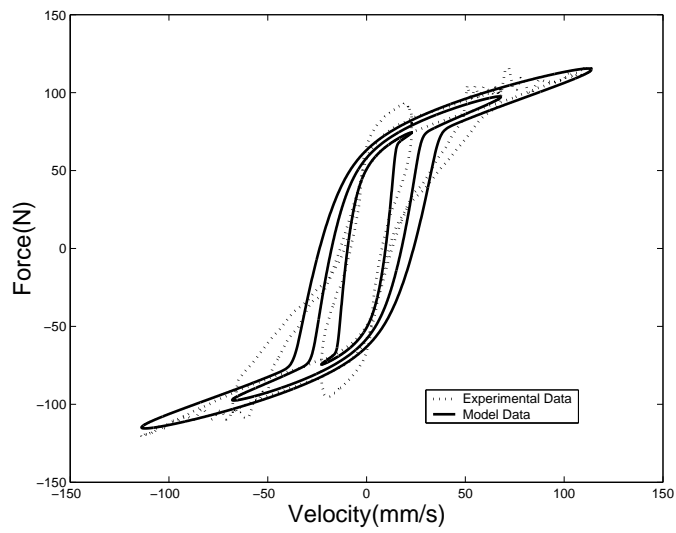


(b) Force-Velocity Diagram

Figure 2.14: Model Fit at 2.5Hz and 0.3A

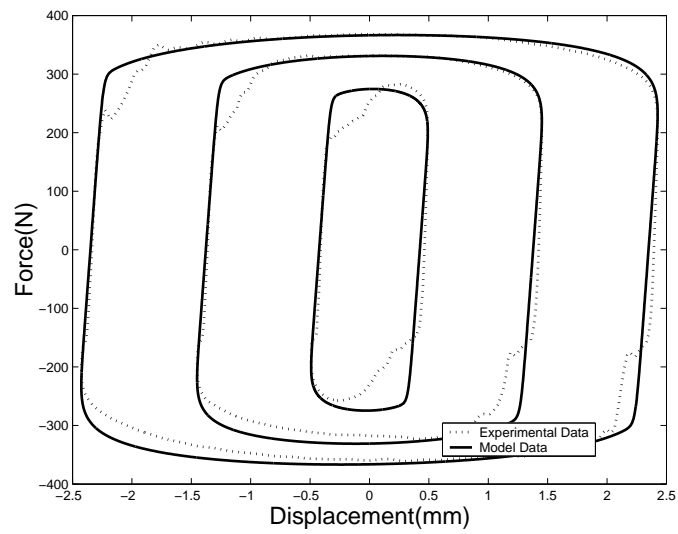


(a) Force-Displacement Diagram

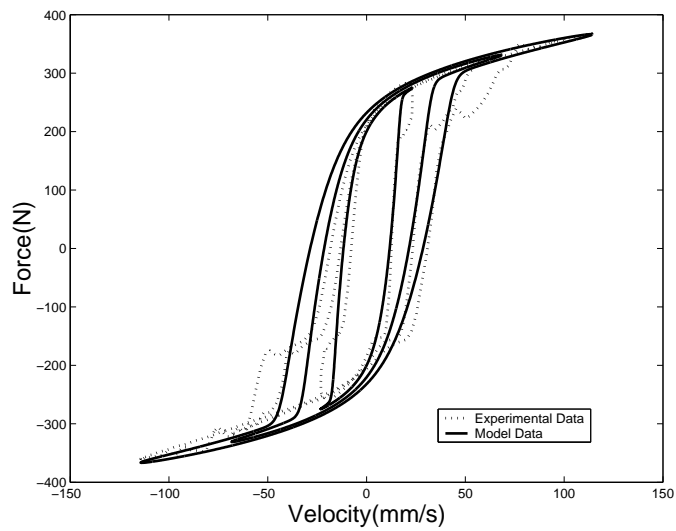


(b) Force-Velocity Diagram

Figure 2.15: Model Fit at 7.5Hz and 0A



(a) Force-Displacement Diagram



(b) Force-Velocity Diagram

Figure 2.16: Model Fit at 7.5Hz and 0.2A

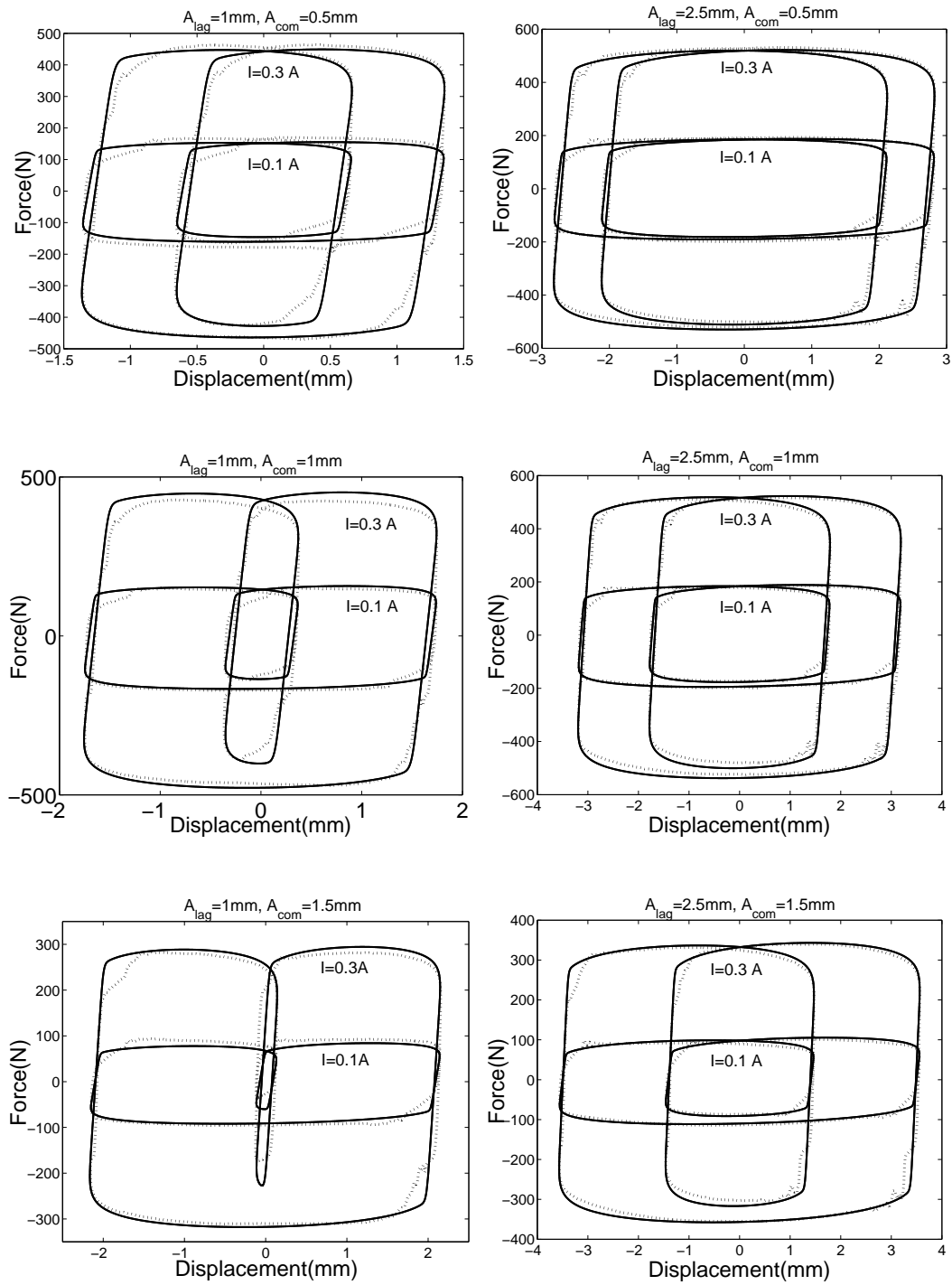


Figure 2.17: Dual Frequency Modeling at 5.0Hz and 2.5Hz

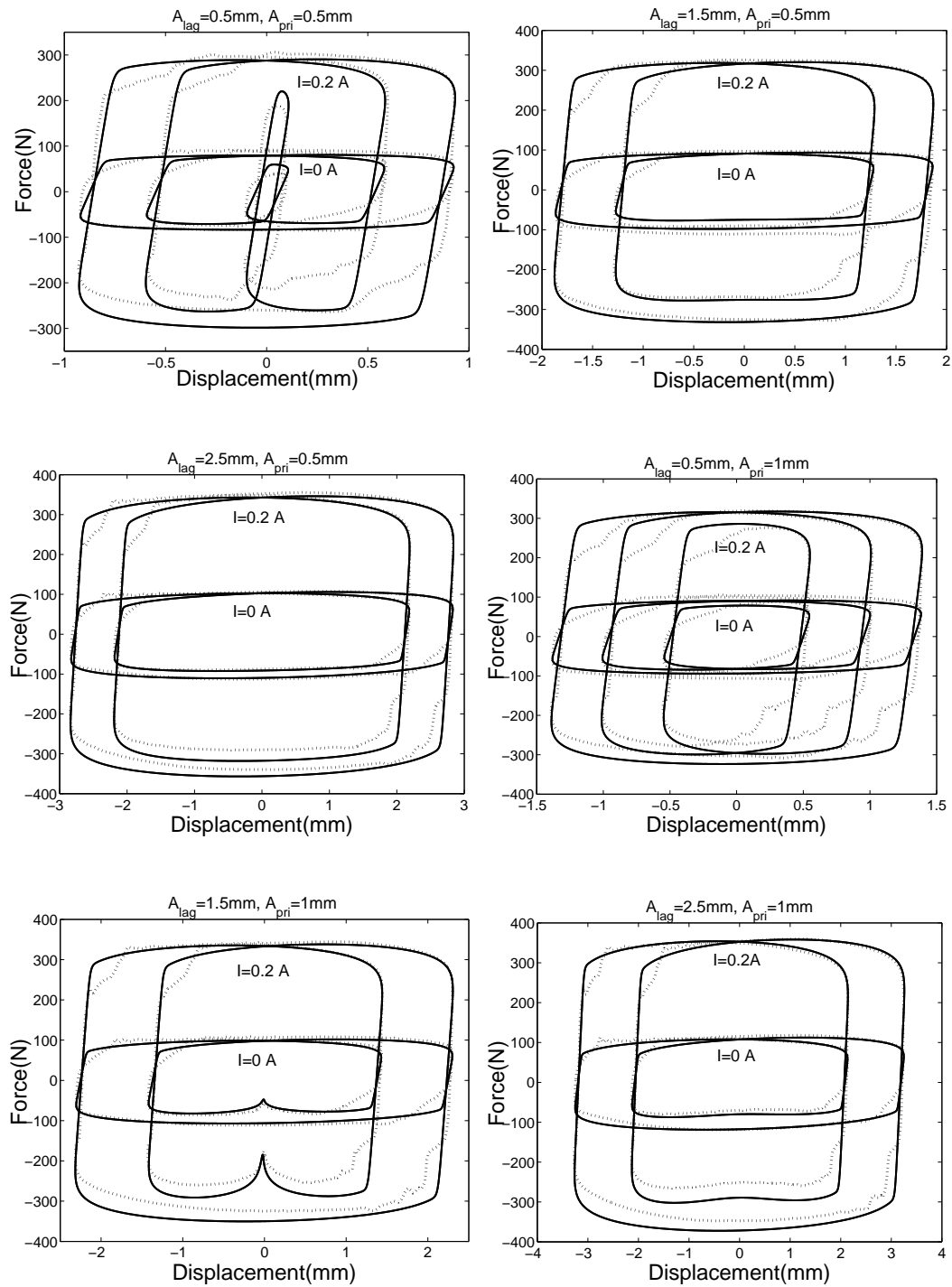


Figure 2.18: Dual Frequency Modeling at 5.0Hz and 7.5Hz

## Chapter 3

# Characterization and Modeling for Elastomeric Materials

As a major component of the MRFE damper, filled elastomer can provide damping and stiffness. The elastomer has proven to be efficient for damping augmentation due to their simple design, low weight and high reliability. However, filled elastomeric materials exhibit significant nonlinearities, especially amplitude dependent and frequency dependent behavior [48]. A precise analytical model is necessary to describe the nonlinear behaviors of an elastomeric damper and to determine the dynamic characteristics when the elastomer is applied in an MRFE damper.

Since the complex modulus method is successful in characterizing viscoelastic materials under harmonic excitation, early modeling efforts focused on linearization using complex moduli at a given frequency, where the storage modulus is a measure of the energy stored over a cycle and the loss modulus is measure of the energy dissipated over a period. This model can be represented as a spring and a dashpot in parallel (Kelvin chain). The complex modulus is a linearization method in the frequency domain which represents the nonlinear force

vs. displacement hysteresis loop with an equivalent ellipse, and is only applicable to steady harmonic forced response analysis. For nonlinear elastomeric materials, the complex modulus is also amplitude dependent. Some researchers extended the basic Kelvin chain to a more complicated mechanism-based modeling approach to describe the nonlinear behavior of elastomers. Felker *et al* [12] developed a nonlinear complex modulus model based on one single Kelvin chain, in which the spring force was a nonlinear function of the displacement, and the damping force was a nonlinear function of displacement and velocity. This model was used to describe the amplitude dependent moduli and to study dual frequency damper motions. In order to display basic behavioral characteristics, such as creep and relaxation, a viscoelastic solid can be represented as a spring in series with Kelvin elements (if one Kelvin element is used, it is called a Zener model [49]). Gandhi and Chopra [50] developed a nonlinear viscoelastic solid model in which a nonlinear leading spring was used in series with a single linear Kelvin chain. Using this model, the variation of the analytical complex moduli with different amplitudes matched closely with experimental data. The parameters in these models were identified using amplitude-dependent complex modulus data, and these models cannot be used to capture the nonlinear hysteresis behavior of elastomers. Kunz [51] similarly used a nonlinear Kelvin chain to capture the nonlinear hysteresis behavior of an elastomeric damper. In this model, the stiffness was expressed as a fourth order polynomial function of displacement, and the damping was described by a second order polynomial function of velocity. Though it can predict the harmonic damper force rather well, this approach is only applicable for a particular amplitude and frequency. In the model developed by Tarzanin *et al* [52], the total damper force was rep-

resented by a nonlinear spring force and a nonlinear Coulomb friction damping force. This model was based on single frequency data and was used to match the value of energy dissipation per cycle. However, a sudden jump in damper modeling force was shown when velocity changed sign, which was unrealistic. Panda *et al* [24] replaced the Coulomb friction damping element with a variable friction damping element whose force was calculated based on the peak displacement of excitation when the velocity was zero. This model correlated well with the experimental hysteresis data, but the effectiveness of this model over a range of amplitudes and frequencies suitable for helicopter lag dampers has not been demonstrated in the literature. In a recent study, Krishnan [53] developed a model which consisted of a linear Kelvin chain and a parallel cubic spring element. Snyder [37] improved this model by adding an elasto-slide element. Both models were developed to capture nonlinear elastomeric damper hysteresis cycles, but the model parameters were still amplitude and frequency dependent.

On the other hand, some elastomeric models were developed using internal variable or nonlinear integral equations. Strganac [55] used a stress shift function to formulate a nonlinear time domain model for elastomers, but the nonlinear integral formulation in the model was difficult to implement in traditional aeromechanical analysis. Lesieutre and Bianchini [56] developed the anelastic displacement field (ADF) method to describe the frequency-dependent behavior of linear materials. It was based on the notion of scalar internal variables or augmenting thermodynamic fields (ATF) [57] that described the interaction of the displacement field with irreversible processes occurring at the materials level. In the ADF approach, the effects of the thermodynamic processes were focused

on the displacement field which consists of both elastic and anelastic parts. The anelastic part may be further subdivided to consider the effects of multiple relaxation processes. Although there is no explicit physical interpretation when multi-anelastic elements are involved, one single ADF model is mechanically analogous to the Zener model. In order to capture the characteristic nonlinear behavior of elastomeric materials, Govindswamy *et al* [58] developed a nonlinear ADF model, in which the linear ADF parameters were replaced with nonlinear terms. The model captured the variations of the complex modulus with amplitude fairly well but did not match the strain-stress hysteresis successfully. Therefore, other functional forms for the ADF parameters were called for to improve hysteresis loop predictions. Brackbill *et al* [59] improved the nonlinear ADF model by adding rate independent nonlinearity, in which friction-damping and linear-spring elements in parallel with the baseline nonlinear ADF model were used to provide additional amplitude dependent relaxation behavior. As many as sixteen parameters were used to construct the model. Although the complex moduli were fitted well along amplitude and frequency ranges, nonlinear stress time histories could still be improved. Moreover, the parameter determination process was difficult because some parameters were chosen by empirical observation. In a recent study, Ramrakhyani *et al* [60] developed an ADF based model containing nonlinear fractional derivatives and frictional elements. This model used eight parameters instead of sixteen parameters to capture the amplitude-dependent and mild frequency-dependent modulus. However, it did not improve prediction of the force response, and the complexity in determining model parameters is still great.

Generally, most existing modeling efforts are based on the viscoelastic as-

assumption for elastomeric characteristics. However, an elastomeric damper usually demonstrates tribo-elastic behavior [48] such that those damper models using linear or nonlinear Kelvin chain combinations cannot capture the elastomeric behavior in reality. Either the model parameters are amplitude dependent or the model poorly describes the hysteretic behaviors of an elastomeric damper. Although in some modeling efforts the Coulomb or friction damping was used to describe the rate-independent damping behavior significantly demonstrated by the elastomer, a single or finite number of Coulomb dampers are not sufficient in modeling. The disadvantage for those modeling efforts is that the excitation amplitude has to be known *a priori* while using these models.

Thus, an efficient and precise model for an elastomeric model will be developed from an empirical understanding of the damping mechanism within the damper. Physically, the amplitude dependent behavior demonstrated by the elastomer is mostly based on the interaction between fillers and rubber compound inside the filled elastomeric materials [61]. Before large deformation of a filled elastomeric damper, an intact filler structure displays a large stiffness and small loss factor for small amplitudes. As the amplitude increases, the filler structure breaks resulting in a stiffness reduction. Moreover, the breaking of filler structures, which is similar to frictional behavior, increases the loss factor. As the amplitude increases further and the frictional effect is fully released, both stiffness and loss factor drop to a substantially reduced level, both of which are then maintained by the remaining polymer chains.

Motivated by the above physical mechanisms, a number of researchers have attempted combinations of springs and frictional slides to represent the filler and rubber compound in filled rubbers or elastomers. As early as 1930, Timoshenko

[62] suggested that the general hysteretic system consist of a large number of ideal elasto-plastic elements with different yield levels. Iwan [63,64] further developed a distributed-element model to study the steady-state dynamic response of a hysteretic system. Instead of specifying a distribution function numerically to agree with experimental data, a constant band-limited statistical function was used to define yield properties of the slide elements in this model. This model proved successful in predicting steady-state frequency response of a hysteretic system using method of linearization. However, the excitation amplitude must be known as *a priori* while this model is applied in the analysis, which is only applicable in steady-state response prediction. The theory of triboelasticity [65] also stated that the behavior of a filled elastomer can be represented by a large or infinite number of alternate springs and frictional slides in series, and each slide has a constant yield force and each spring has a constant stiffness. Coveney et al [48] developed a three-parameters standard triboelastic solid (STS) based on theory of triboelasticity and further developed a four-parameter rate-dependent triboelastic (RT) model. These models gave a satisfactory representation of material behavior. However, since the yield force is fixed along different slides, these models shows less flexibility to represent the amplitude dependent behavior for different filled-level materials.

To describe the nonlinear behavior of elastomers, a distributed rate-dependent elasto-slide model was developed to describe the amplitude dependent behavior for filled elastomeric dampers. Since a filled elastomer exhibits frictional behavior, this physically motivated model consists of a large number of ideal rate-dependent elasto-slide elements with different yield levels and a parallel polymer remaining stiffness. Similar to the MR damper modeling method, the elasto-slide

element is used to emulate friction behavior demonstrated by the filler structure in the elastomer, and the linear spring represents the remaining polymer stiffness. Extensive tests including single frequency and dual frequency tests are conducted on an elastomeric specimen and a linear stroke elastomeric lag damper using a material testing machine, and complex modulus method is used to characterize the elastomeric specimen and damper. The model parameters are determined using a virtual initial loading curve identified from single frequency force-displacement hysteresis cycles. Efficient numerical algorithms are developed to apply the elastomer model to damper analysis. The modeling results for single frequency and dual frequency damper behavior are correlated quite well with experimental results in a broad amplitude and moderate frequency range. This model is successfully applied to predicting the forced response while the specimen is subjected to slowly varying cyclic loading conditions. To analytically study the influence of a nonlinear elastomeric damper on the stability performance for a dynamic system, the elastomer model is incorporated into a one single degree of freedom dynamic system and the transient response is compared with the results using corresponding viscous damping. It is shown that the non-uniform distributed rate-dependent elastomer model is applicable in complex loading conditions without any prior information, and the flexibility in determining the distribution function provides a potential to improve the model and to apply the model to elastomers with different filler structures.

### 3.1 Experimental Setup

To characterize elastomeric materials and evaluate the model, dynamic tests were conducted on two different elastomeric devices to evaluate model adaptability in various elastomers. The first elastomeric device was a double lap shear specimen, or flat linear bearing, hereinafter called the elastomeric specimen. The second elastomeric device was a linear concentric tubular bearing or damper, hereafter called the elastomeric damper. Testing was carried out with varying excitation amplitudes and frequencies, and all tests were conducted at room temperature (25°C).

A test setup for the elastomeric specimen is shown in Figure 3.1 and was designed and built for the purpose of obtaining the elastomeric specimen response data. The silicone based filled elastomeric specimen, in the form of double lap shear, were provided by Paulstra-Vibrachoc. As shown in Figure 3.2, the specimen have three parallel brass plates between which the elastomeric material is sandwiched symmetrically. To study the effect of preload on damper behavior, the elastomeric specimen tests were conducted using no preload and preload conditions, respectively. The elastomeric specimen was applied preload by compressing the double lap shear specimen at 10% of the width of the specimen using a simple vise. A 24.466 kN (5000 lbs) servo-hydraulic MTS test machine was used to test these dampers. Fixtures and grips were designed and machined appropriately to hold the damper specimens in place. The hydraulic power supply (HPS) supplied the servo fluid to the testing machine for power, and the specimens were loaded and tested on the load frame. The actuator on the load frame moved according to the signal sent by the server. A displacement LVDT sensor was used for displacement measurement and a load cell for measuring the

force. The machine can be operated in two ranges for both displacement  $\pm 127$  mm and  $\pm 12.7$  mm ( $\pm 5''$  and  $\pm 0.5''$ ) and force  $\pm 24.466$  kN and  $\pm 2.4466$  kN ( $\pm 5000$  lbs and  $\pm 500$  lbs). Single and dual frequency tests were conducted by using this machine. In dual frequency test, a HP 8904A multi-function synthesizer was used to generate and sum the sinusoidal signals for both frequencies. The single frequency test was conducted with displacement control for excitation amplitude range from 0.25 mm to 5 mm (2.5% to 50% shear) in increments of 0.25 mm. The frequency range was chosen appropriate for a helicopter rotor system:  $\Omega_1 = 7.5$  Hz was assumed to be the 1/rev frequency or rotor RPM,  $\Omega_{lag} = 5$  Hz was assumed to be the lag/rev frequency, and  $\Omega = 2.5$  Hz was a lower harmonic of these two frequencies. The dual frequency testing was carried out at 1/rev frequency of  $\Omega_1 = 7.5$  Hz and the lag/rev frequency of  $\Omega_{lag} = 5$  Hz. The range of the lag/rev amplitudes were the same as for the single frequency tests, and the 1/rev amplitudes respectively tested were 0.5, 1.5, 2.5, 3.5, and 4.5 mm.

An important effect of filler materials in the filled elastomeric specimen is stress-softening. If an elastomer sample is stretched for the first time to 100% followed by a release in the strain and then stretched again to 200%, there is a softening in the strain of up to 100% after which it continues in a manner of following the first cycle. This stress softening effect was first discovered by Mullins and is called the 'Mullins Effect' [74]. To account for this phenomenon, the test samples were first cycled and loosened before the actual tests by exciting them at 1 Hz frequency and 5 mm for 300 cycles because 5 mm is the maximum amplitude during tests. Stress relaxation is also shown in the case of dynamic loading. As the material is subjected to cycling loading, energy dissipation in

the material heats up the material and results in high temperature softening. Usually, material self-heating and other unsteady effects require about 250 seconds to stabilize and reach a steady state. Hence, in order to ensure temperature stabilization and consistency of data, during a normal test, the elastomer sample was typically excited at the test frequency and amplitude for 300 seconds before collecting data. For simplification, the stress softening and relaxation effects were not considered in the modeling process such that the distribution function was independent of the loading level and temperature. However, in principle this model could be used to account for those observed behaviors if the distribution function includes these effects.

A linear concentric tubular elastomeric lag damper was also used to evaluate the performance of the modeling method. The linear stroke elastomeric damper test setup is shown in Figure 3.3. As shown in Figure 3.4, the elastomeric damper is made of two concentric cylindrical metal tubes and one elastomeric layer sandwiched between an outer and inner tubes. The volume enclosed by the inner tube forms a cylindrical inner chamber, and a threaded trapezoidal column is attached to one end of the inner tube. When the damper is installed in the main rotor, the outer tube is attached to the rotor head, and the inner tube connected to the blade root. Thus, the lead-lag motion of the blade induces a relative translation between the inner tube and the outer tube which in turn leads to a shear deformation of the elastomer along the damper body length. The deformation of the elastomer provides required stiffness and damping for the lead-lag mode of the rotor blade. To simulate the loading conditions applied on the elastomeric lag damper by the MTS servo-hydraulic testing machine, the inner tube of the damper is connected with the load cell of the MTS machine

by a screw adapter, and the outer tube of the elastomeric damper is connected to the actuator on the MTS loading frame using a tension rod configuration. Thus, the axial translation of the actuator results in shear deformation of the elastomeric component. The lag damper was excited in displacement control by a sinusoidal signal to simulate damper motion due to the lag motion of a blade. The displacement and force were measured by LVDT sensor and load cell of the MTS machine. The excitation amplitude ranged from 0.25 mm (10 mil) to 1 mm (40 mil) in increments of 0.25 mm (10 mil) at three different frequencies of  $\Omega_1$ ,  $\Omega_{lag}$  and  $\Omega_{com}$ , respectively.

All test data were collected using a high sampling frequency (2048 Hz) such that most higher harmonic components in the nonlinear force were included. To reduce the noise of the sinusoidal displacement signal, a Fourier series was used to reconstruct the input displacement. The reconstructed displacement signal was then differentiated to obtain the velocity signal. The Fourier series expansion of the input displacement is

$$x(t) = \frac{x_0}{2} + \sum_{k=1}^{\infty} [X_{c,k} \cos(k\omega t) + X_{s,k} \sin(k\omega t)] \quad (3.1)$$

where

$$\begin{aligned} X_{c,k} &= \frac{\omega}{\pi} \int_0^{\frac{2\pi}{\omega}} x(t) \cos(k\omega t) dt \\ X_{s,k} &= \frac{\omega}{\pi} \int_0^{\frac{2\pi}{\omega}} x(t) \sin(k\omega t) dt \end{aligned} \quad (3.2)$$

For single frequency data processing, any bias and higher harmonics were filtered, so that only the frequency of interest,  $\omega$ , remained where  $\omega = \Omega$ ,  $\Omega_{lag}$ , or  $\Omega_1$ . For dual frequency testing, the general equation for the input dual displacement signal is written as

$$x(t) = X_{lag} \sin(\Omega_{lag} t) + X_1 \sin(\Omega_1 t) \quad (3.3)$$

The signal is periodic with a frequency corresponding to the highest common factor of both harmonics, i.e., 2.5 Hz in our case. The displacement signal was filtered using  $\Omega = 2.5$  Hz as the base frequency. The first three harmonics were needed to reconstruct the dual frequency displacement signal in order to capture the lag/rev and the 1/rev frequencies. The Fourier series was also used to reconstruct the measured force. However, due to nonlinearity of elastomers, the higher harmonics of the measured force were not filtered.

## 3.2 Elastomer Characterization

A typical approach used for characterizing elastomer behavior is the complex stiffness. The linearized complex stiffness,  $K^*$ , is composed of the in-phase or storage stiffness,  $K'$ , and the quadrature or loss stiffness,  $K''$ , as follows:

$$K^* = K' + jK'' \quad (3.4)$$

Therefore, the damper force can be written as the summation of an in-phase spring force and a quadrature damping force, and the damper force can be approximated by the first Fourier sine and cosine components at the frequencies  $\omega = \Omega$ ,  $\Omega_{lag}$ , and  $\Omega_1$ :

$$\begin{aligned} F(t) &= F_c \cos(\omega t) + F_s \sin(\omega t) \\ &= K' x(t) + \frac{K''}{\omega} \dot{x}(t) \end{aligned} \quad (3.5)$$

where  $F_c$  and  $F_s$  are the first harmonic Fourier coefficients of the measured force. The storage stiffness,  $K'$ , and the loss stiffness,  $K''$ , are determined by

the following equations:

$$\begin{aligned} K'(\omega) &= \frac{F_c X_c + F_s X_s}{X_c^2 + X_s^2} \\ K''(\omega) &= \frac{F_c X_s - F_s X_c}{X_c^2 + X_s^2} \end{aligned} \tag{3.6}$$

where,  $X_c$ ,  $X_s$  are the first harmonic Fourier coefficients of  $x(t)$ .

The typical linear characterization results of the elastomeric specimen are shown in Figure 3.5 where no preload was applied to the elastomeric specimen. These plots indicate that the linearized storage stiffness and loss stiffness of the specimen are highly amplitude dependent at low amplitudes. For smaller amplitudes, the rate of change of the storage stiffness and the loss stiffness is much greater than one for larger amplitudes. However, the complex stiffness does not change substantially over the narrow frequency range tested. The loss factor,  $\eta$ , is also strongly dependent on amplitude. The maximum value of the loss factor is as high as 1.025 for this filled elastomer. This is much higher than the values for existing lag damper materials. This elastomeric material performs most effectively within the amplitude range of 0.76 - 1.27 mm (30 - 50 mils) where  $\eta > 1$ . Similar results are demonstrated by the elastomer with preload. Thus, it can be concluded that the linearized behavior of the elastomeric specimen is highly amplitude dependent and weakly frequency dependent in this frequency range.

The complex modulus and loss factor of the elastomeric lag damper are shown in Figure 3.6. Both inphase and quadrature stiffness demonstrate moderate amplitude dependence and weak frequency dependence. In contrast to the characterization of the elastomeric specimen, the inphase stiffness of the elastomeric damper is much higher than the quadrature stiffness, and both inphase and quadrature stiffness vary with the displacement amplitude at a similar rate.

Thus, the loss factor of the elastomeric damper is quite low (around 0.25 to 0.3) and almost constant along different displacement amplitudes and frequencies, as shown in Figure 3.6(c).

The single frequency linear characterization can capture the general trends of the in-phase and quadrature stiffness for a filled elastomer. However, this linear analysis cannot be used to accurately reconstruct the nonlinear amplitude dependent hysteresis behavior exhibited by the elastomer. Therefore, a new nonlinear modeling effort will be presented in the following section.

### 3.3 Distributed Rate-dependent Elasto-slide Model

The distributed rate-dependent elasto-slide model is shown in Figure 3.7, in which a series of elasto-slide elements are combined in parallel with a constant linear spring or elastic modulus. The model can be applied either in force-displacement relations or in stress-strain relations, but only the force-displacement formulation will be used in this paper. Each elasto-slide element consists of a leading spring with stiffness  $k/N$  in series with a rate-dependent slide which has a yield force  $f_i^*/N$  and a transition velocity  $v_r$  between preyield and postyield region, where  $N$  is the total number of elements. The yield force for each element is different, and the stiffness for each leading spring is assumed to be a constant. The rate-dependent slide is used to describe the friction behavior of a filler structure element which includes a preyield slip and a postyield viscous motion. When  $v_r$  approaches zero, the rate-dependent slide demonstrates ideal Coulomb behavior. For each ideal element, when a loading displacement  $x$  is so small that the consequent leading spring force is smaller than the yield force,

only the spring is deformed to provide a forced response. After the spring force reaches the yield force, the slide is yielded and moves, and the resisting force of the element remains constant with the same value as the yield force. Since each element is assumed to have a different yield force level, this model shows gradual stiffness reduction as amplitude increases until such a condition as all elements have yielded. At that time, only the parallel spring,  $k_0$ , remains to represent polymer stiffness of the elastomer. As the elastomer is a continuum, the total number of elements,  $N$ , approach infinity, and, in the limit, the discrete yield force for a single slide is replaced by a distributed density within a certain yield force range.

The existence of the filler structures inside the elastomer leads to hysteretic behavior when the damper is cycled between fixed deflection limits. Analytically, a distribution function of yield force is denoted as  $\varphi(f^*)$  such that the density of the slides with yield force  $f^*$  is expressed as  $\varphi(f^*)df^*$ . Using the ideal slide assumption, the slide behaves as a Coulomb friction element. Thus, upon initial loading, the leading spring at a certain yield element stretches with the displacement  $x$  until it reaches the maximum slide yield force, i.e.

$$\begin{aligned} df &= kx\varphi(f^*)df^*, \dot{x} > 0, 0 \leq x \leq \frac{f^*}{k} \\ df &= f^*\varphi(f^*)df^*, \dot{x} > 0, x \geq \frac{f^*}{k} \end{aligned} \quad (3.7)$$

If the direction of loading is reversed, the force-deflection relation is more complicated. Including the yielded and not yielded elements, the force-deflection

relation will become

$$\begin{aligned}
df &= [f^* - k(A - x)]\varphi(f^*)df^*, \dot{x} < 0, A - 2\frac{f^*}{k} \leq x \leq A, f^* \leq kA \\
df &= -f^*\varphi(f^*)df^*, \dot{x} < 0, x \leq A - 2\frac{f^*}{k}, f^* \leq kA \\
df &= kx\varphi(f^*)df^*, \dot{x} < 0, f^* > kA
\end{aligned} \tag{3.8}$$

where  $A$  is the maximum deflection that occurred with  $\dot{x} > 0$ . An expression similar to Eq. 3.8 is obtained when the loading reaches the minimum deflection and is reversed again so that  $\dot{x} > 0$ . This process continues until the loading is stopped. Clearly, at each time, only part of the elasto-slide elements have yielded. The total resisting force can be obtained by integrating all of the elasto-slide forces along the yield distribution region and by adding the spring force due to the residual polymer stiffness. Thus, from Eq. 3.7, the initial loading force is given as

$$f = \int_0^{kx} f^*\varphi(f^*)df^* + kx \int_{kx}^{\infty} \varphi(f^*)df^* + k_0x, \dot{x} > 0 \tag{3.9}$$

Similarly, the resisting force due to the reversed loading is obtained by integrating Eq. 3.8

$$\begin{aligned}
f &= \int_0^{\frac{k(A-x)}{2}} -f^*\varphi(f^*)df^* + \int_{\frac{k(A-x)}{2}}^{kA} [kx - (kA - f^*)]\varphi(f^*)df^* \\
&+ kx \int_{kA}^{\infty} \varphi(f^*)df^* + k_0x, \dot{x} < 0, x \leq A
\end{aligned} \tag{3.10}$$

Thus, while an elastomer is under the cyclic displacement loading

$$x = A \sin(\omega t) \tag{3.11}$$

an analytical force-deflection hysteresis cycle can be computed and is shown as a dashed line in Figure 3.8, where  $A$  is 2.5 mm and the frequency is 2.5 Hz.

Compared with the experimental hysteresis as shown in dotted line, the model prediction gives a good match to the non-elliptical hysteresis cycle.

The distributed elasto-slide model resembles the physical mechanism of an elastomer, so it can account for nonlinear characteristics of the behavior demonstrated by an elastomer under a cyclic loading either in single frequency or multi frequencies. However, using Coulomb slide, the cyclic limit at turning point must be known for response calculation, which makes it impossible for the model to describe elastomer behavior under complex loading conditions. The ideal elasto-slide is also incapable of modeling any frequency dependent properties and non-hysteresis behavior in the time domain such as stress relaxation or creep. In reality, the Coulomb slide is only an idealized friction model. The practical friction behavior includes preyield slip and postyield steady resistance which lead to rate dependent damping effect [75, 76]. Thus, a rate-dependent elasto-slide model is introduced to improve the modeling performance.

In the rate-dependent elasto-slide model, the Coulomb slide is replaced with a non-Coulombic friction function and the coupling between a slide and a leading spring is described by an internal displacement denoted as  $x_0$  such that the slide force for a certain yield region is written as

$$df = f^* \varphi(f^*) df^* \left( \frac{\dot{x}_0}{v_r} \right)^{\frac{1}{p}} \quad (3.12)$$

where  $p$  is a positive odd integer. Coupled with the lead spring  $k\varphi(f^*)df^*$ , the internal displacement  $x_0$  at certain yield region is obtained using the function

$$\frac{\dot{x}_0}{v_r} = \left[ \frac{k}{f^*} (x - x_0) \right]^p \quad (3.13)$$

By integration over the whole yield force region, the damper force due to any

deflection loading,  $x$ , is determined by

$$f = \int_0^\infty k(x - x_0)\varphi(f^*)df^* + k_0x \quad (3.14)$$

Eq. 3.13 is a typical well-posed initial-value problem, and numerical solution for this differential equation can be obtained given an initial condition. The simplest way to guarantee a stable solution for such a stiff initial-value problems is to adopt a predictor-corrector approach with the corrector iterated to convergence(PECE) [79]. In this application, the numerical algorithm is based on the Adams-Bashforth four-step method as the predictor step and one iteration of the Adams-Moulton three-step method as the corrector step, with the starting values obtained from a Runge-Kutta method of order four [79]. In accordance with the ratio of yield force and stiffness,  $\frac{k}{f^*}$ , and an appropriate choice of  $p$ , the Adams-Bashforth-Moulton method gives relatively stable and fast convergence of a solution within a limited number time steps.

For an elastomer under loading as in Eq. 3.11, the steady-state response predicted by the rate-dependent elasto-slide model is shown as a solid line in Figure 3.8. The predicted hysteresis cycle correlates much better with the experimental data, especially at turning points of the loading deflection. It should be noted that there is no requirement for excitation amplitude information in this modeling process. Thus, the distributed rate-dependent elasto-slide model can predict forced response of an elastomer in the time-domain in response to a sinusoidal displacement excitation.

In order to apply the elastomer model to a dynamic system, a numerical method using MATLAB ODE algorithm was also evaluated. For a dynamic

system with governing equations

$$M\ddot{x} + C\dot{x} + Kx + F_d(x, \dot{x}) = F(t) \quad (3.15)$$

where,  $M$ ,  $C$ , and  $K$  are mass matrix, equivalent damping matrix, and stiffness matrix, respectively,  $F_d(x, \dot{x})$  is used to describe the force due to an elastomeric damper, and  $F(t)$  is a loading vector applied on the system. The size of the matrix depends on the degree of freedom of the system. For simplicity, only a 1-DOF system is considered. In the distributed rate-dependent elasto-slide damper model, there are infinite internal variable  $x_0$ 's theoretically. However, the distributed yield stress is usually within a limit range. Therefore, according to the form of a distribution function, the continuous yield force distribution area can be uniformly decomposed into  $n$  discrete elements from minimum to maximum yield force and each element has a yield force range,  $\Delta f^*$ . At each yield stress,  $f_i^*$ , the corresponding distribution is equal to the area of that element,  $\varphi(f_i^*)\Delta f^*$ . Thus, each element has an internal variable denoted as  $x_{0i}$ ,  $i = 1, \dots, n$ , and each  $x_{0i}$  satisfies the Eq. 3.13. Thus, the damper force  $F_d$  can be described by

$$F_d = k \sum_{i=1}^n \varphi(f_i^*)\Delta f^* (x - x_{0i}) + k_0 x \quad (3.16)$$

Rewrite Eq. 3.15 into a first order form and combine Eq. 3.13 and 3.16, the

state equation of the system is expressed as

$$\begin{aligned}
\dot{x} &= \dot{x} \\
\ddot{x} &= \frac{F(t)}{M} - \frac{1}{M} [(K + k_0)x - k \sum_{i=1}^n \varphi(f_i^*) \Delta f^*(x - x_{0i})] - \frac{C}{M} \dot{x} \\
\dot{x}_{01} &= \left[ \frac{k}{f_1^*} (x - x_{01}) \right]^p v_r \\
\cdot &\quad \cdot \quad \cdot \\
\cdot &\quad \cdot \quad \cdot \\
\cdot &\quad \cdot \quad \cdot \\
\dot{x}_{0n} &= \left[ \frac{k}{f_n^*} (x - x_{0n}) \right]^p v_r
\end{aligned} \tag{3.17}$$

This is a  $(n + 2)$ th order state function. Using the ODE23 algorithm, the forced response due to  $F(t)$  or the transient response due to the initial condition  $x(0)$  and  $\dot{x}(0)$  can be solved numerically. For the system with more degrees of freedom or elastomeric dampers, the state function can easily accommodate these additions by using a larger number of states.

### 3.4 Determination of Model Parameters

As seen in the construction of the model, the major parameters to be determined are the leading spring,  $k$ , and yield force distribution function,  $\varphi(f^*)$ , for the distributed elasto-slide element, and the parallel spring,  $k_0$ , for the remaining polymer stiffness. In the absence of the knowledge of the elastomer structure, the selection of these parameters are only based on experimental data though the elasto-slide distribution could be determined by the properties of the filler structures in the elastomer. One possible selection of methods would be to make use of an experimentally determined initial loading curve.

The definition of the distribution function implies that  $\varphi(f^*)$  has to obey the

following three constraints:

$$\begin{aligned}\int_0^{\infty} \varphi(f^*)df^* &= 1 \\ \varphi(f^*) &\geq 0 \\ 0 &\leq f^* \leq \infty\end{aligned}\tag{3.18}$$

From the initial loading curve Eq. 3.9, yields

$$\frac{df}{dx} = k \int_{kx}^{\infty} \varphi(f^*)df^*\tag{3.19}$$

where,

$$f^* = kx\tag{3.20}$$

Then

$$\frac{d^2f}{dx^2} = -k^2\varphi(f^*)\tag{3.21}$$

Thus, the distribution function would be related to the curvature of the initial loading curve by the formula

$$\varphi(f^*) = -\frac{1}{k^2} \frac{d^2f}{dx^2}\tag{3.22}$$

And the determination of the distribution function relies on the identification of the initial loading curve from the experimental data.

In the view of distributed elasto-slide model using ideal Coulomb slide, the initial loading curve is independent of loading rate such that the maximum force of the initial loading responds to the maximum displacement in cyclic loading. As a result, an initial loading curve can be obtained using a series of experimental hysteresis loops at different amplitudes. An example of the initial loading curve is shown in Figure 3.9, the initial loading curve at three different frequencies are

obtained from hysteresis cycles of the elastomeric specimen by identifying the force at corresponding maximum displacement. The analytical initial loading curve is determined by considering the influence of the rate-dependent slide. This curve appears an elasto-plastic behavior, which is described as

$$f = \frac{1}{\varphi_0}(1 - e^{-k\varphi_0x}) + k_0x \quad (3.23)$$

Notably,  $\varphi_0$  is a distribution constant and an index of the post yield force level.  $k$  and  $k_0$  are the stiffness of the leading spring and the remaining polymer stiffness respectively. Summation of the leading spring and the polymer stiffness is just the slope of the force-displacement curve when  $x \rightarrow 0$ . This is conceivable since there only exists the influence of the springs while all slide elements are not yielded. Substituting Eq. 3.23 into Eq. 3.22, yields a very simple distribution function as

$$\varphi(f^*) = \varphi_0 e^{-\varphi_0 f^*} \quad (3.24)$$

The distribution area for the elastomeric specimen is shown as shadow area in Figure 3.10. It is easily shown that the distribution function satisfies all the properties of Eq. 3.18.

The initial loading curve is determined from the experimental hysteresis diagrams, and the distribution function or  $\varphi$ ,  $k$  and  $k_0$  can be determined by fitting Eq. 3.23 with the test data. For the distributed elasto-slide model using Coulomb slide, the steady-state forced response of the damper under cyclic loading will be predicted with determined  $\varphi_0$ ,  $k$  and  $k_0$  as follows:

$$\begin{aligned} f &= \frac{1}{\varphi_0}(1 + e^{-k\varphi_0x_{max}} - 2e^{-k\varphi_0\frac{x-x_{min}}{2}}) + k_0x, \dot{x} > 0 \\ f &= -\frac{1}{\varphi_0}(1 + e^{-k\varphi_0x_{max}} - 2e^{-k\varphi_0\frac{x_{max}-x}{2}}) + k_0x, \dot{x} < 0 \end{aligned} \quad (3.25)$$

where  $x_{max}$  and  $x_{min}$  are the displacement at turning points while  $\dot{x} < 0$  and  $\dot{x} > 0$  respectively.

For the rate-dependent elasto-slide model, the reference velocity  $v_r$  and the exponent  $p$  were determined as follows. The choice of  $v_r$  is based on steady state force-velocity curves in which the boundary between preyield slip and postyield flow is approximated. Analytically,  $p$  should be as large as possible such that the post yield force rapidly transitions to a constant value, which is similar to friction behavior. However, large values of  $p$  result in a stiffer system. Thus,  $p$  was chosen by trading off between both factors. For the elastomeric specimen, the determined model parameters are shown in Table 3.1, in which the elastomeric damper has two preload conditions. For elastomeric damper with 10% preload, the distribution constant  $\varphi_0$  is lower than that without preload. This means that the yield force level can be increased by the normal force in the preload condition. Similarly, the preload force also can increase the stiffness. As a result, the addition of preload perpendicular to the loading axis tends to increase the equivalent stiffness and damping over the entire amplitude range. This effect is due to the compressive preload increasing the friction response of the filler in the elastomer, and is not reflected in the distributed elasto-slide model. Thus, the model parameters are different for different preloading conditions. For the elastomeric lag damper, the determined model parameters are shown in Table 3.2. Notably, the elastomeric material in the elastomeric damper is much stiffer than the elastomeric specimen since the stiffness of the leading spring and remaining spring is much higher than the elastomeric specimen. Thus, the loss factor of the elastomeric damper appears much lower than the elastomeric specimen though the yield force level of the elastomeric damper is higher than the elastomeric

specimen.

## **3.5 Model Applications**

As stated before, the distributed rate-dependent elasto-slide model resembles the behavior of filler structures in the elastomer such that it can predict forced response of an elastomer in the time domain. In this section, single frequency and dual frequency steady-state hysteresis data are used to evaluate the fidelity of the model, in which the model is validated over an appropriate amplitude and frequency range for helicopter lag dampers. Since the intention is to apply these materials in a lag damper in a helicopter rotor, the damper forced response under dual frequency loading with slowly varying amplitude is also correlated with model predictions. In order to determine the soundness of the model and the underlying numerical algorithms while applied to a dynamic system, the elastomeric model is incorporated into a one degree of freedom dynamic system. The transient response due to the initial disturbance is predicted, and the result is compared with the transient response obtained using equivalent viscous damping.

### **3.5.1 Single Frequency Modeling Results**

For the elastomeric specimen, three sets of single frequency hysteresis cycle data are used to verify the fidelity of the modeling results. Each set of data is obtained by measuring the forced response while the elastomeric specimen is under sinusoidal displacement loading at 2.5 Hz, 5.0 Hz and 7.5 Hz, respectively. At each frequency, the loading amplitude is chosen as 1 mm, 2 mm, 3 mm and

4 mm. In Figure 3.11(a)(b)(c), the experimental data at three frequencies are shown compared with the modeling results. Basically, the modeling results correlate quite well with the experimental results while the displacement amplitude  $x_0$  is in the moderate amplitude range ( $2 < x_0 < 5$  mm). In the small amplitude range  $x_0 < 2$  mm, the elastomer model under-predicts the area enclosed by the hysteresis cycle. The reason for that is partly because the lower yield region for the elasto-slide element is replaced with a non-zero constant yield force for numerical consideration and the influence of this approximation is amplified at small deflection loading.

The complex modulus determined by the elastomeric model is also compared with the experimental result. As shown solid lines in Figure 3.12, the storage stiffness and loss stiffness predicted by the model have the same amplitude dependent trend as the experimental result. The analytical moduli are well matched by the experimental moduli at moderate amplitude range except that the moduli over small amplitude range are under-predicted especially for loss stiffness. Model predictions are also compared with experimental data for loss factor. The predicted loss factor shares common features of the elastomer. Clearly, at small amplitude, most of the filler structures, or corresponding elasto-slide elements, have not yielded, so that the loss factor is small. As the amplitude increases, breaking filler structures or yielding of slides leads to a rise in the loss factor. After all of the slide elements have yielded, the loss factor decreases again. In Figure 3.12, it also shows that both experimental and predicted moduli are weakly dependent on frequency. This phenomenon is consistent with the tribo-elastic mechanism of elastomeric materials [65].

Similar single frequency modeling results for the elastomeric lag damper are

shown in Figure 3.13 as force-displacement diagrams for different amplitudes at 2.5 Hz (Fig. 3.13(a)), 5 Hz (Fig. 3.13(b)) and 7.5 Hz (Fig. 3.13(c)) respectively. Clearly, the elastomeric model captures the amplitude and frequency dependent behavior of the elastomeric damper.

### 3.5.2 Dual Frequency Modeling Results

In a helicopter lag damper, the elastomer would experience multi-frequency excitation, especially as a combination of regressive lead-lag frequency and  $1/\text{rev}$  rotor frequency, while the helicopter is in the forward flight condition. Under such a circumstance, the potential loss of damping at the lag frequency due to limitation of stroke is well known [12], so it is important to predict the response of the elastomeric dampers under dual frequency excitation. Dual frequency force-deflection experimental data of the elastomeric specimen are used to evaluate the adaptability of the model under complex loading conditions.

In stable forward flight conditions, the blade motion at  $1/\text{rev}$  is constant at a given amplitude. Thus, the test data were obtained while the amplitudes at both frequencies (lag/rev and  $1/\text{rev}$ ) were held constant. For each test condition, the amplitude for lag frequency and  $1/\text{rev}$  frequency ranges from 0.25 mm to 5 mm, and the sum of both amplitudes must not exceed 5 mm, which corresponds to maximum allowable strain of 50%. The modeling result at each dual frequency loading condition is correlated with the corresponding experimental result. Some of these dual frequency modeling results are presented in Figure 3.14, 3.15, 3.16 and 3.17. The figures are grouped according to the  $1/\text{rev}$  frequency amplitude. Figure 3.14 shows the modeling results for 3.5 mm amplitude at the  $1/\text{rev}$  frequency and at four different amplitudes at lag frequency. Clearly,

as the lag amplitude increases, the ability of the elastomer model to capture the hysteresis cycle is also increased. Over the small amplitude range, the model under-predicts the forced response due to inadequacy of the elasto-slide elements in describing the effect of viscous damping. In the moderate amplitude range, the model accurately captures the outer hysteresis loop and fairly captures the inner loop. Similar results are shown in Figure 3.15, 3.16 and 3.17. In general, the distributed rate-dependent elasto-slide model performs well in the moderate amplitude range except it over-predicts the inner loop in some cases. The model also should be improved to predict the response over the small amplitude range.

In unstable forward flight conditions, the lead-lag damper may encounter a slowly-varying amplitude modulated periodic loading. For simplicity, the analytical and experimental simulation results are only shown for one scenario, in which the amplitude for 1/rev frequency is 1.5 mm and the amplitude for lag frequency is assumed as

$$A_{lag} = 1.5[1 + 0.2 \sin(0.2\pi t)]mm \quad (3.26)$$

The predicted forced response is shown in Figure 3.18(a) and (b) compared with the experimental results for two different time scales. Similarly, the modeling force-displacement hysteresis cycle is also compared with the experimental data as shown in Figure 3.18(c). As seen, the predicted force output due to the slowly varying loading has the same varying trend, and also the force value is tracked quite well. Clearly, the proposed elastomeric model performs fairly well in predicting dual frequency response, and especially the distributed elasto-slide model can predict the behavior of the elastomeric damper under any complex loading conditions.

### 3.5.3 1-DOF Dynamic Response Analysis

To examine the influence of an elastomeric damper in a dynamic system, the proposed elastomeric model is included in a dynamic oscillator. Figure 3.19 shows the schematic of a dynamic oscillator with a damper. This model is representative of the lag dynamics of a helicopter rotor blade, so that the mass,  $M$ , represents the blade lag inertia, the system damping,  $C$ , includes the effect of structural damping,  $C_{\text{struc}}$ , and aerodynamic damping,  $C_{\text{aero}}$ , and the spring,  $K$ , is the blade lag stiffness. The damper force is denoted as  $F_d$ , and the system transient response is calculated either using a nonlinear elastomeric damper or an equivalent viscous damper such that the effect of the nonlinear elastomeric damping can be obtained compared with the viscous damping. The equation of motion for this oscillator is shown in Eq. 3.15. For simplicity, the natural frequency of this system is set at 5 Hz, and the required damping ratio is assumed to be 5%. It is also assumed that the damping coefficient for the viscous damper is equal to the equivalent damping of the elastomeric damper at 1 mm amplitude. Thus, the effective mass is 1524 Kg, the effective stiffness is 1504 N/mm, and equivalent damping is 4.8 Nmm/s. Given an initial displacement perturbation  $x(0) = 3$  mm, the transient response of the system can be obtained by solving Eq. 3.17 using MATLAB ordinary differential equation solver.

Due to the aerodynamic effect, the aerodynamic damping,  $C_{\text{aero}}$ , can be reduced and even become negative. Thus, the response of the oscillator at different aerodynamic damping conditions are studied. First, the damping effect of the elastomeric damper and the viscous damper is obtained using nominal system damping (5% damping ratio). As shown in Figure 3.20, with the same initial perturbation, the decay rate of the viscous damper is faster than that for

the nonlinear elastomeric damper. Moreover, compared with the constant oscillation frequency for the viscous damping case, the oscillation frequency for the elastomeric damper case increases as response amplitude decreases. This is caused by the stiffness of the elastomer over the small amplitude range being stiffer than that at larger amplitudes. Second, to examine whether the elastomeric model can reproduce limit cycle oscillation which is observed in the real elastomeric damper, the system transient response is solved with a simulated negative aerodynamic damping, i.e. the system damping,  $C$ , is reduced to zero due to a negative aerodynamic damping. Figure 3.21 shows that with the same zero system damping and displacement perturbation, the transient response due to the viscous damping still diminishes within several seconds, but the transient response due to the elastomeric damping settles to constant or slowly decayed oscillations (jitter phenomenon). Therefore, the elastomeric damper model captures this characteristic of the elastomer.

### 3.6 Conclusions

Modeling methods for elastomeric material behavior in simple shear were investigated. Most prior models introduced nonlinear terms into the conventional Kelvin model or Zener model. As filled elastomers are anelastic materials, friction mechanism damping proves useful to model rate-independent damping. Nonlinearity in tested elastomeric materials was manifested in two ways. First, the forced response of an elastomer is nonlinear which means the response cannot be predicted by linear differential and integral equations. The other is that the stiffness and damping of elastomers vary as a function of amplitude and fre-

quency. Therefore, different modeling emphases result in different model effectiveness. While some models capture the amplitude dependent complex moduli very well with constant parameters, they cannot predict stress-strain hysteresis accurately. On the other hand, those hysteresis models can predict stress time histories quite well, but their parameters are usually amplitude and frequency dependent. The methods require amplitude and frequency as prior information when these models are implemented or simulated.

Developed from a hysteresis modeling method, a distributed rate-dependent elasto-slide elastomeric model is used to describe the amplitude dependent characteristics of an elastomer. This physically motivated damper model resembles the behavior of filler structures in the elastomer under loading. The method to determine the model parameters was presented. It was found that a unique exponential function can be used to describe the yield force distribution for elastomers. Numerical algorithms were developed for model applications. Dynamic test conducted on an elastomeric specimen and an elastomeric lag damper are used respectively to evaluate the modeling method. The fidelity of the model was verified by the good correlation between predicted single and dual frequency force-deflection hysteresis and the experimental results except that the damping at lower amplitude range can not be fully predicted by the model. Since the proposed model is a time domain model, the adaptability of the model in predicting damper response under complex loading was evaluated. The predicted force response for slowly varying amplitude loading correlated quite well with the corresponding experimental data. Finally, a single degree of freedom system was used to study the influence of the elastomeric damper on the blade lag motion. The transient response and limit cycle oscillation were simulated and predicted

by the model.

In conclusion, the distribute rate-dependent elasto-slide elastomeric damper model is a time-domain modeling approach to capture nonlinear behavior of the elastomer. The damper model can easily be implemented into the dynamic systems. Since the model is physically motivated, the flexibility in determining the distribution function provides a potential to improve the model performance especially in small amplitude range. Though only a one-dimensional elastomeric model is described in this paper, the distributed elasto-slide model can also be extended into a three-dimensional form such that it can be implemented easily into a finite element analysis for a complex elastomeric damper configuration.

The distributed elasto-slide model was successfully applied to elastomeric materials. Thus, the behavior of both MR fluids and elastomeric materials can be well described using similar elasto-slide mechanism. An MRFE damper includes the effect of the MR fluids and elastomer, and the MRFE model then can be developed by combining MR and elastomeric models. In the following chapters, a design analysis of an concentric bearing type MRFE damper is described, and then the experimental behavior of the damper is correlated with the modeling results.

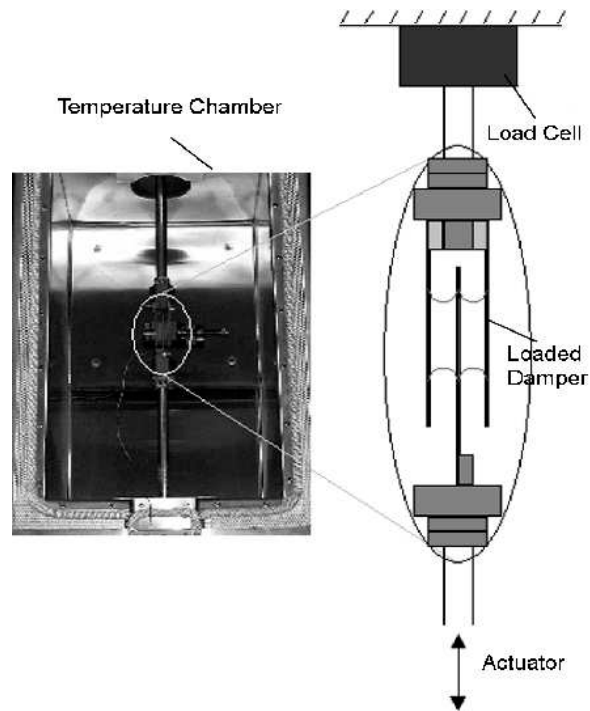


Figure 3.1: Elastomeric Specimen Test Setup

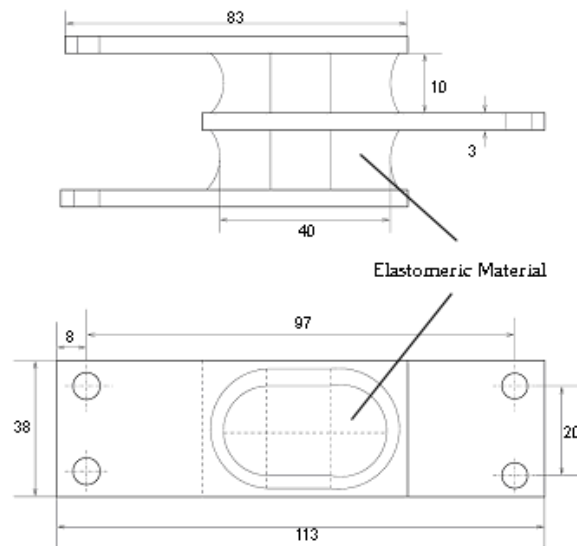


Figure 3.2: Schematic of the Elastomeric Double Lap Shear Specimen (Dimensions in mm)

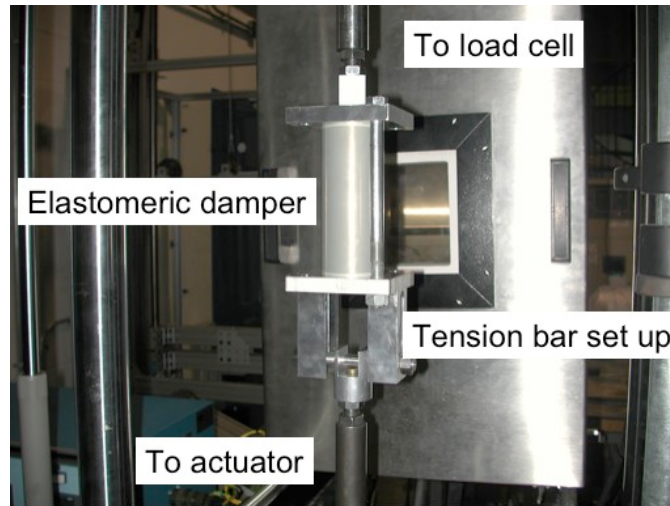


Figure 3.3: Elastomeric Lag Damper Test Setup

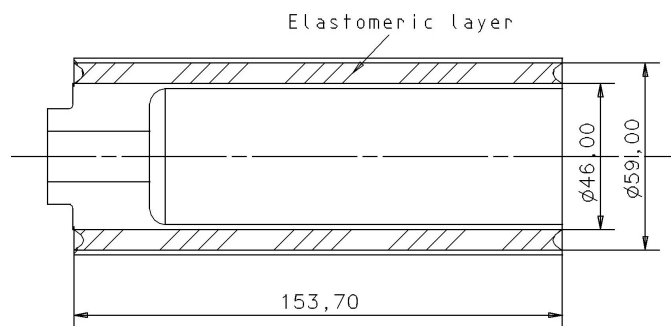


Figure 3.4: Cross Section of Concentric Bearing Elastomeric Lag Damper (Dimensions in mm)

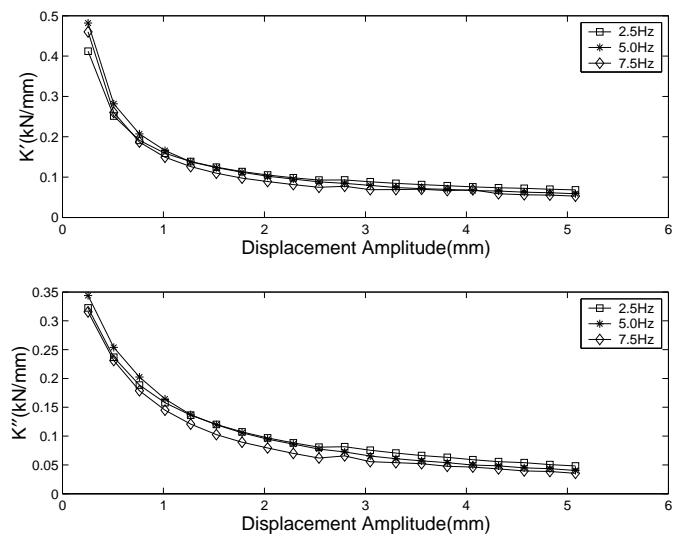


Figure 3.5: Linear Characterization of an Elastomeric Specimen

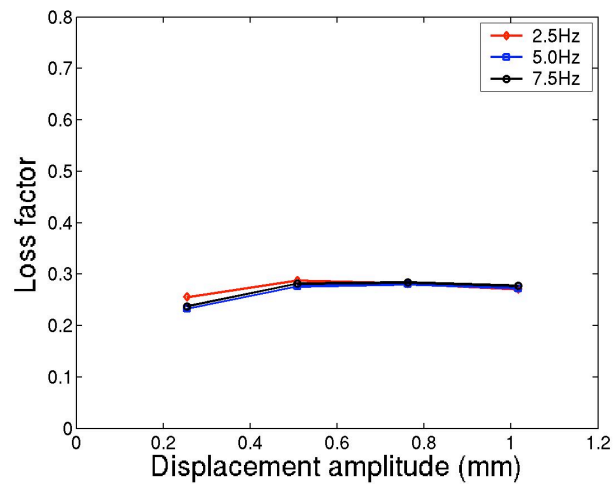
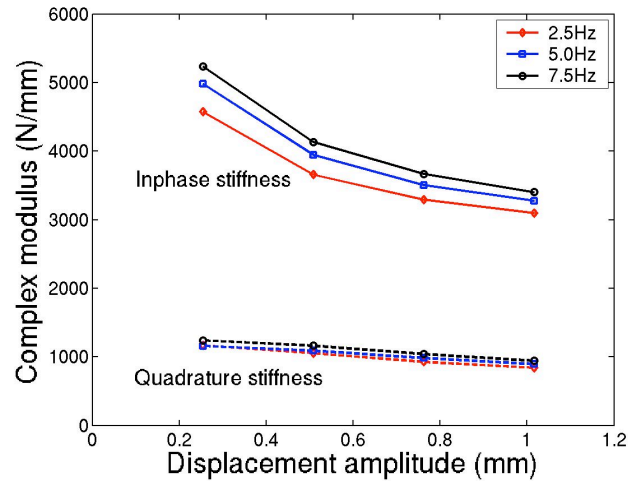


Figure 3.6: Linear Characterization of the Elastomeric Damper

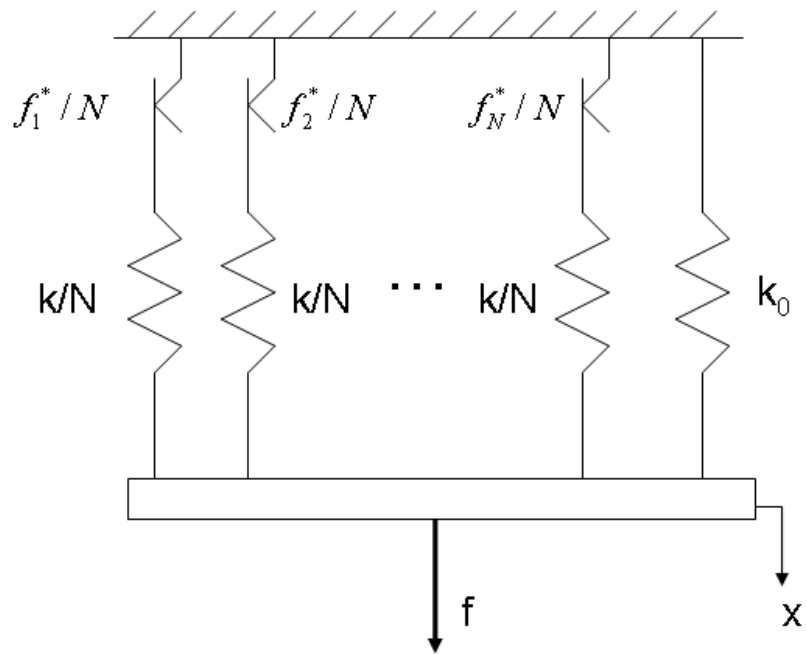


Figure 3.7: Distributed Elasto-Slide Model

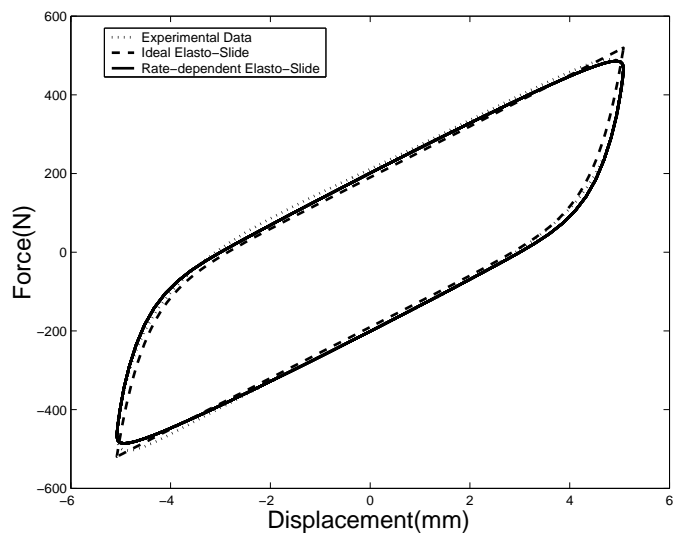


Figure 3.8: Hysteresis Modeling for Elastomeric Specimen

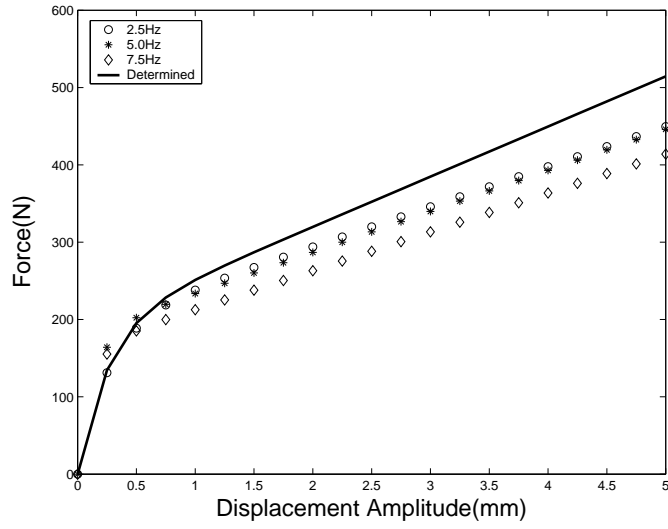


Figure 3.9: Determination of the Initial Loading Curve for Elastomeric Specimen

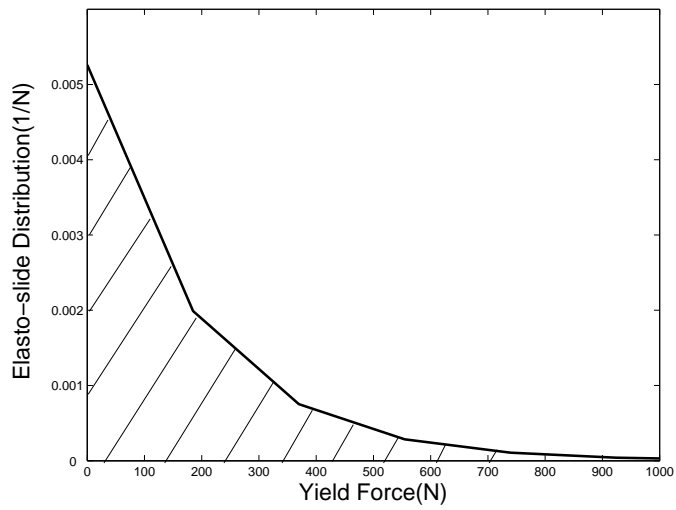


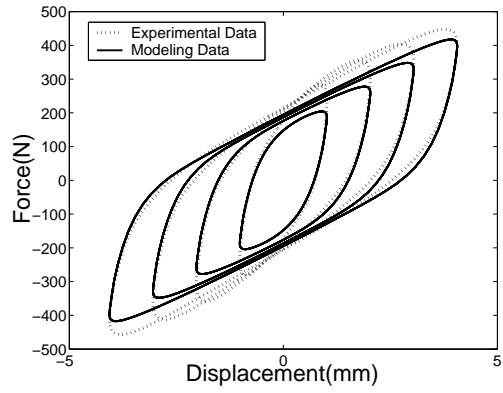
Figure 3.10: Elasto-slide Distribution for Elastomeric Specimen

Table 3.1: Model Parameters for Elastomeric Specimen

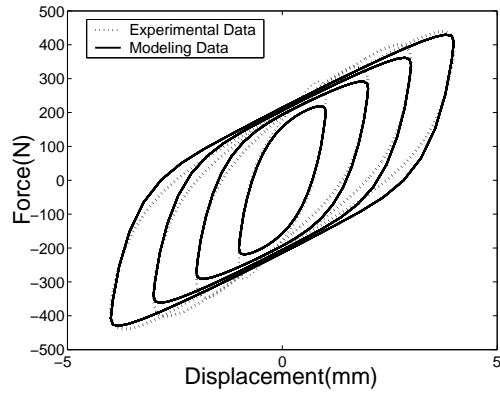
| Parameter              | No Preload | 10% Preload |
|------------------------|------------|-------------|
| $\varphi_0$ (1/Newton) | 0.0068     | 0.0053      |
| $k$ (N/mm)             | 504.51     | 739.40      |
| $k_0$ (N/mm)           | 44.44      | 64.87       |
| $v_r$ (mm/s)           | 50         | 50          |
| $p$                    | 7          | 7           |

Table 3.2: Model Parameters for Elastomeric Damper

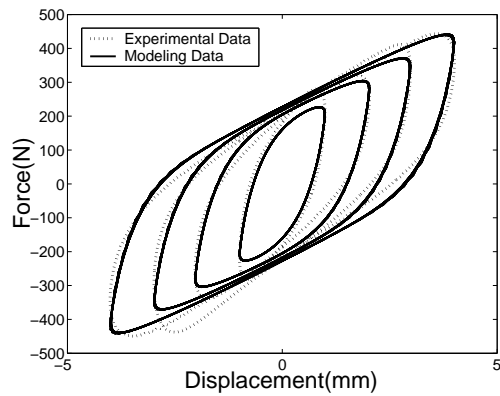
| Parameter              | No Preload |
|------------------------|------------|
| $\varphi_0$ (1/Newton) | 0.0015     |
| $k$ (N/mm)             | 6436       |
| $k_0$ (N/mm)           | 2915       |
| $v_r$ (mm/s)           | 15         |
| $p$                    | 7          |



(a) 2.5Hz

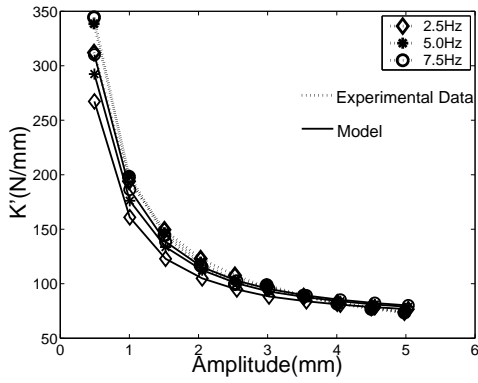


(b) 5.0Hz

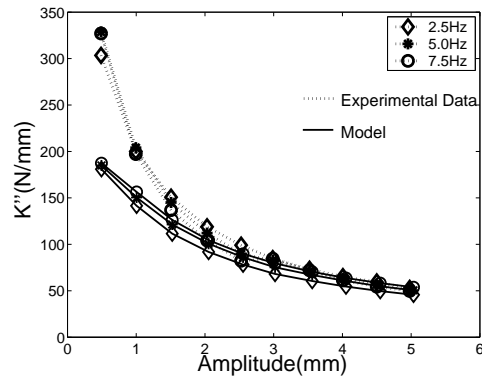


(c) 7.5Hz

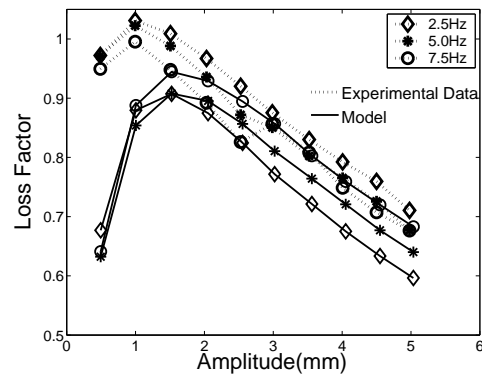
Figure 3.11: Single Frequency Hysteresis Modeling for Elastomeric Specimen



(a) In-phase Stiffness

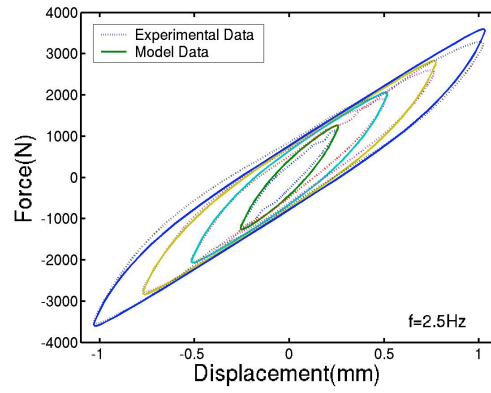


(b) Quadrature Stiffness

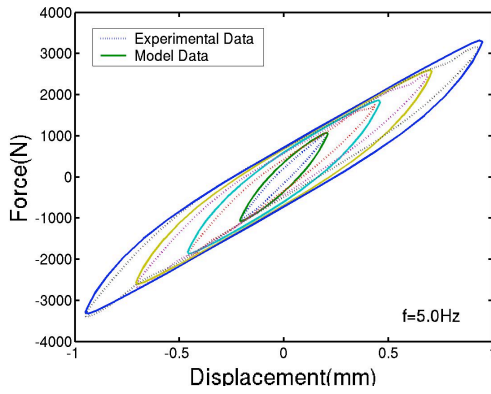


(c) Loss factor

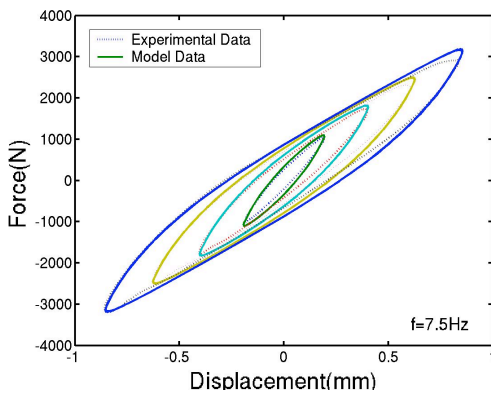
Figure 3.12: Variation of Complex Modulus with Dynamic Amplitude for Elastomeric Specimen



(a) 2.5Hz

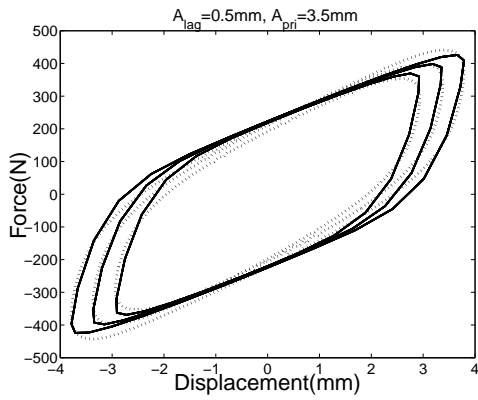


(b) 5.0Hz

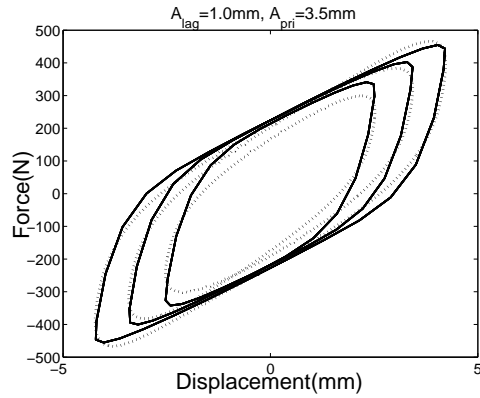


(c) 7.5Hz

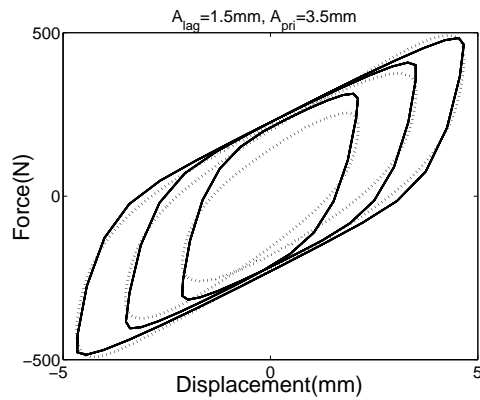
Figure 3.13: Single Frequency Hysteresis Modeling for Elastomeric Damper



(a) 3.5mm @ 7.5Hz, 0.5mm @ 5.0Hz

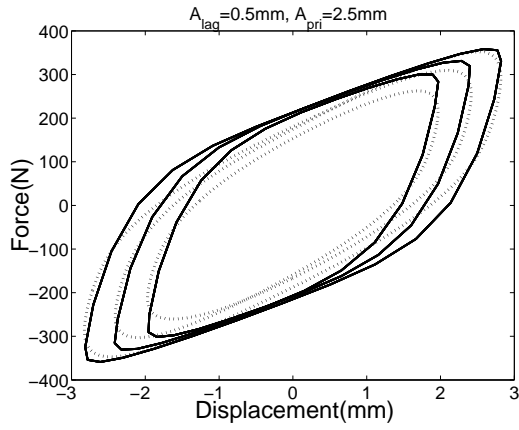


(b) 3.5mm @ 7.5Hz, 1.0mm @ 5.0Hz

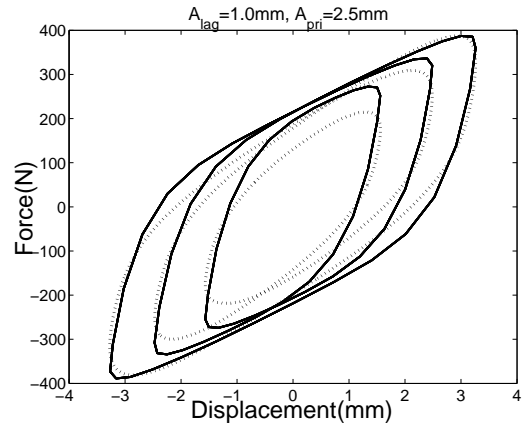


(c) 3.5mm @ 7.5Hz, 1.5mm @ 5.0Hz

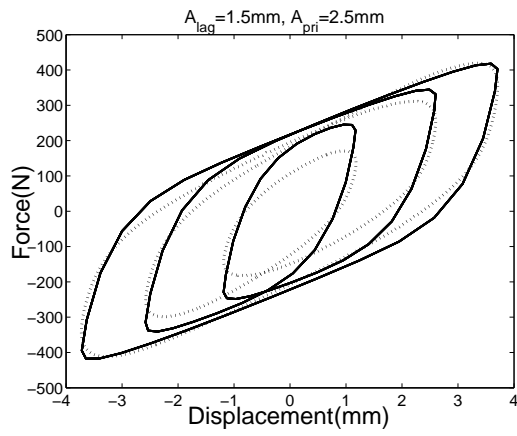
Figure 3.14: Dual Frequency Hysteresis Modeling for Elastomeric Specimen



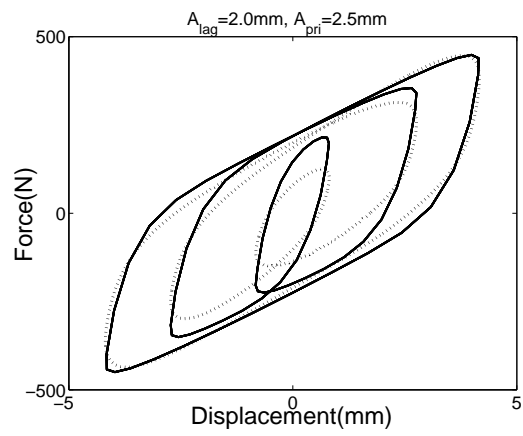
(a) 2.5mm @ 7.5Hz, 0.5mm @ 5.0Hz



(b) 2.5mm @ 7.5Hz, 1.0mm @ 5.0Hz

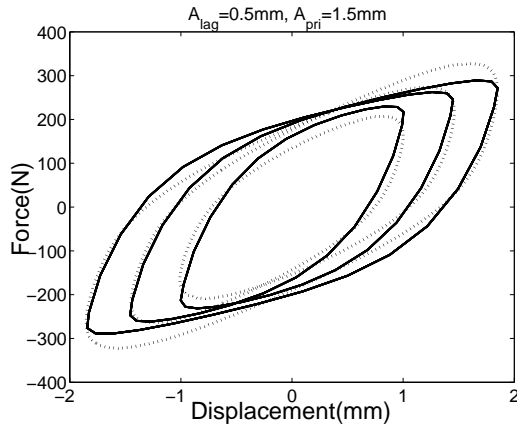


(c) 2.5mm @ 7.5Hz, 1.5mm @ 5.0Hz

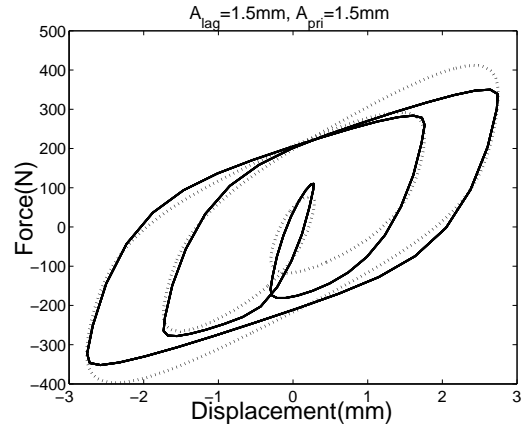


(d) 2.5mm @ 7.5Hz, 2.0mm @ 5.0Hz

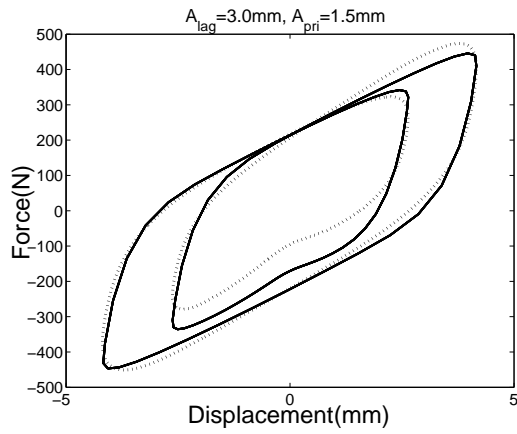
Figure 3.15: Dual Frequency Hysteresis Modeling for Elastomeric Specimen



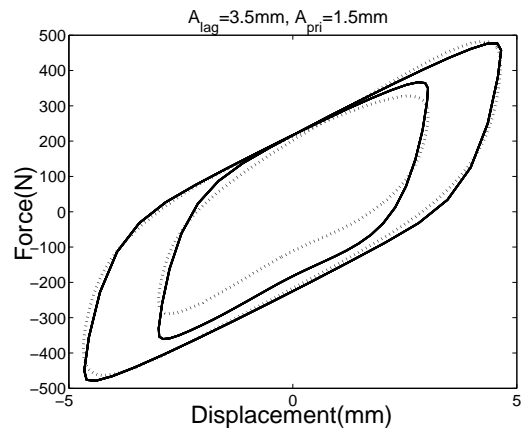
(a) 1.5mm @ 7.5Hz, 0.5mm @ 5.0Hz



(b) 1.5mm @ 7.5Hz, 1.5mm @ 5.0Hz

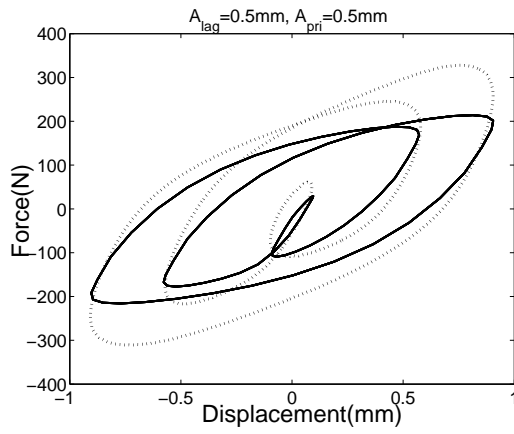


(c) 1.5mm @ 7.5Hz, 3.0mm @ 5.0Hz

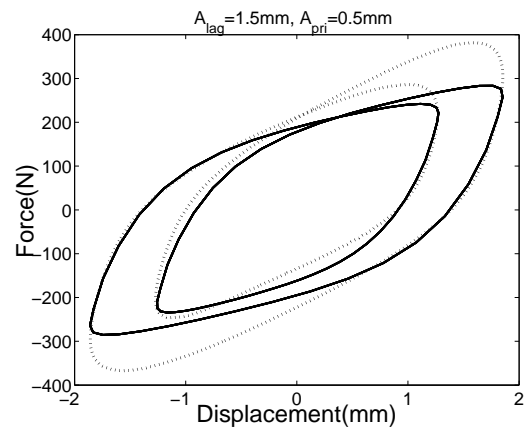


(d) 1.5mm @ 7.5Hz, 3.5mm @ 5.0Hz

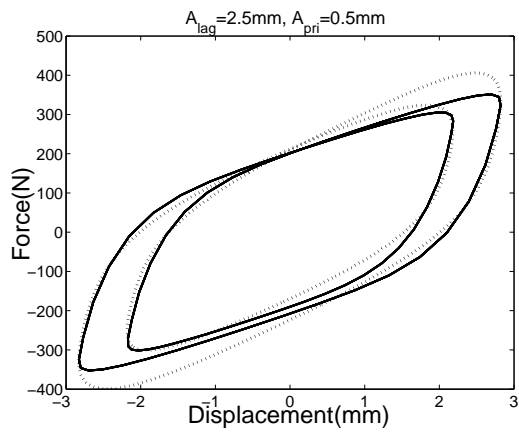
Figure 3.16: Dual Frequency Hysteresis Modeling for Elastomeric Specimen



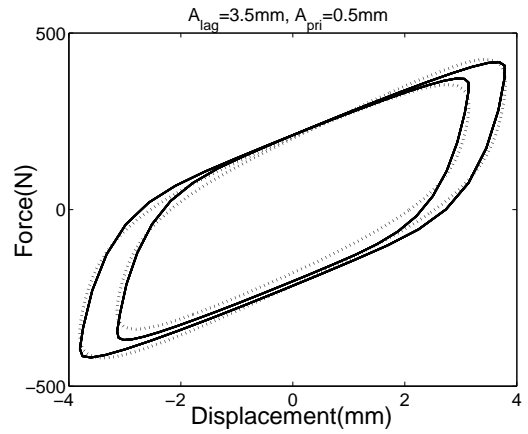
(a) 0.5mm @ 7.5Hz, 0.5mm @ 5.0Hz



(b) 0.5mm @ 7.5Hz, 1.5mm @ 5.0Hz

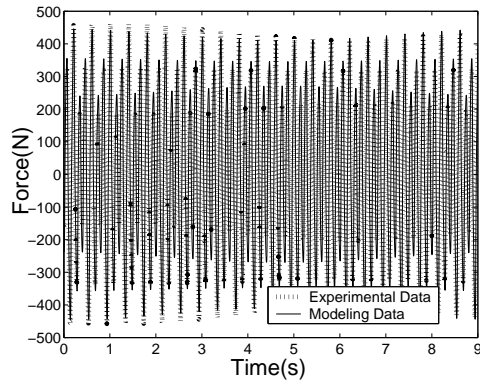


(c) 0.5mm @ 7.5Hz, 2.5mm @ 5.0Hz

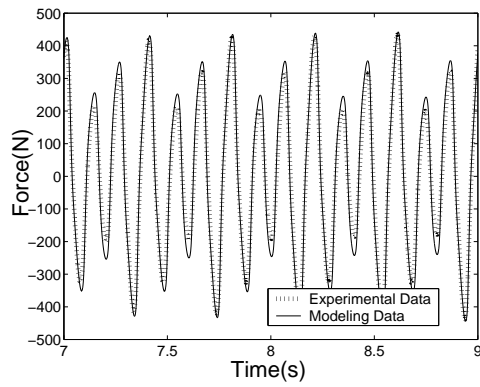


(d) 0.5mm @ 7.5Hz, 3.5mm @ 5.0Hz

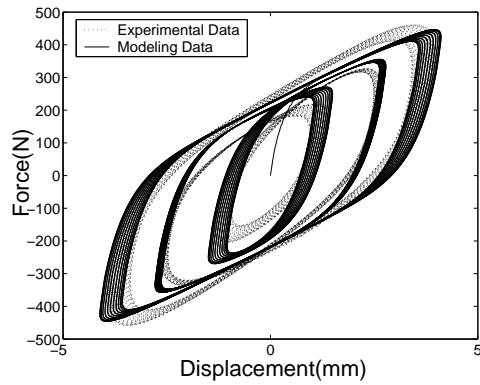
Figure 3.17: Dual Frequency Hysteresis Modeling for Elastomeric Specimen



(a) Forced Response (0-9 Seconds)



(b) Forced Response (7-9 Seconds)



(c) Force-Displacement Hysteresis

Figure 3.18: Modeling Results for Dual Frequency with Slowly Varying Amplitude

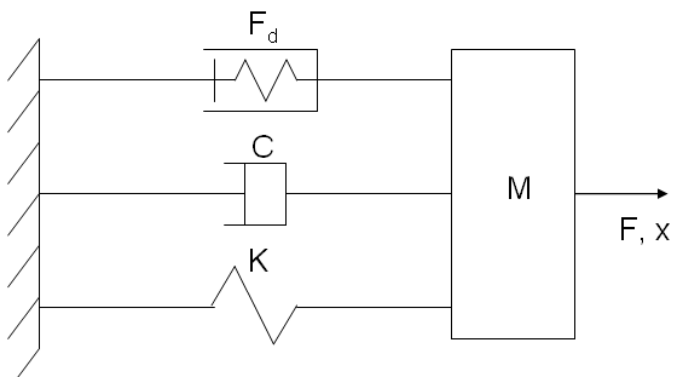


Figure 3.19: Dynamic Oscillator

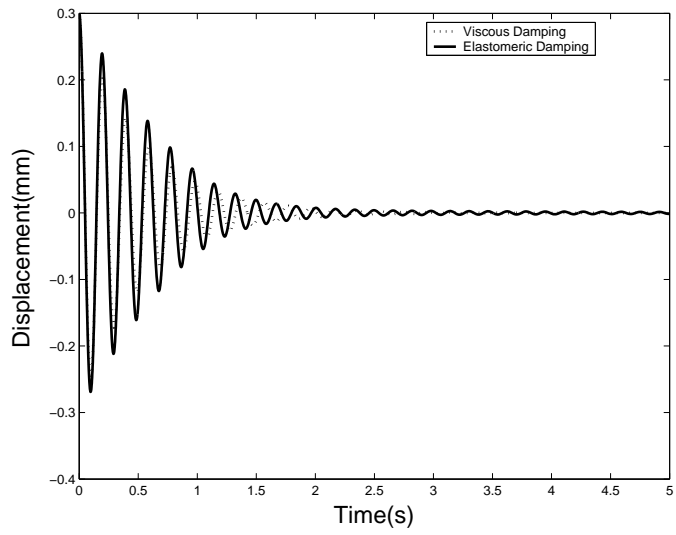


Figure 3.20: Transient Response with Displacement Perturbation and Nominal System Damping Ratio 5%

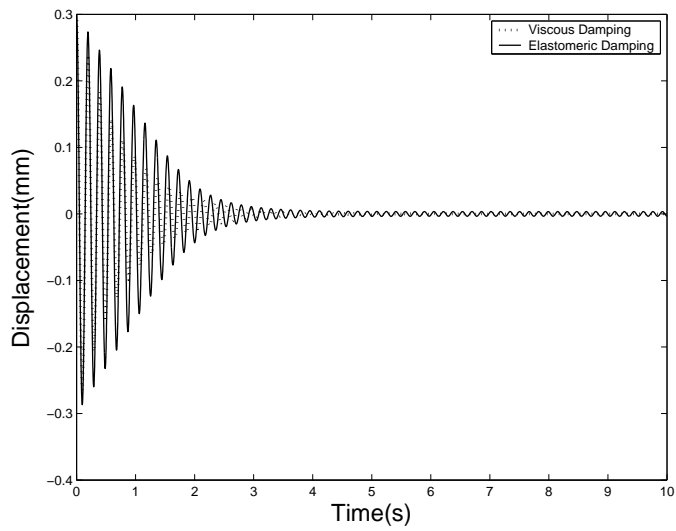


Figure 3.21: Transient Response with Displacement Perturbation and Zero System Damping

## Chapter 4

# MRFE Damper Design and Analysis

Magnetorheological (MR) fluids have attracted much attention as a functional fluid for improving the properties of mechanical systems and in the development of new devices. Many MR device design methods have been developed, and several design parameters related with MR or similar ER damper have been established for design optimization (Refs. [67–70]). However, most design methods are based on an idealized MR valve in which only field activated gaps were considered. In this chapter, an MR valve fluid dynamic analysis is conducted based on a flow-mode MR valve configuration. The effect of the MR circuit and leaking path on the damping performance of the MR valve is investigated. Combined with experimentally obtained elastomeric data, damping performance of an MRFE damper is evaluated using analytical equivalent damping. As a basis for developing a comprehensive MRFE damper design code, design directives are established and a damping objective is given.

## 4.1 MR Flow Mode Analysis

The MR component to be incorporated into the proposed MRFE damper is a flow-mode MR damper, and the design analysis will be carried out using the flow-mode analysis [35]. The MR fluid behavior in steady shear flow mode is characterized by an idealized Bingham plastic model, in which the constitutive relationship between the post-yield shear stress,  $\tau$ , and the shear strain,  $\gamma$ , can be expressed as:

$$\tau = \tau_y \text{sgn}(\dot{\gamma}) + \mu \dot{\gamma}, \tau > \tau_y \quad (4.1)$$

Here,  $\tau_y$  is a field dependent yield stress, and  $\mu$  is a plastic viscosity. Both  $\tau_y$  and  $\mu$  are MR material properties. Performance of an MR valve resides not only in MR fluid properties but also in the hydraulic mechanism design of the MR valve.

In a flow mode valve, there are two flow paths existing in the MR valve, and the damping force due to an applied shaft velocity is developed because of the pressure drop through the flowing paths. Figure 4.1 shows the schematic of an flow mode MR valve, in which a piston is seated inside a fluid chamber. One major flow path is the active flow path shown as the gap across the piston, in which  $d_a$  is the gap width and  $L$  is the total length of the gap. In certain MR valve configurations, an interior volume of fluid in the gap length  $L_m$  cannot be activated due to the existence of the magnetic circuit, so only the fluid in the length  $L_a$  is field activated. As a result, the pressure drop  $\Delta P$  across the active flow path consists of effects of  $L_a$  and  $L_m$ , denoted as  $\Delta P_a$  and  $\Delta P_m$ , respectively. An additional passive flow path appears between the piston and the chamber wall since the piston translates relatively to the chamber, and the

width and length of the passive flow path are denoted as  $d_p$  and  $L_p$ , respectively. Thus, the damper force includes the effect of the active and passive volumes of fluid, i.e. the effect of  $d_a$ ,  $d_p$ ,  $L_a$ ,  $L_m$  and  $L_p$ .

The MR valve is assumed to operate in a quasi-steady state. Thus, neglecting fluid inertia effect, the governing equation for flow through the field activated gap, is

$$\frac{d\tau}{dy} = -\frac{\Delta P_a}{L_a} \quad (4.2)$$

where,  $y$  is the local coordinate perpendicular to the axis of the active gap. To predict the damping force developed by forcing fluid through the field activated valve, the velocity profile through the gap must be first predicted as a function of the piston or shaft velocity,  $v$ . The typical velocity profile across the gap in a flow mode valve is illustrated in Figure 4.2, where  $u(y)$  is the fluid velocity inside the gap. Since the pressure distribution across the gap width is assumed uniform while using the parallel plate assumption, the velocity profile is symmetric about the center of the annular gap. Thus, let the coordinate  $y$  originate at the centerline of the parallel plates, and decompose the velocity profile into three regions. Regions 1 and 3 are post-yield regions, in which the shear stress exceeds the dynamic yield stress  $\tau_y$  and the material is in fluid mode. In both regions, the velocity gradient,  $\frac{du}{dy}$ , is not equal to zero, and the fluid properties can be described by the Bingham model, as

$$\begin{aligned} \tau_1(y) &= \tau_y + \mu \frac{du}{dy} \\ \tau_3(y) &= -\tau_y - \mu \frac{du}{dy} \end{aligned} \quad (4.3)$$

Region 2 is the pre-yield region, where the velocity across the region is constant. Therefore, the flow behavior in region 2 is similar to a solid plug, and the thickness of the plug is denoted as  $\delta$ . The plug thickness and its location in the gap

can be determined using the shear stress boundary conditions. Using symmetry arguments for the parallel plate geometry assumed here, the plug is located symmetrically about the flow velocity axis as shown in Figure 4.2. Thus, the top edge of the plug is located at

$$y = \frac{\delta}{2} \quad (4.4)$$

and the bottom edge is located at

$$y = -\frac{\delta}{2} \quad (4.5)$$

Moreover, the shear stress in the plug is given by integrating Eq. 4.2,

$$\tau = -\frac{\Delta P_a}{L_a}y + A_2 \quad (4.6)$$

Since the boundary conditions for region 2 are

$$\begin{aligned} \tau\left(-\frac{\delta}{2}\right) &= \tau_y \\ \tau\left(\frac{\delta}{2}\right) &= -\tau_y \end{aligned} \quad (4.7)$$

yields an expression for the plug thickness

$$\delta = \frac{2L_a\tau_y}{\Delta P_a} \quad (4.8)$$

The plug thickness is a key parameter for the valve action in MR valves. As the field dependent  $\tau_y$  increases, the plug thickness also increases thereby constricting the flow through the valve, increasing the pressure drop and the damping force. On the other hand, the plug will disappear if no field is applied or  $\tau_y = 0$ , so that the flow is nearly Newtonian. To obtain the velocity profile in each region, boundary conditions, compatibility conditions and symmetry conditions must be satisfied. For convenience, the velocity profile in the  $i$ th region is denoted as

$u_i(y)$ . Since for ideal viscous laminar flow there is no slip at the upper and lower walls, so that

$$\begin{aligned} u_1\left(-\frac{d_a}{2}\right) &= 0 \\ u_3\left(\frac{d_a}{2}\right) &= 0 \end{aligned} \quad (4.9)$$

For symmetry geometry, velocity compatibility requires

$$\begin{aligned} u_1\left(-\frac{\delta}{2}\right) &= u_2\left(-\frac{\delta}{2}\right) \\ u_3\left(\frac{\delta}{2}\right) &= u_2\left(\frac{\delta}{2}\right) \end{aligned} \quad (4.10)$$

Velocity gradient compatibility conditions must also be satisfied as the flow governing equation implies that shear stress across the gap should be continuous. Note that the plug moves at a constant velocity, so that the velocity gradient across the plug must be zero. Then, it leads to

$$u'_1\left(-\frac{\delta}{2}\right) = u'_3\left(\frac{\delta}{2}\right) = 0 \quad (4.11)$$

Thus, in region 1 and 3, substituting Eq. 4.1 into Eq. 4.2, the velocity profile is obtained by direct integration, so that

$$u(y) = -\frac{\Delta P_a}{2\mu L_a} y^2 + Ay + B \quad (4.12)$$

Using the boundary conditions,

$$\begin{aligned} u\left(\pm\frac{d_a}{2}\right) &= 0 \\ u'\left(\pm\frac{\delta}{2}\right) &= 0 \end{aligned} \quad (4.13)$$

leads to the velocity profile for region 1,

$$u_1(y) = \frac{\Delta P_a}{2\mu L_a} \left[ \left( \frac{d_a}{2} - \frac{\delta}{2} \right)^2 - \left( y + \frac{\delta}{2} \right)^2 \right] \quad (4.14)$$

and the velocity profile for region 3,

$$u_3(y) = \frac{\Delta P_a}{2\mu L_a} \left[ \left( \frac{d_a}{2} - \frac{\delta}{2} \right)^2 - \left( y - \frac{\delta}{2} \right)^2 \right] \quad (4.15)$$

In region 2, considering velocity continuity Eq. 4.10, the velocity of the pre-yield plug is obtained

$$u_2(y) = \frac{\Delta P_a}{2\mu L_a} \left( \frac{d_a}{2} - \frac{\delta}{2} \right)^2 \quad (4.16)$$

Considering the effect of the magnetic circuit and the passive flow path, the MR fluid flowing through the passive gap is characterized by the Newtonian behavior. Thus, the velocity profile along the passive gap is described by

$$u_m(y) = \frac{\Delta P_m}{2\mu L_m} \left[ \left( \frac{d_a}{2} \right)^2 - y^2 \right] \quad (4.17)$$

and

$$u_p(y) = \frac{\Delta P_p}{2\mu L_p} \left[ \left( \frac{d_p}{2} \right)^2 - y^2 \right] \quad (4.18)$$

where,  $u_m(y)$  is the velocity profile in the passive region of the active flow path and the gap width is assumed the same as the active gap width, and  $u_p(y)$  is the velocity profile in the passive flow path.

The volume flux through the active flow path,  $Q_a$ , can be obtained by integrating the velocity profile along the active gap width as

$$\begin{aligned} Q_a &= A_a \int_{-\frac{d_a}{2}}^{\frac{d_a}{2}} u(y) dy \\ &= \frac{\Delta P_a A_a d_a^2}{12\mu L_a} (1 - \bar{\delta})^2 \left( 1 + \frac{\bar{\delta}}{2} \right) \end{aligned} \quad (4.19)$$

where,  $A_a$  is the cross-sectional area of the active gap, and

$$\bar{\delta} \triangleq \frac{\delta}{d_a} \quad (4.20)$$

Since the MR volume flux through the active region of the active flow path is the same as the volume flux through the passive region due to the magnetic circuit,  $Q_a$  is also described by

$$Q_a = \frac{\Delta P_m A_a d_a^2}{12\mu L_m} \quad (4.21)$$

As the pressure drop across the piston is

$$\Delta P = \Delta P_a + \Delta P_m \quad (4.22)$$

$Q_a$  can be rewritten as a function of  $\Delta P$  as

$$Q_a = \frac{\Delta P A_a d_a^2}{12\mu L_a} \frac{(1 - \bar{\delta}^2) \left(1 + \frac{\bar{\delta}}{2}\right)}{\left(\frac{L}{L_a} - 1\right) (1 - \bar{\delta}^2) \left(1 + \frac{\bar{\delta}}{2}\right) + 1} \quad (4.23)$$

Similarly, the MR volume flux through the passive flow path is determined as

$$Q_p = \frac{\Delta P A_p d_p^2}{12\mu L_p} \quad (4.24)$$

where,  $A_p$  is the cross-sectional area of the passive gap. Due to the continuity of flow, equating the volume flux through the flow paths to the volume flux displaced by relative motion between the piston and chamber wall with a constant velocity, yields

$$Q = Q_a + Q_p = vA \quad (4.25)$$

where,  $A$  is an effective cross-sectional area of the piston, and  $v$  is the velocity of the relative motion. The relationship between  $\Delta P$  and shaft velocity  $v$  is described as

$$\frac{\Delta P d_a^2}{12\mu L_a} \left[ A_a \frac{(1 - \bar{\delta}^2) \left(1 + \frac{\bar{\delta}}{2}\right)}{\left(\frac{L}{L_a} - 1\right) (1 - \bar{\delta}^2) \left(1 + \frac{\bar{\delta}}{2}\right) + 1} + A_p \frac{d_p^2 L_a}{d_a^2 L_p} \right] = vA \quad (4.26)$$

Using Eq. 4.26, the MR valve behavior can be determined for either an applied load or an applied velocity. Moreover, equivalent damping analysis and MR valve design code can be developed from Eq. 4.26.

## 4.2 MR Valve Design

Since the controllable damping capability of the MRFE damper is determined by the MR valve, the main task for the MRFE damper design is the MR valve design. To design an effective MR valve, the MR fluid flow path geometry should be determined to induce required minimum and maximum damping, and the configuration of the MR circuit also should be determined to apply a significant magnetic field on the MR fluids to obtain a controllable damping objective.

### 4.2.1 Determine MR Valve and Performance

As a basis for MRFE damper design, equivalent viscous damping is used to evaluate semi-active damping capability of the MRFE damper compared with the experimental results. Since  $\Delta P$  is related to the damping force due to the MR valve,  $F_{MR}$ , as

$$\Delta P = \frac{F_{MR}}{A} \quad (4.27)$$

From Eq. 4.26, the MR valve behavior can be described by an equivalent damping which is defined as the ratio between the damping force and the shaft velocity, and is expressed as

$$\begin{aligned} C^{MR} &\triangleq \frac{F_{MR}}{v} \\ &= \frac{12\mu L_a}{A_a} \left(\frac{A}{d_a}\right)^2 \frac{\left(\frac{L}{L_a} - 1\right) (1 - \bar{\delta}^2) \left(1 + \frac{\bar{\delta}}{2}\right) + 1}{(1 - \bar{\delta}^2) \left(1 + \frac{\bar{\delta}}{2}\right) \left(1 + \frac{A_p}{A_a} \frac{d_p^2}{d_a^2} \frac{L - L_a}{L_p}\right) + \frac{A_p}{A_a} \frac{d_p^2}{d_a^2} \frac{L_a}{L_p}} \end{aligned} \quad (4.28)$$

As  $\bar{\delta} = 0$ , the Field-OFF Newtonian damping,  $C_0^{MR}$ , is obtained by

$$C_0^{MR} \triangleq 12\mu L_a \left(\frac{A}{d_a}\right)^2 \frac{1}{A_a \frac{L_a}{L} + A_p \left(\frac{d_p}{d_a}\right)^2 \left(\frac{L_a}{L_p}\right)} \quad (4.29)$$

which represents the viscous damping in the absence of field. When  $\bar{\delta} = 1$ , a Field-ON viscous damping,  $C_1^{MR}$ , is determined by:

$$C_1^{MR} \triangleq 12\mu L_a \left( \frac{A}{d_a} \right)^2 \frac{1}{A_p \left( \frac{d_p}{d_a} \right)^2 \left( \frac{L_a}{L_p} \right)} \quad (4.30)$$

which represents the viscous damping when the flow through the field activated gap is blocked. Since  $\bar{\delta}$  varies between 0 and 1 as the applied field and velocity are varied, the damping coefficient of the MR valve is varied between  $C_0^{MR}$  and  $C_1^{MR}$ . To determine  $\bar{\delta}$  and then  $C^{MR}$ , substitute Eq. 4.20 into Eq. 4.26, and yields a quadrinomial function as

$$\left[ \frac{6\mu v}{\tau_y d_a} \frac{A}{A_a} \left( \frac{L}{L_a} - 1 \right) \bar{\delta} - 1 \right] (1 - \bar{\delta}^2) \left( 1 + \frac{\bar{\delta}}{2} \right) + \frac{6\mu v}{\tau_y d_a} \bar{\delta} - \frac{A_p}{A_a} \left( \frac{d_p}{d_a} \right)^2 \frac{L_a}{L_p} = 0 \quad (4.31)$$

Since a piston shaft velocity and an applied field are known, the nondimensional plug thickness is determined using Eq. 4.31 and the MR valve equivalent damping is found from Eq. 4.28. Thus, the MR valve performance can be evaluated using the equivalent damping as a function of the applied field and the velocity.

In addition, the quasi-steady relationship between damping force and the shaft velocity of the MR valve can be obtained using Eq. 4.28 for four different configuration conditions, i.e. (a) ideal valve (no effect of the magnetic circuit and the passive flow path), (b) effect of the magnetic circuit only, (c) effect of the passive flow path only, and (d) effect of both circuit and passive flow path. As shown in Figure 4.3, the effect of the magnetic circuit is demonstrated by a increase in postyield viscous damping, and the effect of the leakage is shown by an emergence of the preyield viscous damping which is the typical preyield behavior demonstrated by a flow mode MR valve or damper. However, both magnetic circuit and leakage path do not lead to dramatic changes for the field-dependent yield force.

Clearly, the MR valve damping at any applied current and velocity can be evaluated using basic MR fluid motion analysis, geometry data and material properties. On the other hand, to design an MR valve, the damper geometry size has to be determined using prescribed design objectives and various constraints. Those design objectives include controllable damping range, maximum or minimum damping force and operating velocity range, etc., and the prescribed constraints usually are maximum diameter and length, damper stroke, and power requirements. Based on the equivalent damping analysis, a practical MR valve design can be conducted using an iterative process as the design parameters are prescribed. The initial valve sizing will be accomplished by the following three constraints:

- The maximum controllable damping objective  $C_{\text{obj}}$  requires

$$C_{\text{obj}} \leq C_1^{\text{MR}} = 12\mu L_a \left( \frac{A}{d_a} \right)^2 \frac{1}{A_p \left( \frac{d_p}{d_a} \right)^2 \frac{L_a}{L_p}} \quad (4.32)$$

such that the first constraint is

$$\text{I} : \frac{A^2 L_p}{A_p d_p^2} \geq \frac{C_{\text{obj}}}{12\mu} \quad (4.33)$$

- Due to the existence of the passive flow path, an optimum damper velocity range is required to obtain a constant maximum equivalent damping within this range, i.e. a damper velocity limit for required maximum equivalent damping,  $v_{\text{cr}}$ , should satisfy

$$v \leq v_{\text{cr}} = \frac{(\tau_y)_{\text{max}}}{6\mu} \frac{A_p}{A} \frac{d_p^2}{d_a} \frac{L_a}{L_p} \quad (4.34)$$

This leads to the second constraint

$$\text{II} : \frac{A_p d_p^2 L_a}{A d_a L_p} \geq \frac{6\mu v_{\text{cr}}}{(\tau_y)_{\text{max}}} \quad (4.35)$$

- A damping control range is defined by a ratio,  $\lambda$ , between the maximum Field-ON and Field-OFF damping:

$$\lambda = \frac{C_1^{\text{MR}}}{C_0^{\text{MR}}} \leq \frac{A_a + A_p \left(\frac{d_p}{d_a}\right)^2 \left(\frac{L_a}{L_p}\right)}{A_p \left(\frac{d_p}{d_a}\right)^2 \left(\frac{L_a}{L_p}\right)} \quad (4.36)$$

results in the third constraint

$$\text{III : } \frac{A_p}{A_a} \left(\frac{d_p}{d_a}\right)^2 \frac{L_a}{L_p} \leq \frac{1}{\lambda - 1} \quad (4.37)$$

In accordance with damper geometry constraints, the effective piston area,  $A$ , can be chosen first. Thus, using the Constraint I, passive flow path parameters,  $A_p$ ,  $d_p$  and  $L_p$  are determined initially, and the thickness and length of the active gap,  $d_a$  and  $L_a$  would be given using Constraint II and Constraint III. If these results do not satisfy the practical geometric constraints, a new choice of  $L_p$  and  $d_p$  are chosen again until the iteration reaches a physically acceptable result.

## 4.2.2 Magnetic Circuit Design

The MR effect of MR fluid is actuated by passing a magnetic field perpendicular to the direction in which the fluid is flowing. This field causes the micron-sized magnetizable particles in the fluid to form chains, which will remain intact below a yield shear stress in the fluid. It is this yield stress which characterizes the magnetorheological properties of MR fluid. The presence of these chains within a fluid obstructs fluid flow through a gap, which is used to alter the damping properties of a fluid damper. Thus, the objective of the magnetic circuit design is to maximize the magnetic field across the fluid gap to increase the yield stress of the fluid, which in turn will increase the performance of the MRFE damper.

In practice, MR circuits use high-magnetic-permeability materials in conjunction with magnetic solenoids to guide a controllable magnetic field across the fluid gap. As shown in Figure 4.1, the magnetic circuit uses the entire of the piston to create the magnetic field. The field first flows through the center of the piston, shunts outward through the upper arms, across the gap across the piston, and then returns the field through the piston. Considerations in designing a magnetic circuit are made to avoid magnetic flux saturation in the circuit, which will decrease the field available at the gap. Saturation can be prevented by increasing the cross-sectional areas of the circuit through which the field flows, or by using a more magnetically-permeable material which can handle higher flux densities.

Several factors should be considered during the initial design of the magnetic circuit. Firstly, the magnetic circuit should have a low reluctance flux conduit to guide and focus magnetic flux into the fluid gap in the MR fluid valve, and sufficient cross-sectional area should be maintained to avoid saturation. Secondly, the size restriction due to the chamber dimension and the damping requirements set a constraint for the magnetic circuit design, and this process is coupled with the MR valve geometry determination. Therefore, the magnetic circuit is designed initially using principle of Continuity of Magnetic Flux, and this design can be optimized by a magnetic FEM analysis.

If the damping objective is known and the magnetic fluid is chosen, the operating point in the MR fluid can be selected to yield a desired yield stress such that the total magnetic flux flowing through the gap is given as

$$\phi = B_g A_g \tag{4.38}$$

where,  $B_g$  is the flux density in the gap and  $A_g$  is the average area of the gap

perpendicular to the magnetic flux. Since the magnetic flux flowing through the magnetic circuit is the same according to the principle of continuity of magnetic flux, the flux density at each cross-section of the magnetic conduit is denoted as

$$B_s = \frac{\phi}{A_s} \quad (4.39)$$

From the B-H curve of the magnetic conduit material, required magnetic field strength at each section,  $H_s$ , is determined. In this step, the cross-sectional area,  $A_s$ , and length,  $L_s$ , of the magnetic conduit can be determined by trading-off between the geometry constrictions and the flux saturation constraint. Then, using Kirchoffs law of magnetic circuits, the required amp-turns of the magnetic circuit would be

$$NI = H_g g + H_s L_s \quad (4.40)$$

where,  $g$  is the gap thickness. After choosing a suitable maximum current,  $I$ , the wire gauge and the required winding turns,  $N$ , can be determined.

### 4.3 MRFE Damping Performance Prediction

Consistent with sinusoidal loading conditions for a helicopter lag damper, single frequency (lag/rev) and dual frequency (lag/rev and 1/rev) sinusoidal loadings are applied to the MRFE damper. As the MR valve is applied by a sinusoidal loading, the damping effect can be characterized by the energy dissipated by the MR valve within one cycle and is quantitatively described by an equivalent viscous damping such that the energy dissipated by a linear viscous damper with this viscous damping over one circle is equal to the energy dissipated by the MR valve. In detail, while a linear viscous damper is applied

by a sinusoidal loading as

$$x = X_0 \sin(\Omega t + \phi) \quad (4.41)$$

the damping force,  $F(t)$ , is proportional to the damper shaft velocity,  $\dot{x}(t)$ , as

$$F(t) = C_{eq}\dot{x}(t) \quad (4.42)$$

and the dissipated energy by the viscous damper is

$$E = \int_0^{\frac{2\pi}{\Omega}} F(t)\dot{x}(t)dt = \pi\Omega X_0^2 \quad (4.43)$$

Similarly, the dissipated energy of the MR valve is

$$E_{MR} = \oint f(t)dx = \int_0^{\frac{2\pi}{\Omega}} f(t)\dot{x}(t)dt \quad (4.44)$$

where  $f$  is the MR valve force under the same loading and is analytically determined by

$$f = C_{MR}\dot{x} \quad (4.45)$$

Since  $C_{MR}$  is the function of  $\dot{x}$ , Eq. 4.44 can be solved numerically using the trapezoidal rule. Equating the energy dissipated by the MR valve to the energy dissipated by the linear viscous damper, the equivalent viscous damping of the MR valve under the sinusoidal loading is:

$$C_{eq}^{MR} = \frac{E_{MR}}{\pi\Omega X_0^2} \quad (4.46)$$

MRFE lead-lag dampers can be designed in different configurations as shown in Figure 1.1(a), 1.1(b), and 1.1(c). However, in each MRFE damper configuration, the contribution of the elastomeric and MR component are considered decoupled. Thus, combined with the determined elastomeric equivalent damping (usually experimentally determined), the total equivalent damping for the MRFE damper is

$$C_{eq} = C_{eq}^{MR} + C_{eq}^{EM} \quad (4.47)$$

where,  $C_{eq}^{EM}$  represents the equivalent damping due to the elastomeric layer in the MRFE damper. The experimental data of the preliminary MRFE damper shown in Figure 1.2 are used to evaluate the equivalent damping performance analysis. In the preliminary MRFE damper, two MR dampers are combined in parallel with an elastomeric damper. The linear stroke MR damper used for this study is a commercially available truck seat damper manufactured by the Lord Corporation [70], and the silicone based filled elastomeric damper, in the form of double lap shear specimen, was provided by Barry Controls [71]. As the MRFE damper is subjected to a sinusoidal loading at a nominal lag frequency (5 Hz), the comparison between the analytical and experimental equivalent damping is shown in Figure 4.4, where the applied currents are 0, 0.1, 0.2 and 0.3 A, respectively. Similar to the experimental equivalent damping (solid line), the analytical equivalent damping (dashed line) demonstrates amplitude dependent behavior and a damping augmentation effect due to the applied current. The equivalent damping characteristics at 1/rev (7.5 Hz) are similar to that at lag/rev (5 Hz) except that the equivalent damping at higher frequency is smaller than damping at lower frequency. Therefore, the equivalent damping analysis can capture both amplitude and frequency dependent damping characteristics demonstrated by the MR valve or damper.

## 4.4 Conclusion

In this chapter, quasi-steady damping analysis was conducted for flow mode MR dampers with an approximate parallel plate assumption. Using idealized Bingham constitutive model to characterize the MR fluid behavior, the equiva-

lent damping as a function of the applied field and velocity was derived. Therefore, for a constant shaft velocity, the damping control capacity under different fields control can be predicted. Based on the quasi-steady analysis, MRFE damper design directives were developed, and the magnetic circuit design was also described. In the next chapter, the development of a concentric bearing type MRFE damper will be introduced, and the damping performance of the MRFE damper will be investigated both analytically and experimentally.

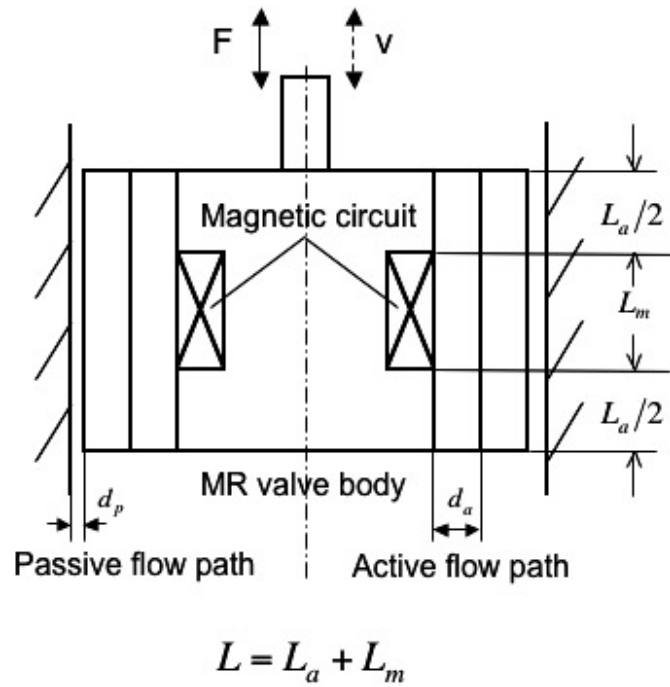


Figure 4.1: Flow-mode MR Valve Mechanism

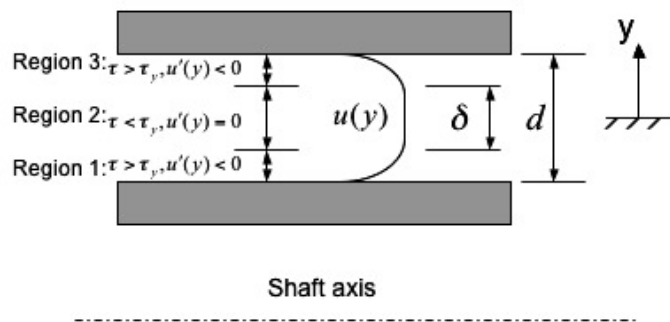
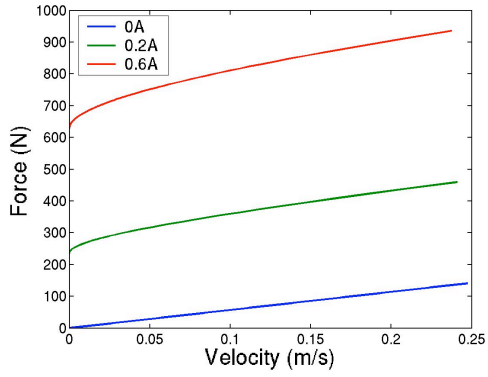
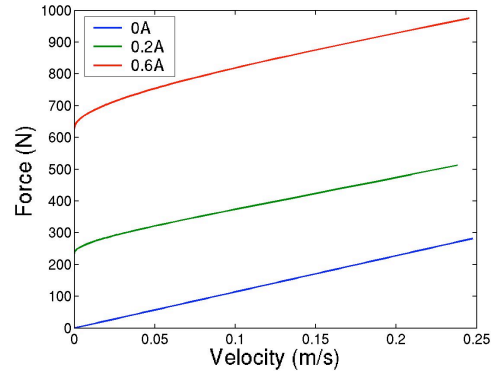


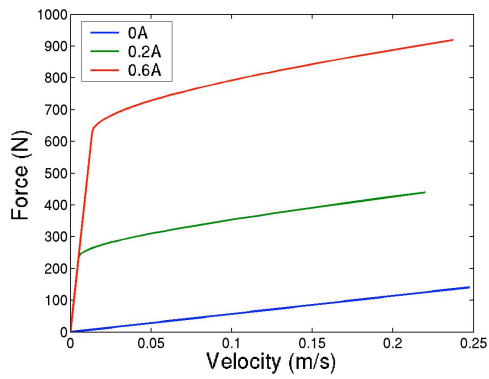
Figure 4.2: Typical Velocity Profile



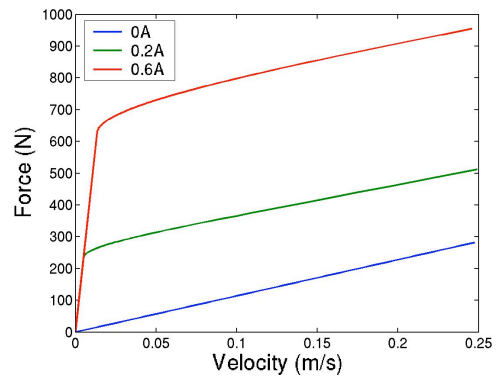
(a) Ideal MR Valve



(b) Effect of Magnetic Circuit

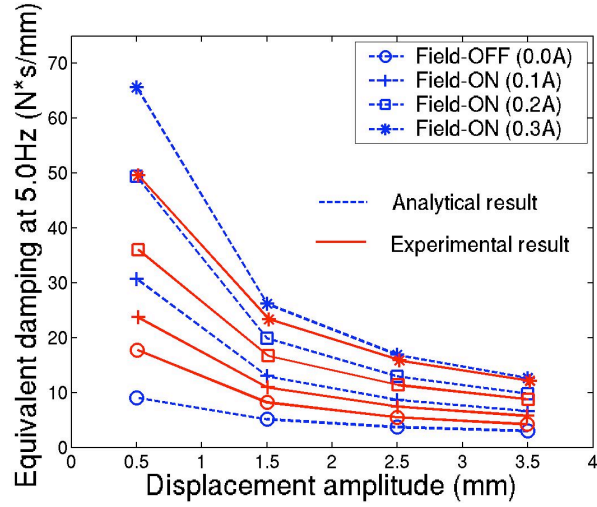


(c) Effect of Passive Flow Path

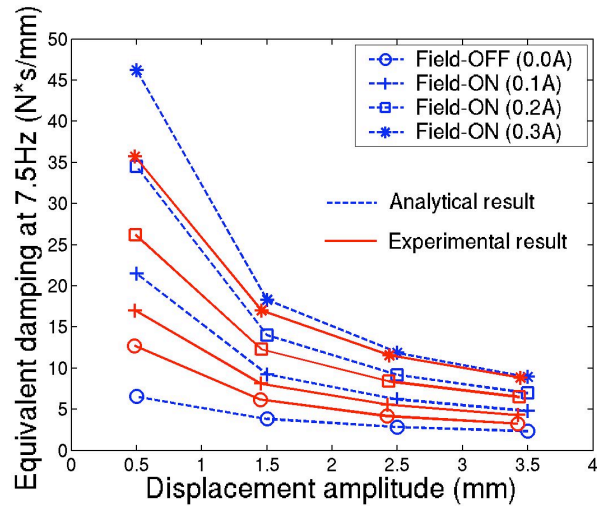


(d) Effect of Magnetic Circuit and Passive Flow Path

Figure 4.3: Analytical Quasi-Steady MR Valve Behavior



(a) Damping Characteristics at lag/rev



(b) Damping Characteristics at 1/rev

Figure 4.4: MRFE Equivalent Damping Prediction

## Chapter 5

# Characterization and Modeling for MRFE Damper

A major concern for an MR lag damper, as for any hydraulic damper, is fluid leakage, so that the combination of elastomeric materials and MR fluids in a lag damper becomes a rational choice ensuring some level of fail-safe damping in the event of fluid loss. First, elastomeric materials can contribute stiffness to the lead-lag mode of blades. Second, an elastomer itself can act as a flexible sealant material to eliminate the possibility of leakage. Third, the kinematical complexity in modern bearingless or hingeless helicopter main rotors requires a flexible damper body to allow for multiple degrees of freedom such that damper chamber is usually made from a laminated stack of alternating elastomeric-metallic rings, and the flexible damper body provides a housing for damping fluids or MR fluids (e.g. Comanche snubber damper) [24, 42]. The feasibility of a combination of MR fluids and elastomeric materials was studied by an emulation of a magnetorheological fluid and elastic (MRFE) composite damper [25]. This experimental feasibility study validated a considerable damping control range provided by the flow mode MR valve in the MRFE damper. While damping

is provided by the combination of the elastomer and MR fluid, this preliminary MRFE damper can actively augment damping over critical frequency ranges and enhance the stability of helicopter rotors. While the stiffness in the elastomer is still available as a design parameter, the MR and elastomeric damping elements of the MRFE damper can augment each other. In addition, the passive damping in both the elastomer and MR damping elements provides a fail-safe damping in the event that control of the field dependent MR damping is lost.

This chapter focuses on developing a linear stroke MRFE lag damper as a retrofit to an existing concentric elastomeric bearing type lag damper and evaluating its controllable damping capacity under loading conditions encountered by the baseline elastomeric damper. The MRFE damper is developed by incorporating an MR valve into the inner chamber of the baseline concentric elastomeric damper. A fixture setup is designed to hold the MRFE damper on a material testing machine such that the uniaxial motion of the loading actuator results in a shear deformation of the elastomer and a uniaxial MR valve translation through an MR fluid reservoir. Complex modulus and equivalent damping are used to characterize the MRFE damper. It will be shown that the Field-OFF damping of the MRFE damper is comparable to that of the baseline elastomeric damper, and the damping capacity of the MRFE damper can be controlled by varying applied field. Performance predictions using quasi-steady nonlinear Bingham-plastic fluid flow analysis and elastomeric characteristic data are conducted as a basis for developing a comprehensive MRFE damper design code, and the analytical equivalent viscous damping is validated by the experimental results.

Linearized constants, such as equivalent viscous damping, are not sufficient to uniquely define the dynamic behavior of the MRFE damper as applied to a

helicopter rotor lag damper, and a precise damper model plays an important role in the choice of the control strategy for a given application [27,29]. Therefore, an MRFE time domain model is developed to describe the nonlinear behavior of the MRFE damper, especially the single and dual frequency hysteretic behavior. In this model, the distributed elasto-slide element is used to describe the behavior of the filled elastomer, and the field dependent elasto-slide is used to represent the behavior of the MR valve. Model parameters are determined by extracting the basic characteristics from a virtual initial loading curve derived from steady state sinusoidal forcing data. Compared with these elastomeric damper models developed in Refs. [50, 51, 54, 58], and MR models developed in Refs. [18, 42, 44, 46], the unique advantage of the MRFE damper model developed in this study is that it can capture amplitude and frequency dependent behavior demonstrated by the MRFE damper and can be applied in any complex loading conditions, by resorting to neither amplitude dependent nor frequency dependent model parameters.

## 5.1 Damper Setup and Testing

The MRFE damper is made from a linear stroke concentric elastomeric bearing damper and an enclosed MR valve, as shown in Figure 5.1. The linear stroke elastomeric damper was provided by Hutchinson Aerospace and is treated as the baseline damper for MRFE damper evaluation. The baseline elastomeric damper is made of two concentric cylindrical metal tubes, with an elastomeric layer sandwiched between the outer and inner tubes. The volume enclosed by the inner tube forms a cylindrical inner chamber, and a threaded trapezoidal col-

umn is attached to one end of the inner tube. The outer tube is attached to the rotor head, and the inner tube connected to the blade root. Thus, the lead-lag motion of the blade induces a relative translation between the inner tube and the outer tube, which in turn leads to a shear deformation of the elastomer along the damper body length. The deformation of the elastomer provides required stiffness and damping for the lead-lag mode of the rotor blade, but the stiffness and damping of the damper are passive and cannot be varied as flight conditions are varied. Therefore, using an MR valve compatible in size with the inner chamber, a simplified full scale MRFE damper is constructed. The MR valve is composed of an MR fluid chamber and a piston seated in the chamber. The fluid chamber is fixed relative to the inner tube, and the piston is fixed relative to the outer tube. The relative motion between the inner and outer tube forces the MR fluid to flow through the field activated gaps in the piston, so that field dependent damping force is added to the output force of the damper.

To simulate the loading conditions applied to the MRFE lag damper, a test fixture was designed to hold the MRFE damper in a 24.466 kN (5000 lbs) MTS servo-hydraulic testing machine. The MRFE test setup is shown in Figure 5.2, in which the inner tube of the baseline damper and MR fluid chamber is connected together with the load cell of the MTS machine by a screw adapter, and the outer tube of the elastomeric damper and the piston of the MR valve are connected to the actuator on the MTS loading frame using a tension rod configuration. Thus, the axial translation of the actuator results in shear deformation of the elastomeric component and MR piston motion inside the MR fluid chamber. The displacement LVDT sensor of the MTS machine was used for displacement measurement and the load cell for measuring the force. The frequency range

of the excitation was chosen appropriate for a rotor system at  $\omega_1=7.5$  Hz, the baseline 1/rev frequency,  $\omega_{lag}=5.0$  Hz, the lag/rev frequency, and  $\omega_{com}=2.5$  Hz, a lower harmonic of these two. An HP 8904A multi-function synthesizer was used to generate and sum the sinusoidal signals for dual frequency tests. A DC power supply provided current control for the MR component during testing. Damper testing was carried out with varying excitation amplitudes and magnetic fields. All tests were conducted at room temperature (25°C).

The applied currents were in the range of 0-0.8 A in increments of 0.2 A. For each applied current, the MRFE damper was tested for single frequency excitation and dual frequency excitation conditions. The single frequency tests were conducted with displacement control for excitation amplitude range from 0.25 mm (10 mil) to 1 mm (40 mil) in increments of 0.25 mm (10 mil) at three different frequencies of  $\omega_1$ ,  $\omega_{lag}$  and  $\omega_{com}$ , respectively. In these tests, 1 mm corresponds to 20% shear strain. For dual frequency tests, the combination of 5 Hz/7.5 Hz was used to evaluate the MRFE damper behavior in helicopter forward flight conditions. The complete array of dual frequency tests for the MRFE damper is given in Table 5.1, in which the symbol  $\times$  indicates the dual frequency test conditions.

During each test, the sampling frequency was chosen as 2048Hz, which is far above the required Nyquist frequency. Nominally, twenty cycles of force and displacement data were measured at each test case. To reduce the noise of the sinusoidal displacement signal, a Fourier series was used to reconstruct the input displacement. The reconstructed displacement signal was then differentiated to obtain the velocity data. Since the MRFE damper produces nonlinear damping force, the measured force was not filtered. However, to reduce the offset in the

measured force due to the presence of the accumulator, the measured bias force was removed using the bias term in the Fourier series expansion of the force.

## 5.2 MRFE Damper Characterization

### 5.2.1 Linearization of Damper Characteristics

To characterize the MRFE damper and compare the MRFE damper with the baseline elastomeric damper, a linearization technique was adopted and equivalent linear constants that serve as comparison metrics were calculated. A typical approach used for characterizing MRFE damper behavior is the complex modulus. The linearized complex modulus,  $K^*$ , is composed of the in-phase or storage stiffness,  $K'$ , and the quadrature or loss stiffness,  $K''$ , as follows:

$$K^* = K' + jK'' \quad (5.1)$$

When the MRFE damper is under single frequency sinusoidal displacement excitation as

$$X = X_c \cos(\omega t) + X_s \sin(\omega t) \quad (5.2)$$

the linearized damper force can be written as the summation of an in-phase spring force and a quadrature damping force, so that the damper force can be approximated by the first Fourier sine and cosine components as

$$\begin{aligned} F(t) &= F_c \cos(\omega t) + F_s \sin(\omega t) \\ &= K' X(t) + \frac{K''}{\omega} \dot{X}(t) \end{aligned} \quad (5.3)$$

where  $F_c$  and  $F_s$  are the first harmonic Fourier coefficients of  $\omega$ . From Eq. 5.2 and Eq. 5.3, the inphase stiffness,  $K'$ , and the quadrature stiffness,  $K''$ , are

determined by the following equations:

$$\begin{aligned} K'(\omega) &= \frac{F_c X_c + F_s X_s}{X_c^2 + X_s^2} \\ K''(\omega) &= \frac{F_c X_s - F_s X_c}{X_c^2 + X_s^2} \end{aligned} \quad (5.4)$$

The loss factor,  $\eta$ , is also used to measure the relative levels of damping to the stiffness. The ratio is written as

$$\eta = \frac{K''}{K'} \quad (5.5)$$

For the case of motion at two or more frequencies simultaneously,  $K'$  and  $K''$  are determined from the oscillatory force and displacement associated with each of the frequencies. Thus, for dual-frequency motion at the frequencies  $\omega_{lag}$  and  $\omega_1$ , the damper response is characterized by  $K_{\omega_{lag}}^*$  and  $K_{\omega_1}^*$  respectively.

Alternatively, a standard linearization technique, equivalent viscous damping, is used to evaluate the damping capacity of the MRFE damper under sinusoidal loading. The equivalent viscous damping is obtained by equating the energy dissipated over a cycle by the MRFE damper to the energy dissipated by an equivalent viscous damper. For a single frequency loading with experimental damper force and displacement data,  $F$  and  $X$ , the dissipated energy of the MRFE damper over a cycle,  $E$ , at frequency,  $\omega$ , is calculated

$$E = \oint F(t) dX = \int_0^{\frac{2\pi}{\omega}} F(t) \dot{X}(t) dt \quad (5.6)$$

and the equivalent viscous damping coefficient is given by

$$C_{eq} = \frac{E}{\pi \omega X_0^2} \quad (5.7)$$

where,  $X_0$  is the amplitude of the displacement input. The equivalent viscous damping can be approximately related to the quadrature stiffness by:

$$C_{eq} \approx \frac{K''}{\omega} \quad (5.8)$$

This relationship is approximate because the complex stiffness considers only the harmonic at frequency  $\omega$ . For dual frequency motion, the equivalent damping at lag frequency is determined by Eq. 5.8 using the quadrature stiffness at the lag frequency.

### 5.2.2 Single and Dual Frequency Characteristics

To evaluate the performance of the MRFE lag damper, the elastomeric lag damper was tested, so that characteristics of damping and stiffness could be recorded as a baseline. The lag damper was excited using displacement control using a sinusoidal signal to simulate damper motion due to the lag motion of a blade. The maximum deformation was chosen to be 1 mm (40 mil) as dictated by the shear deformation limitation of the elastomeric damper. One example of an experimental hysteresis cycle is shown in Figure 5.3, in which the loading frequency is 5 Hz and the loading displacement amplitudes are from 0.25 mm to 1 mm. As shown by the hysteresis cycle, the elastomeric damper mostly provides stiffness together with some damping. Using the linearization method, the complex modulus and loss factor of the elastomer are shown in Figure 5.4. Both inphase and quadrature stiffness demonstrate moderate amplitude dependence and weak frequency dependence. Further, the loss factor of the elastomeric damper is quite low (around 0.25 to 0.3) and almost constant for different displacement amplitudes and frequencies.

In comparison, typical force versus sinusoidal displacement data of the MRFE damper are shown in Figure 5.5, in which the baseline elastomeric damper data are shown together with the MRFE damper data at a fixed displacement amplitude and several different applied currents. Clearly, though an MR valve is

combined with the baseline damper, the Field-OFF characteristics of the MRFE damper are similar to those of the baseline damper. This implies that the viscous damping of the MR valve is nearly zero over this amplitude range (0-1 mm), but it may not be true for higher amplitudes. The damping in the MRFE damper, which is represented by the area enclosed within the force versus displacement diagram, includes the effect of both elastomeric and MR components. As the applied current increases, the area enclosed by the force vs. displacement curve, hence the damping, increases dramatically. The slope of the MRFE force vs. displacement curves reflects the stiffness of the elastomer, which varies slightly as current varies implying that most stiffness is contributed by the elastomer.

Complex modulus was also used to characterize the MRFE damper. At a single frequency, the complex modulus and loss factor of the damper are shown in Figure 5.6. Compared with the baseline damper, the Field-OFF MRFE damper provides similar inphase stiffness and quadrature stiffness. As the applied current increases, the index of the damping, i.e. the quadrature stiffness, increases dramatically. Comparatively, the inphase stiffness increases much less than the quadrature stiffness. Thus, the loss factor of the MRFE damper increases significantly over the entire amplitude range (0.5 vs. 0.3 between maximum Field-ON and Field-OFF status). This increase in loss factor implies that the MRFE damper can provide a substantial damping control range (minimum 70% damping increase). Notably, as the applied current increases over 0.8 A, the MR component cannot provide more damping augmentation due to the saturation of the MR circuit. The characteristics of the MRFE damper at different frequencies are also evaluated in terms of inphase stiffness and loss factor as shown in Figure 5.7. As mentioned before, the baseline damper demonstrates weak

frequency dependence over the tested frequency range. For the MRFE damper, the nonlinearity of the MR component leads to a stronger frequency dependent behavior, but the frequency dependence is still insignificant. Comparatively, the complex modulus of the MRFE damper demonstrates similar amplitude dependent behavior to the baseline damper, and the loss factor at each applied current is almost constant along the current amplitude range.

Helicopter lag dampers encounter multi-frequency excitations, especially for regressive lead-lag frequency and 1/rev rotor frequency. Under such a circumstance, the complex modulus of an elastomeric damper at lag frequency decreases significantly due to its amplitude dependent property. Similarly, the complex modulus of the MRFE damper at the lead-lag frequency is reduced as the motion at the 1/rev frequency is increased as shown in Figure 5.8. This effect is particularly dramatic for small lead-lag motion amplitudes. However, as field is applied to the MRFE damper (0.6 A), the complex modulus in Figure 5.8(b) increases dramatically compared with the Field-OFF modulus in Figure 5.8(a).

This damping augmentation effect is also demonstrated by the dual frequency force-displacement hysteresis cycle as shown in Figure 5.9. Notably, as the applied current increases, the area enclosed by the force vs. displacement curve, hence, the damping, increases dramatically.

### **5.2.3 Equivalent Damping of the MRFE Damper**

As a basis for MRFE damper design, analytical equivalent damping is used to evaluate semi-active damping capability of the MRFE damper compared with the experimental results. Since the MR valve in the MRFE damper is in flow mode, damping force is developed because of the pressure drop,  $\Delta P$ , through

a field activated annular gap in the piston,  $d$  in thickness, and a passive gap between the piston and chamber wall,  $d'$  in thickness. The damping force can be determined by equating volume flux through the gaps to the volume flux displaced by the piston. The volume flux flowing through the passive gap,  $Q_{d'}$ , is determined using laminar flow analysis as

$$Q_{d'} = \frac{\Delta P d'^2 A_{d'}}{12\mu l'} \quad (5.9)$$

where,  $A_{d'}$  and  $l'$  are the passive gap area and length, respectively, and  $\mu$  is the post-yield viscous damping of the MR fluid. As the MR fluid behavior is described by the Bingham plastic model, the volume flux flowing through the active gap,  $Q_d$ , is known as (Ref. 25)

$$Q_d = \frac{\Delta P d^2 A_d}{12\mu l} (1 - \bar{\delta})^2 \left(1 + \frac{\bar{\delta}}{2}\right) \quad (5.10)$$

where,  $A_d$  and  $l$  are the active gap area and length, respectively. In addition,

$$\bar{\delta} \triangleq \frac{\delta}{d} = \frac{2l\tau_y}{\Delta P d} \quad (5.11)$$

is the non-dimensionalized plug thickness, and  $0 \leq \bar{\delta} \leq 1$ . The plug thickness  $\delta$  is the flow region in the active gap where the shear stress has not exceeded the yield stress, i.e.  $\tau \leq \tau_y$ .

The yield stress is the function of an applied field or current. The ideal relationship between the yield stress and applied current for the MR fluid is shown in Figure 5.10, which is obtained by an empirical equation as [70]:

$$\tau_y = 271700\nu^{1.5239} \tanh(1.1078I) \quad (5.12)$$

In this equation,  $\nu$  is the volume fraction of the iron particles in the MR fluid, and  $I$  is the applied current. In Figure 5.10, the yield stress of the MR fluids

increases proportionally to the applied current, but saturates above 1 Amp. As the MR valve geometry and the yield force of the MR fluid are known, the quasi-static yield force of the MR valve can be known as shown in Figure 5.11. Similarly, the MR valve demonstrates a small increase in yield behavior for the range of applied current above 1 Amp, as opposed to the much large increase below 1 Amp.

Due to the continuity of flow, equating the volume flux through the gaps to the volume flux displaced by the piston with a constant velocity, yields

$$Q = Q_d + Q_{d'} = vA \quad (5.13)$$

where,  $A$  is the piston area, and  $v$  is a constant shaft velocity. Since  $\Delta P$  is related to the damping force of the MR valve,  $F_{MR}$ , as

$$\Delta P = \frac{F_{MR}}{A} \quad (5.14)$$

From Eq. 5.13, the MR behavior can be described by an equivalent MR damping which is defined as the ratio between the damping force and the shaft velocity, and is expressed as

$$\begin{aligned} C^{MR} &\triangleq \frac{F_{MR}}{v} \\ &= 12\mu l \frac{\left(\frac{A}{d}\right)^2}{(1 - \bar{\delta})^2 \left(1 + \frac{\bar{\delta}}{2}\right) A_d + A_{d'} \left(\frac{d'}{d}\right)^2 \frac{l}{l'}} \end{aligned} \quad (5.15)$$

As  $\bar{\delta} = 0$ , the Field-OFF Newtonian damping,  $C_0^{MR}$ , is obtained by

$$C_0^{MR} \triangleq 12\mu l \left(\frac{A}{d}\right)^2 \frac{1}{A_d + A_{d'} \left(\frac{d'}{d}\right)^2 \left(\frac{l}{l'}\right)} \quad (5.16)$$

which represents the viscous damping in the absence of field. When  $\bar{\delta} = 1$ , a Field-ON viscous damping,  $C_1^{MR}$ , is determined by:

$$C_1^{MR} \triangleq 12\mu l \left(\frac{A}{d}\right)^2 \frac{1}{A_{d'} \left(\frac{d'}{d}\right)^2 \left(\frac{l}{l'}\right)} \quad (5.17)$$

which represents the viscous damping when the flow through the field activated gap is blocked. Since  $\bar{\delta}$  varies between zero and one as the applied field and velocity are varied, the damping coefficient of the MR valve is varied between  $C_0^{MR}$  and  $C_1^{MR}$ . To determine  $\bar{\delta}$  and then  $C^{MR}$ , substitute Eq. 5.11 into Eq. 5.15, and yields a cubic polynomial function as

$$\frac{\bar{\delta}^3}{2} - \left( \frac{3}{2} + \frac{6\mu v}{\tau_y d} \frac{A}{A_d} \right) \bar{\delta} + \left[ 1 + \frac{A'_d}{A_d} \left( \frac{d'}{d} \right)^2 \frac{l}{l'} \right] = 0 \quad (5.18)$$

Since a piston shaft velocity and an applied field are known, the nondimensional plug thickness is determined using Eq. 5.18 and the MR equivalent damping is found from Eq. 5.15.

As the damping coefficient of the MR valve is obtained, the analytical equivalent viscous damping of the MR valve under a sinusoidal loading can be known using Eq. 5.7, and is denoted as  $C_{eq}^{MR}$ . Combined with the experimental elastomeric equivalent damping, the total equivalent damping for the MRFE damper is

$$C_{eq} = C_{eq}^{MR} + C_{eq}^{EM} \quad (5.19)$$

where,  $C_{eq}^{EM}$  represents the equivalent damping due to the elastomeric layer in the MRFE damper. As the MRFE damper is excited by a sinusoidal loading at 5 Hz, the comparison between the analytical and experimental equivalent damping is shown in Figure 5.12, where the applied currents are 0, 0.4 and 0.8 A, respectively. Similar to the experimental equivalent damping (gray line), the analytical equivalent damping (dotted line) demonstrates amplitude dependent behavior and a damping augmentation effect due to the applied current. Notably, due to the effect of the passive gap (the effect of the accumulator pressure is not considered here), the equivalent damping at small displacement amplitude range

approaches a constant value as the applied current increases. The equivalent damping characteristics at 2.5 Hz and 7.5 Hz are similar to that at 5 Hz. In general, the single frequency equivalent damping characteristic of the MRFE damper can be evaluated using quasi-steady MR fluid flow analysis.

For the dual frequency case, of particular interest is the equivalent damping that is available at lag/rev (5 Hz), since it affects the rotor stability characteristics. As shown in Figure 5.13, the lag damping degradation as a function of 1/rev (7.5 Hz) excitation amplitude is found when the MRFE damper is under dual frequency excitation. The damping at the lead-lag frequency is generally reduced by 1/rev motion, and the loss of the equivalent viscous damping at lag frequency is substantial at lower amplitudes as the amplitude of the 1/rev excitation increases. However, compared with the damping behavior under both current inputs, the damping loss at the lag frequency can be recovered significantly by applying a field to the MRFE damper. For instance, as the displacement amplitude at 7.5 Hz is 0.25 mm and the displacement amplitude at 5.0 Hz is 0.75 mm, the equivalent damping of the lag mode can be varied from 30 Ns/mm to 60 Ns/mm by applying a moderate field (0-0.6 A).

Apparently, the equivalent damping of the MRFE damper can be varied dramatically as a function of the applied current. In other words, the dissipated energy of the MRFE damper due to sinusoidal loading can be varied with little energy input. In Figure 5.14, the dissipated energy due to the MR valve at three different currents is compared with the input control power. At the whole amplitude range except at very small displacement, the input control power is only few percents of the dissipated power. Meanwhile, as the displacement amplitude (or velocity as the product of frequency and displacement amplitude)

increases, the dissipated power of the MR valve increases much faster than the input power. Thus, the MRFE damper as a semi-active damper can provide significant damping dissipation capability with low power consumption.

### 5.3 MRFE Damper Modeling

Linearized characteristics, such as complex modulus and equivalent damping, are appropriate for determining the damping capacity of the MRFE damper in the frequency domain, but they cannot be used to predict the nonlinear forced response demonstrated by the MRFE damper. Thus, based on a distributed elasto-slide elastomer model and a rate-dependent elasto-slide MR model, an MRFE analytical model is developed in this section to describe nonlinear behavior of the MRFE lag damper in time and frequency domain. Since contributions of the elastomeric and MR component in the MRFE damper are considered decoupled, the MRFE model is constructed by a linear combination of elastomeric and MR model. Model parameters are determined using experimental force-displacement hysteresis data, and modeling results are correlated with single frequency and dual frequency hysteresis cycles.

The structure of the MRFE damper model is shown in Figure 5.15, in which the elastomeric model and MR model are combined in parallel. The elastomeric component model consists of a distributed elasto-slide element. In each rate-dependent elasto-slide element,  $k/n$  is the stiffness of the spring in series, and  $f_i^*/n$  is the yield force of the  $i$ th slide. For a continuous elastomer, the total number of elements  $n$  approaches to infinity, and the yield force is described by a distribution function denoted as  $\varphi(f^*)$  such that the number of elasto-slides

with yield force  $f^*$  is  $\varphi(f^*)df^*$ . Behavior of the MR component is described by a single field-dependent elasto-slide and a viscous dashpot. The MR elasto-slide consists of a stiff spring,  $K$ , which accounts for the pre-yield stiffness, and a rate dependent slide,  $N^*$ , which is a pseudo-Coulombic friction function of velocity and is dependent on an applied field. The linear viscous dashpot,  $C_0$ , is parallel to the elasto-slide element to represent a post-yield viscous damping. In addition, a parallel spring in the MRFE model,  $k_0$ , accounts for the stiffness effect of the elastomeric polymer and MR valve. The yield behavior of the elastomer or MR slide is shown in Figure 5.15(a), in which an ideal rate-dependent friction behavior is sketched.

As a displacement loading,  $X$ , is applied to the MRFE damper, the damper force is developed by the elastomeric component and MR valve as:

$$\begin{aligned} F &= F^{EM} + F^{MR} \\ &= \int_0^\infty f^* \varphi(f^*) df^* + N^* + K_0 X + C_0 \dot{X} \end{aligned} \quad (5.20)$$

The yield force,  $f_i^*$  or  $N^*$ , for each elasto-slide element, can be denoted by a rate-dependent function as

$$\begin{aligned} N^* &= K(X - x_0) \\ &= N \left( \frac{\dot{x}_0}{v_r} \right)^{\frac{1}{p}} \end{aligned} \quad (5.21)$$

where,  $x_0$  is an internal displacement coupled between the slide and the elasto spring for each elasto-slide element,  $p$  is a positive odd integer, and  $v_r$  is a constant reference velocity at which the slide goes from the pre-yield region to the post-yield region. For elastomer,  $N$  and  $K$  are replaced with  $f^*$  and  $k$ , respectively. For MR valve,  $N$  is dependent on an applied field or current. Eq.

5.21 leads to

$$\dot{x}_0 = v_r \left[ \frac{K}{N} (X - x_0) \right]^p \quad (5.22)$$

Since the internal velocity,  $\dot{x}_0$ , is the function of internal displacement,  $x_0$ , and loading displacement,  $X$ , as shown in Eq. 5.22, the internal displacement was solved using a variable step ODE solver (ODE23 in MATLAB) and the model force was calculated using Eq. 5.20.

### 5.3.1 Determine Model Parameters

For a single elastomeric damper or MR valve, model parameters are determined from estimated initial loading curves. Using force-displacement hysteresis data, the initial loading curve is identified as the maximum force as displacement amplitudes increases. For the elastomeric component only, the loading curve is represented by an exponential function as

$$F = F^* \left( 1 - e^{-\frac{kx}{F^*}} \right) + k_0x \quad (5.23)$$

The distribution function can then be deduced:

$$\varphi(f^*) = \frac{1}{F^*} e^{-\frac{f^*}{F^*}} \quad (5.24)$$

where,  $F^*$  is the total yield force, and the total stiffness of the spring in the distributed elasto-slide element,  $k$ , is the slope of the loading curve at zero displacement input while the effect of the stiffness,  $k_0$ , is excluded. For MR component only, the initial loading curve is optimized by the same exponent function as Eq. 5.23, but the yield force and preyield stiffness are denoted by  $N$  and  $K$ , respectively. Similarly, the model parameters of the MRFE damper can also be determined using the initial loading curve of the MRFE damper. Ideally,

the initial loading curve should be optimized by a summation of two exponent functions to represent the effect of elastomer and MR valve as shown below:

$$F = F^* \left(1 - e^{-\frac{kx}{F^*}}\right) + N \left(1 - e^{-\frac{Kx}{N}}\right) + k_0x \quad (5.25)$$

However, for numerical simplicity, several assumptions are made to determine model parameters. First, the initial loading curve can be fitted to a single exponential function. Second, the Field-OFF initial loading curve is only governed by the elastomeric component and the effect of the MR valve is trivial. Thus, the yield force distribution for the elastomer and the parallel spring can be determined from the Field-OFF initial loading curve as Eq. 5.23. From the Field-ON initial loading curves at different applied currents, the yield force and preyield stiffness are determined using Eq. 5.23, and they are proven to be the same as the ones determined using Eq. 5.25. By subtracting determined Field-OFF yield force and preyield stiffness from the Field-ON values, the field dependent model parameters related to the MR valve can be identified. The postyield viscous damping due to the MR valve,  $C_0$ , is determined by postyield slope of force-velocity curves. In addition, parameters related to the elasto-slide, such as  $v_r$  and  $p$ , are determined as follows. The choice of  $v_r$  is based on force-velocity curves in which the boundary between preyield slip and postyield flow is approximated. Analytically,  $p$  should be as large as possible, such that the post yield force approaches a constant, which is similar to friction behavior. However, a too large value of  $p$  results in a stiff mathematical model. Thus,  $p$  was chosen by trading off between both factors. Finally, the determined model parameters are shown in Table 5.2. In Figure 5.16, the field dependent yield force and preyield stiffness are shown as a function of the applied current. The determined yield force is compared with the analytical results which is obtained using Eq. 5.15.

As shown in Figure 5.16(a), the determined yield force for the MRFE model is consistent with the predicted results except over the higher applied current range ( $>1\text{A}$ ), so the method for determining the model parameters is validated.

### 5.3.2 Modeling Results

Three sets of single frequency hysteresis cycle data were used to verify the fidelity of the modeling results. Each set of data was obtained by measuring the forced response while the MRFE damper was under sinusoidal displacement loading at 2.5 Hz, 5.0 Hz and 7.5 Hz, respectively. At each frequency, the loading amplitude was chosen as 0.25 mm, 0.50 mm, 0.75 mm and 1.00 mm, and the applied current was varied from 0.0 A to 0.8 A. In Figure 5.17, 5.18 and 5.19, the experimental data at three frequencies were compared to the modeling results. Clearly, the modeling results correlate very well with the experimental results, and especially the proposed model captures the amplitude-dependent behavior of the MRFE damper.

Since a helicopter lag damper experiences multi-frequency excitation, especially for regressive lead-lag frequency and 1/rev rotor frequency. Under such a circumstance, the potential loss of damping at lag frequency has been known, so it is important to predict the response of the MRFE damper under dual frequency excitation. At various combinations of dual frequency amplitudes and currents, the force-displacement hysteresis data are used to evaluate the MRFE damper model. The modeling results for combination of 5.0 Hz and 7.5 Hz are shown in Figure 5.20, 5.21, and 5.22, in which  $A_{lag}$  is the amplitude of the sinusoidal signal at 5Hz and  $A_1$  is the amplitude at 7.5 Hz. In Figure 5.20 and 5.21, the amplitude of the sinusoidal loading at 7.5 Hz is 0.5 mm, and the modeling

results for different applied current (0.0 A and 0.4 A) are correlated with the experimental results. In Figure 5.22, the amplitude for 7.5 Hz is 0.75 mm, and the applied current is 0.0 A and 0.6 A, respectively. Clearly, the MRFE damper model performs quite well in predicting the dual frequency behavior over this broad amplitude and frequency range.

## 5.4 Conclusions

Helicopter lag dampers are important to augment helicopter stability, such as to mitigate air and ground resonance. While simple and reliable elastomeric dampers have proven efficient for damping augmentation in helicopter rotors, they show strong nonlinearity in amplitude, frequency and temperature, which leads to lag damping degradation under adverse conditions. On the other hand, an MR damper can augment lag mode damping during specific flight conditions by the application of a controllable magnetic field. Therefore, a linear stroke MRFE damper was studied to demonstrate the feasibility of augmenting lag damping with little stiffness variation.

As a retrofit of a baseline elastomeric lag damper, a preliminary linear stroke MRFE damper was designed and experimentally evaluated. It was shown that the MR component in the MRFE damper could provide most damping while the elastomeric component provided stiffness and some passive damping. The Field-OFF MRFE damper behaves similarly to the baseline elastomeric damper. As the current is applied to the MR component, the damping of the MRFE damper can be varied dramatically (loss factor was increased from the baseline value of 0.3 to 0.5), and meanwhile the effective stiffness is not changed substantially

by the application of field. The MRFE damping performance and controllability were well predicted using equivalent damping analysis. Compared with the baseline elastomeric damper, the MRFE damper demonstrates similar amplitude dependence and stronger frequency dependence characteristics.

To describe the nonlinear hysteresis behavior of the MRFE damper, a damper model was developed based on the modeling methods developed for elastomeric and MR damper, respectively. The model structure is a linear superposition of both elastomer and MR model since the elastomeric and MR component in the MRFE damper are not coupled. The fidelity of the MRFE model was justified by the good correlation with experimental single and dual frequency test data. Since the proposed model is a time domain model, it also can be used to predict damper behavior under quasi-steady or complex dynamic loading conditions. Because the relationship between model parameters and the applied current is known, the damper model can predict the behavior of the MRFE damper when subjected to a continuously controlled magnetic field.

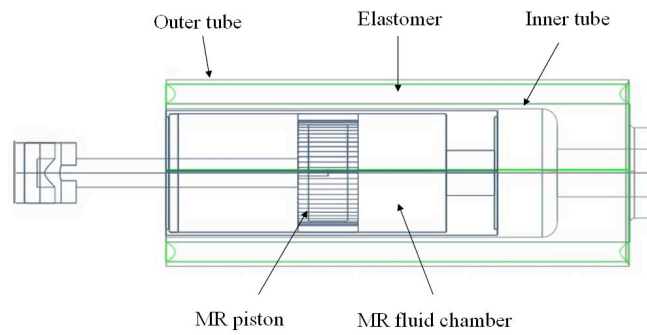


Figure 5.1: Schematic of MRFE Damper

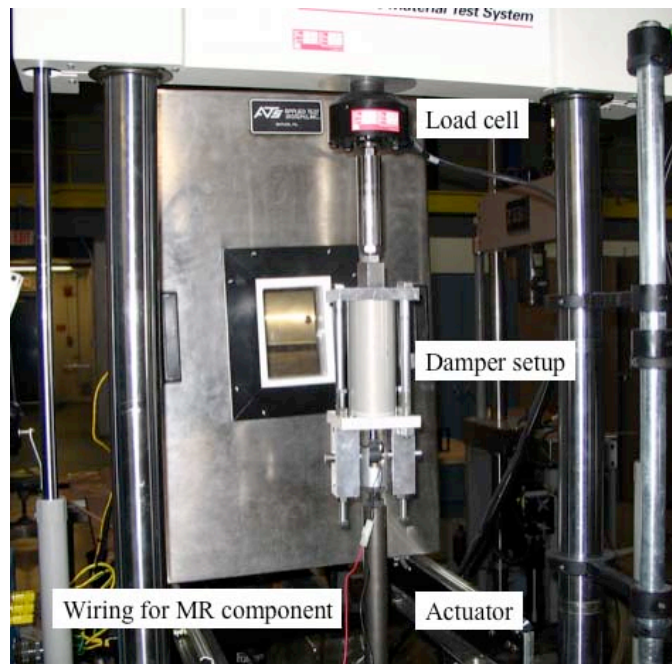


Figure 5.2: MRFE Damper Experimental Setup

Table 5.1: Dual Frequency Test Matrix

| 5Hz\7.5Hz | 0.25 mm | 0.50 mm | 0.75 mm |
|-----------|---------|---------|---------|
| 0.25 mm   | x       | x       | x       |
| 0.50 mm   | x       | x       |         |
| 0.75 mm   | x       |         |         |

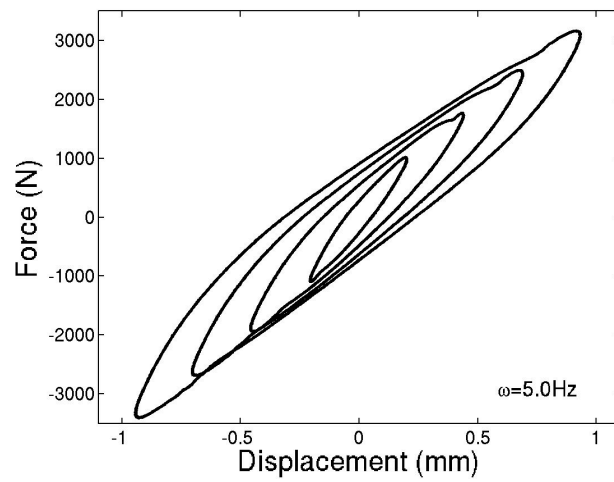


Figure 5.3: Typical Hysteresis Cycles of the Baseline Damper for Varying Displacements

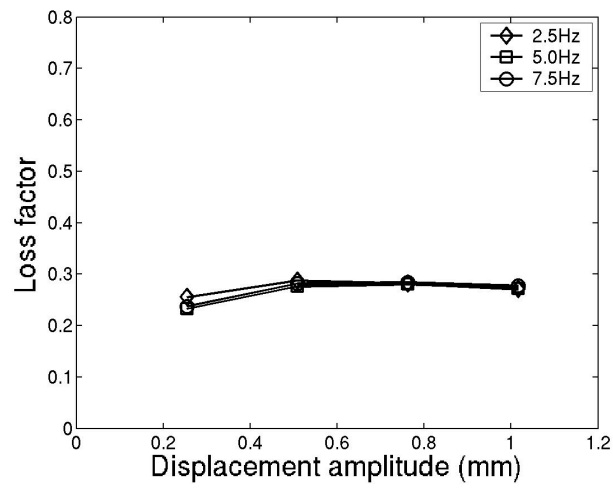
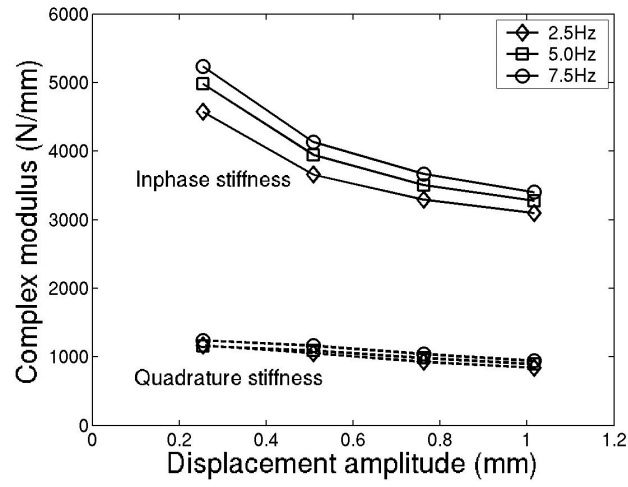


Figure 5.4: Linear Characterization of the Baseline Damper

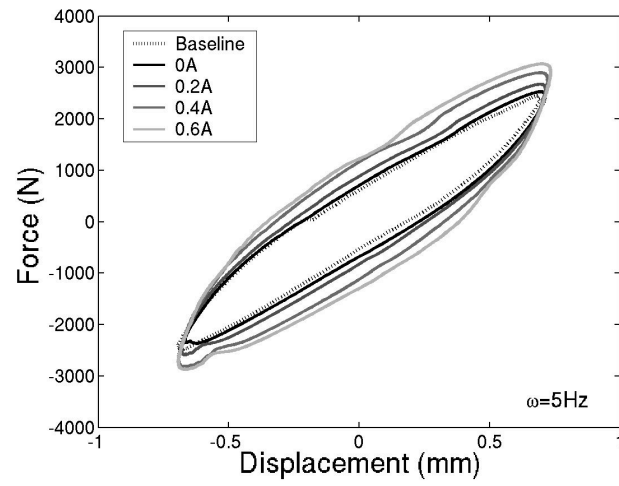


Figure 5.5: Hysteresis of the MRFE Damper

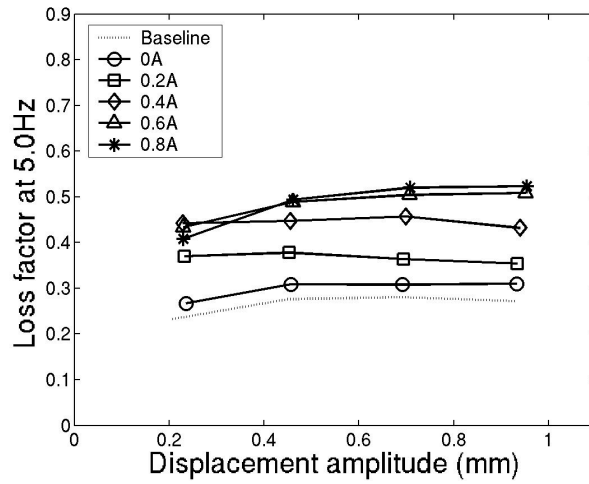
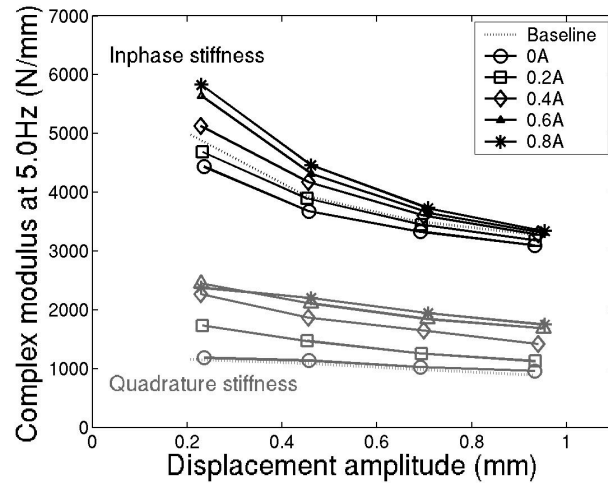


Figure 5.6: Linear Characterization of MRFE Damper at Single Frequency

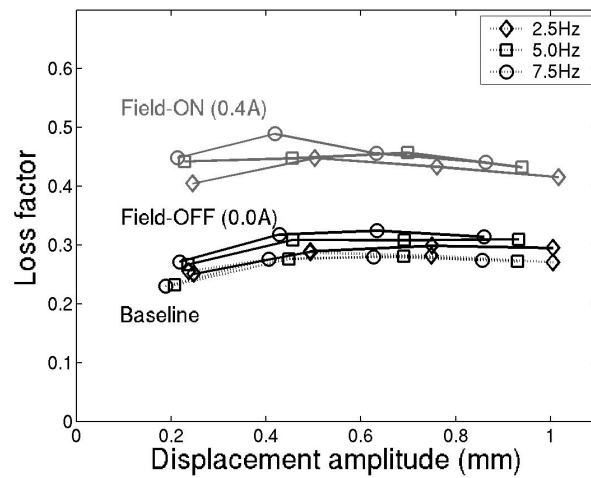
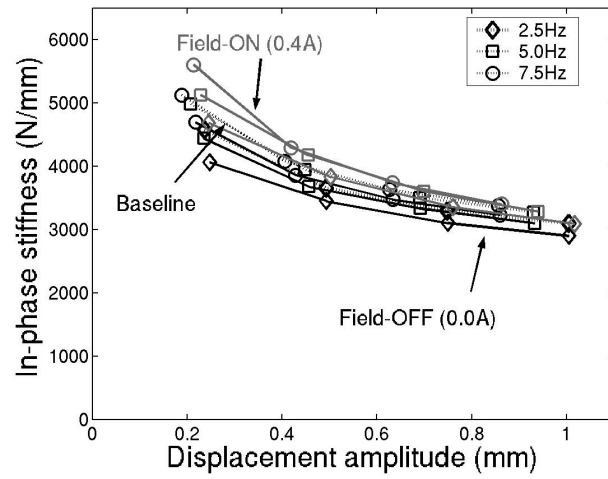
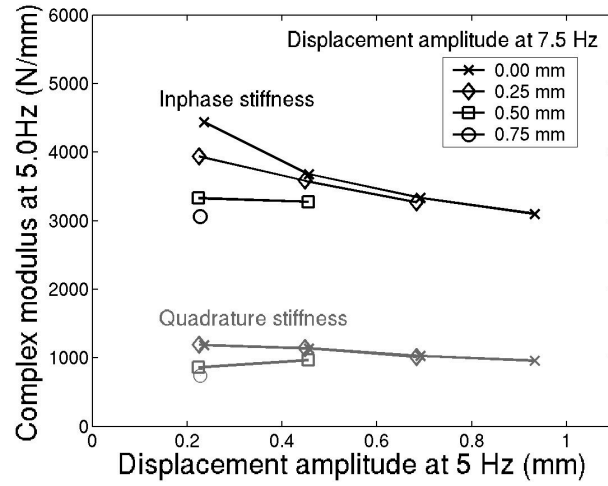
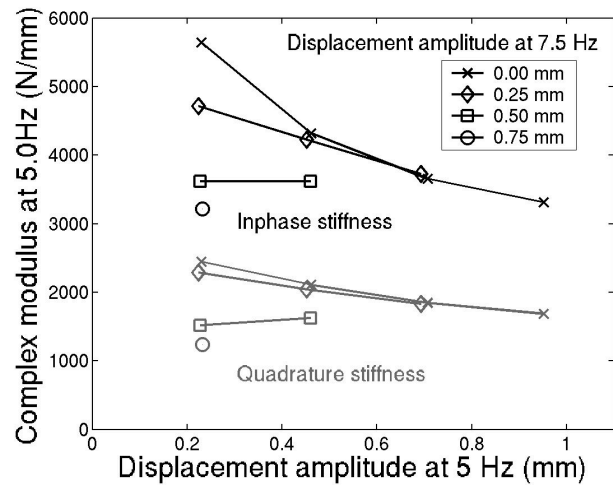


Figure 5.7: Linear Characterization of MRFE Damper at Different Frequencies



(a) Field-OFF (0.0 A) MRFE Damper



(b) Field-ON (0.6 A) MRFE Damper

Figure 5.8: Dual Frequency Characterization

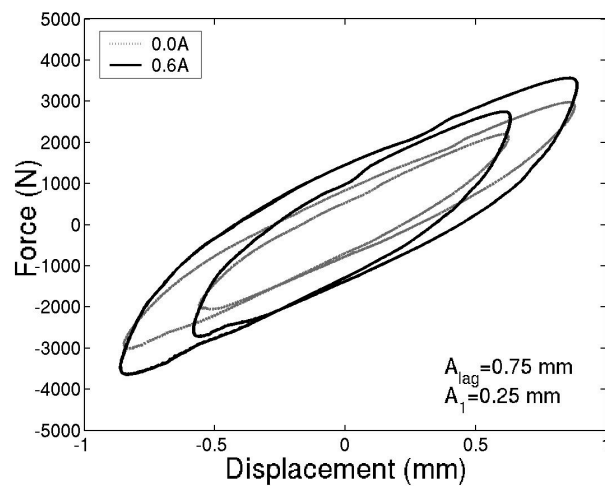


Figure 5.9: Dual Frequency Hysteresis

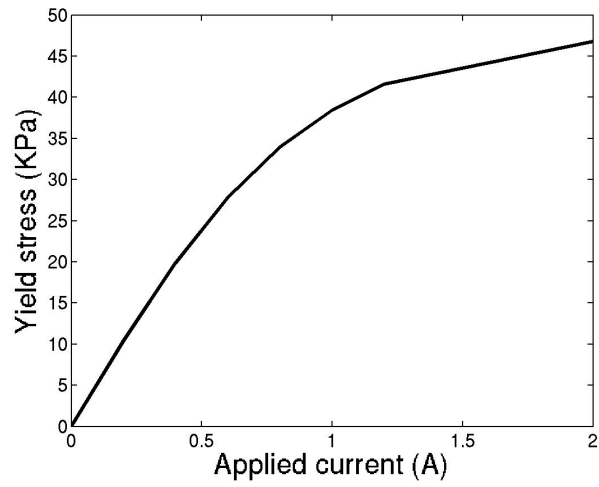


Figure 5.10: Empirical Relationship between Yield Stress and Current

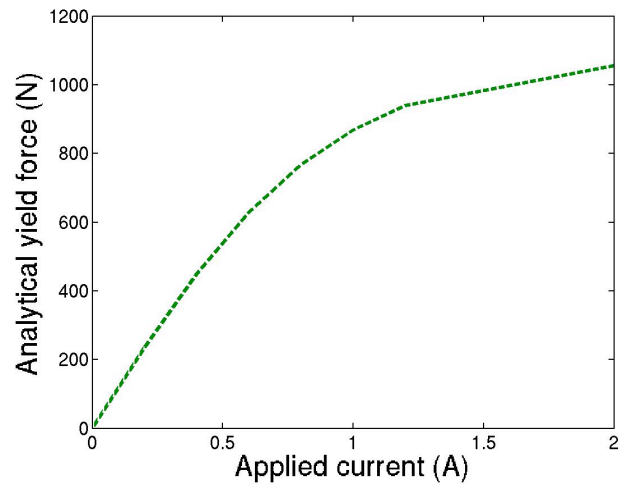


Figure 5.11: Empirical Relationship between Yield Force and Current

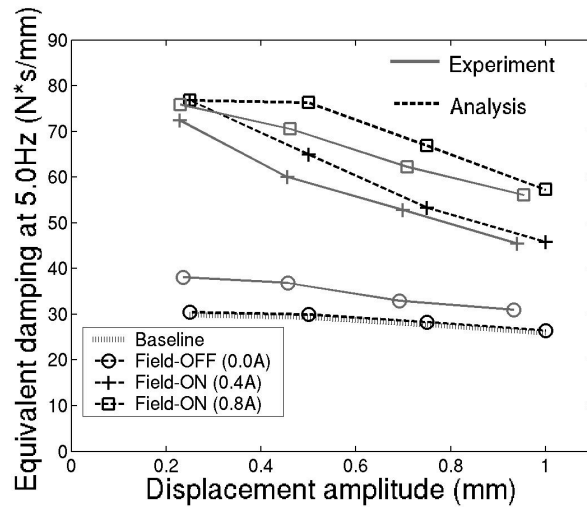


Figure 5.12: MRFE Equivalent Damping Prediction

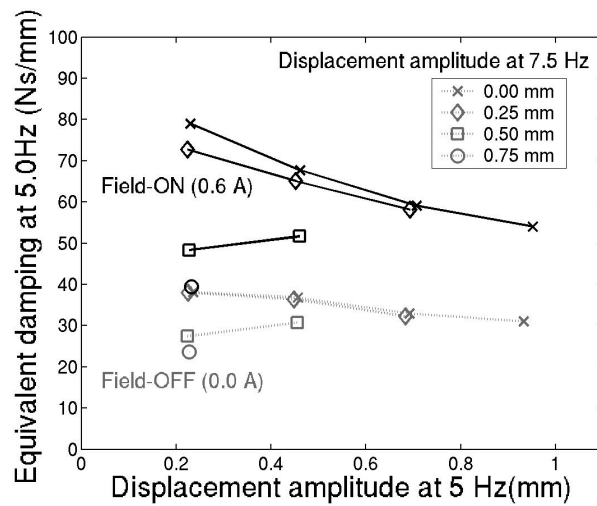


Figure 5.13: Dual Frequency Equivalent Damping

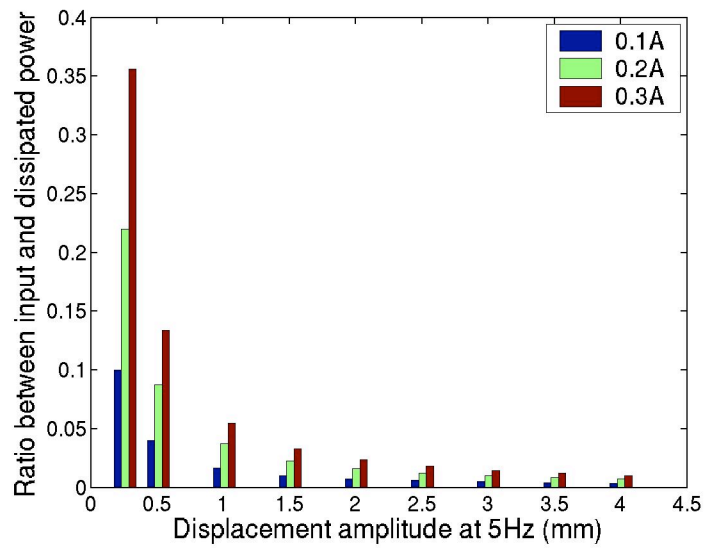
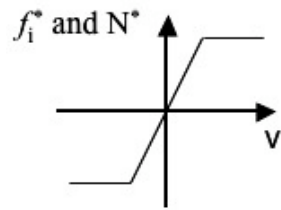
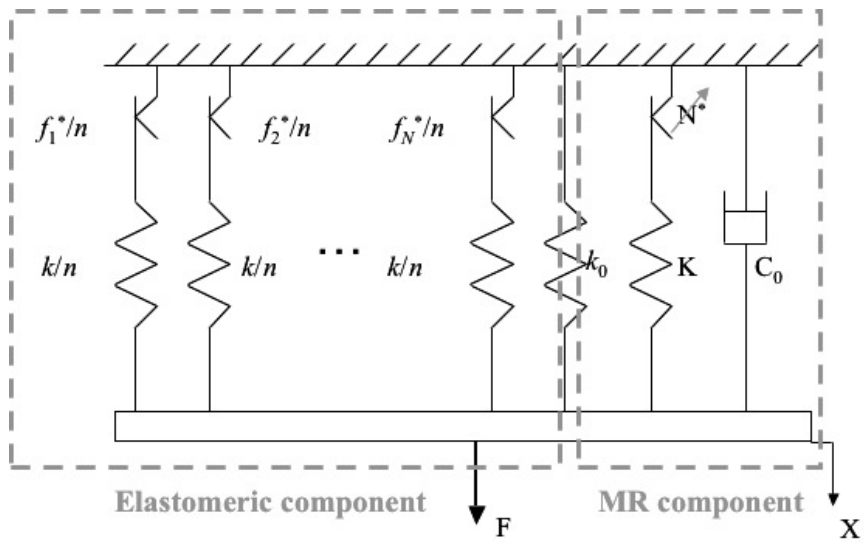


Figure 5.14: Semi-active MR Damping Power Characteristics



(a) Slide Function

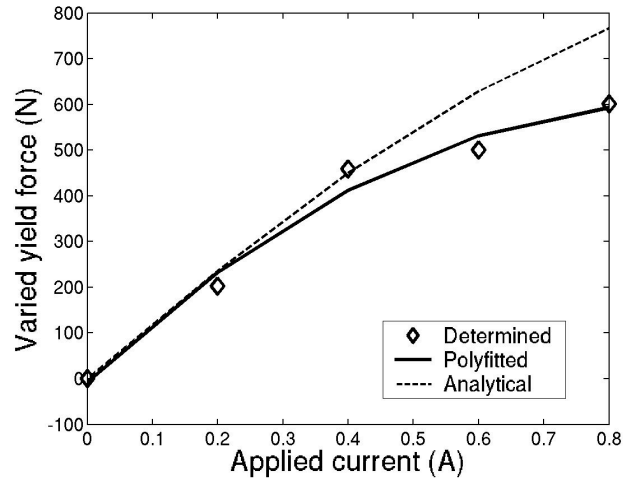


(b) MRFE Mechanical Model

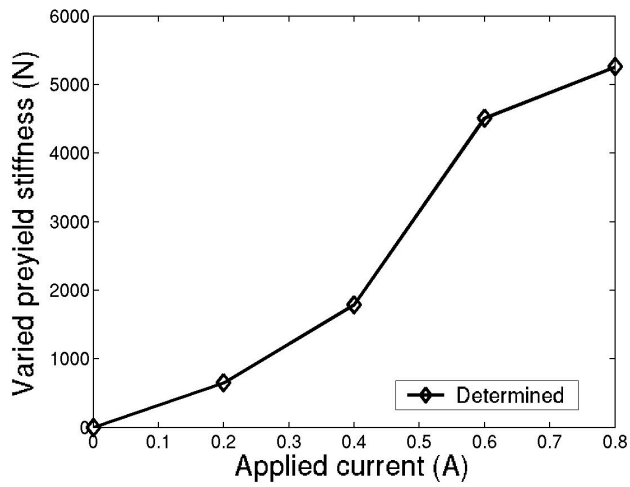
Figure 5.15: MRFE Model Structure

Table 5.2: Model Parameters

| Parameter        | Elastomer | MR valve       |
|------------------|-----------|----------------|
| $F^*/N$ (Newton) | 851       | Figure 5.16(a) |
| $k/K$ (N/mm)     | 4635      | Figure 5.16(b) |
| $v_r$ (mm/s)     | 15        | 50             |
| $p$              | 7         | 7              |
| $C_0$ (Nmm/s)    |           | 0.25           |
| $k_0$ (N/mm)     | 2550      |                |

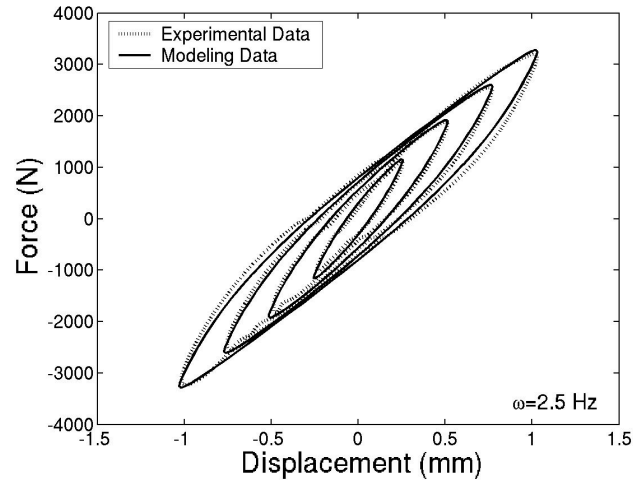


(a) Yield Force

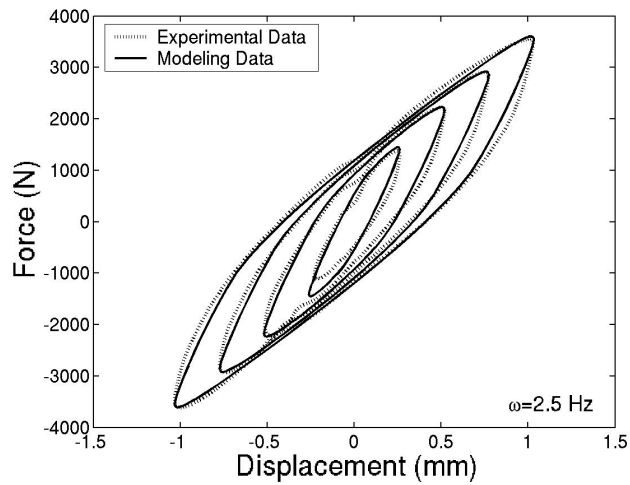


(b) Preyield Stiffness

Figure 5.16: Field Dependent N and K

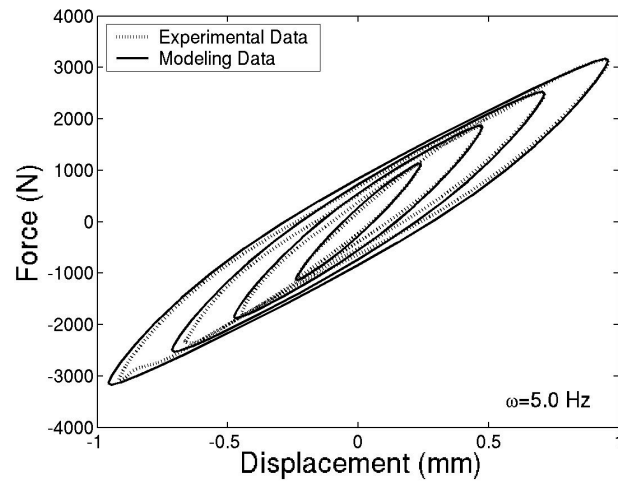


(a) Field-OFF (0.0 A)

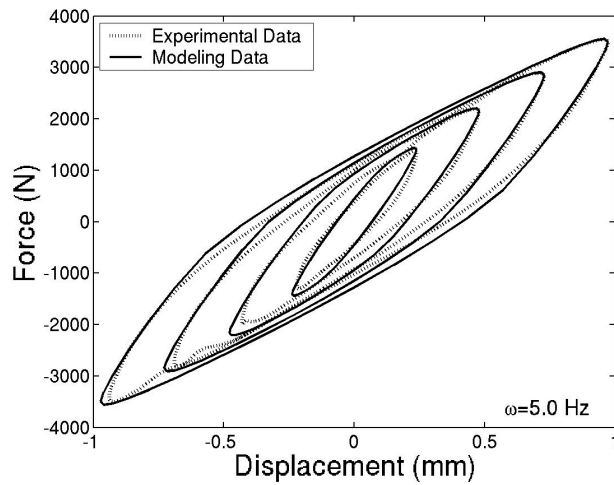


(b) Field-ON (0.4 A)

Figure 5.17: Force-Displacement Hysteresis Modeling at 2.5 Hz, Four Amplitude Cases: 0.25, 0.50, 0.75 and 1 mm

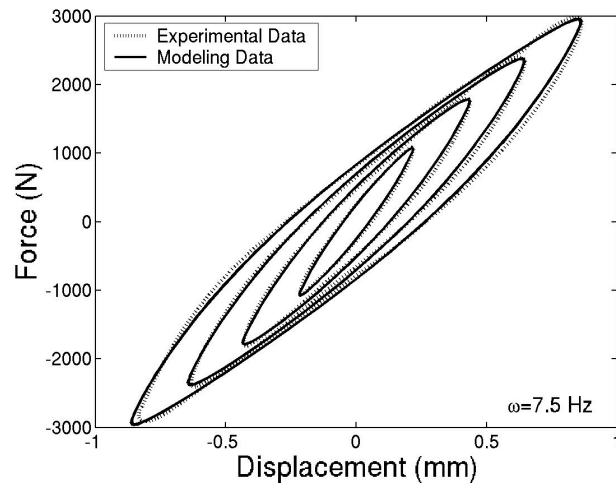


(a) Field-OFF (0.0 A)

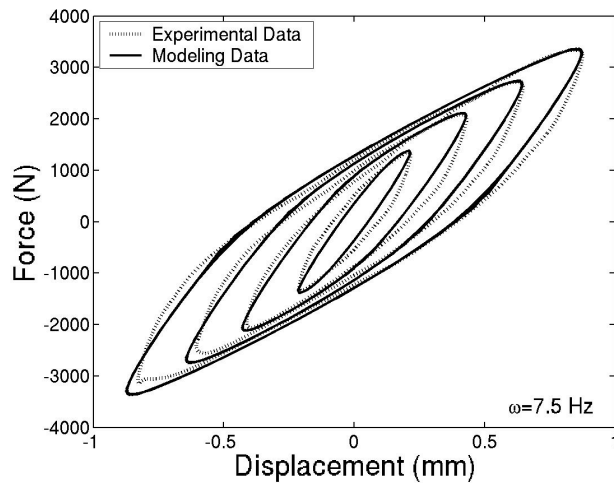


(b) Field-ON (0.4 A)

Figure 5.18: Force-Displacement Hysteresis Modeling at 5.0 Hz, Four Amplitude Cases: 0.25, 0.50, 0.75 and 1 mm

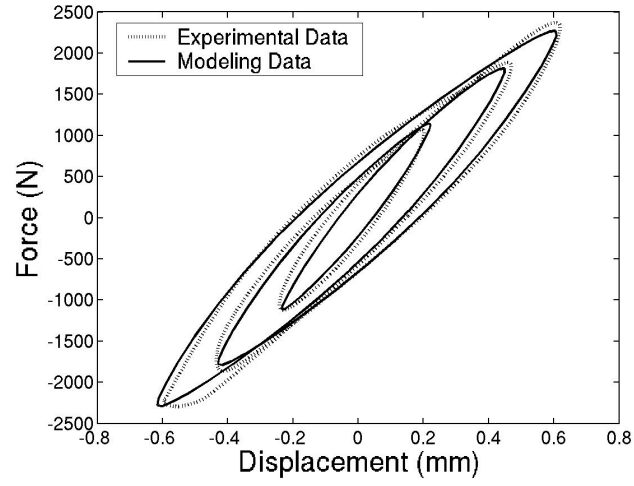


(a) Field-OFF (0.0 A)

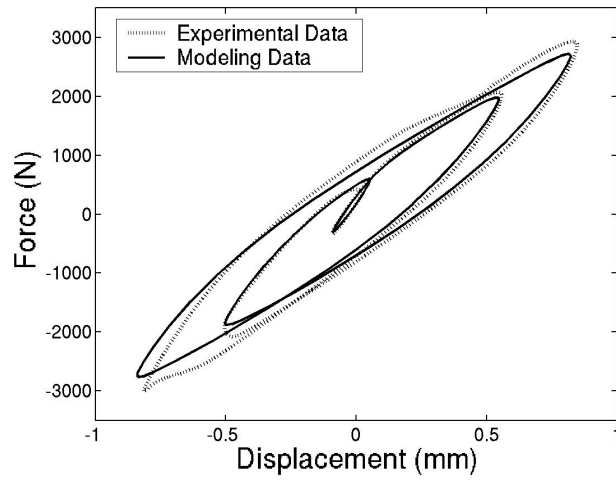


(b) Field-ON (0.4 A)

Figure 5.19: Force-Displacement Hysteresis Modeling at 7.5 Hz, Four Amplitude Cases: 0.25, 0.50, 0.75 and 1 mm

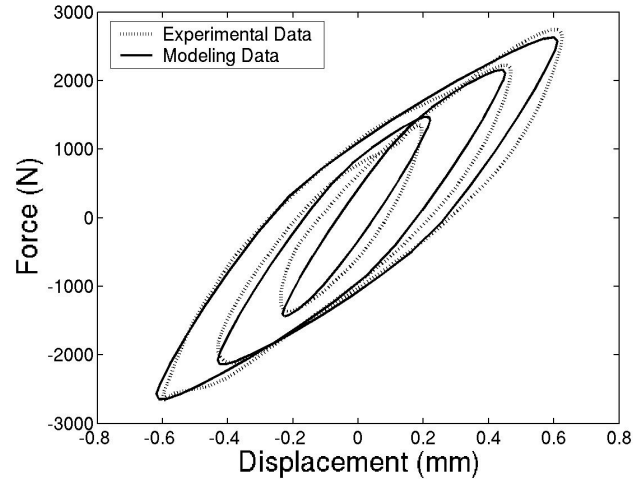


(a)  $A_{lag}=0.25$  mm,  $A_1=0.50$  mm

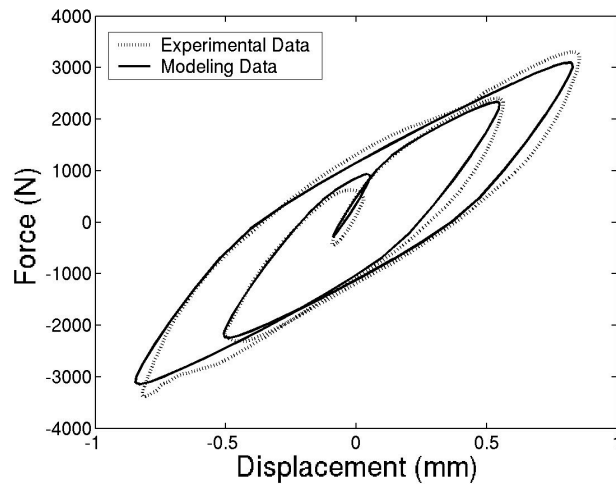


(b)  $A_{lag}=0.50$  mm,  $A_1=0.50$  mm

Figure 5.20: Field-OFF (0.0 A) Dual Frequency Modeling

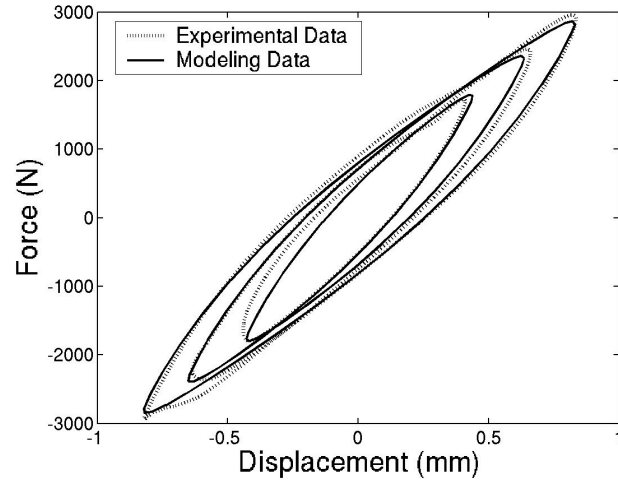


(a)  $A_{lag}=0.25$  mm,  $A_1=0.50$  mm

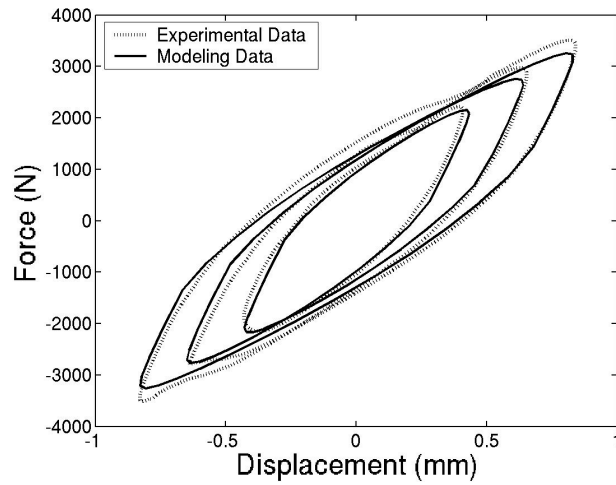


(b)  $A_{lag}=0.50$  mm,  $A_1=0.50$  mm

Figure 5.21: Field-ON (0.4 A) Dual Frequency Modeling



(a) Field-OFF (0.0 A)



(b) Field-ON (0.6A)

Figure 5.22: Dual Frequency Modeling:  $A_{lag}=0.25$  mm,  $A_1=0.75$  mm

## Chapter 6

# Summary and Conclusions

This research focused on the development of semi-active MRFE damper technology, in which two goals were accomplished including MRFE damper experimental evaluation and modeling of damper response. First, MRFE damper configurations and design parameters were explored to evaluate the feasibility of an MRFE damper in lag damping augmentation, and the experimental result of the prototype MRFE damper demonstrated that the MRFE damper could provide fail safe lag damping, control of single frequency damping loss and control of dual frequency damping loss. The specific contributions in developing and evaluating MRFE dampers are:

1. Design and fabrication of a concentric bearing type magnetorheological fluid and elastic damper especially in parameter studies to identify key design parameters that affect MRFE damper performance.
2. Experimental evaluation of the MRFE damper and damping augmentation investigation on the MRFE damper activated by a continuously variable magnetic field.

3. Exploration of the feasibility of the MRFE technology in different lag damper configurations.

Second, characterization of elastomeric materials and MR fluids were conducted extensively, and new modeling strategies for elastomeric and MR dampers were developed to provide significant improvements over prior modeling efforts in describing amplitude and frequency dependent behavior demonstrated by the elastomer and MR damper. Using these models, modeling of response to sinusoidal loadings was conducted for MR dampers, elastomeric dampers and MRFE dampers, respectively. The detailed modeling contributions are:

1. Development of a distributed elasto-slide elastomer model to describe non-linear triboelastic behavior demonstrated by elastomers. This time domain model is developed based on physical damping mechanisms of the elastomer. Using a simpler model structure and constant damper parameters, the damper model can describe amplitude and frequency dependent behavior of the elastomer or elastomeric dampers.
2. Investigation of behavior of an elastomeric damper under slowly varying loading conditions using the new modeling approach and experimental results.
3. Development of a rate-dependent elasto-slide MR model, in which the model parameters are amplitude and frequency independent which is unique compared with the other existing models.
4. Development of an MRFE damper model based on the elastomeric and MR model.

Specifically, this research can be summarized according to the following: material characterization and modeling, MRFE damper design and analysis, and MRFE damper characterization and modeling. The following conclusion sections are arranged in this order.

## 6.1 MR Damper Modeling

A rate-dependent elasto-slide (RDES) model for a linear stroke MR damper was developed. The MR damping mechanism was developed using the Bingham model of MR fluids and the parallel plate assumption. The relationship between model parameters and damper mechanisms was studied. The model parameters were determined using identified virtual loading curves from force-displacement and force-velocity hysteresis data. A stable numerical method was chosen to predict the model response under various loading conditions. The predicted forced response correlated very well with the single and dual frequency experimental results. Significantly, the nonlinear amplitude dependent behavior of the MR damper was described by this six constant parameter model. The RDES model can be used in a variety of applications such as initial or forced response analysis of the system using MR dampers and a wide range of proposed control strategies dealing with the MR damper.

In conclusion, the rate-dependent elasto-slide model is a physically motivated time domain model. It captures the nonlinearity of the MR damper using a simple model structure. The model parameters are predictable using MR fluids and damper geometry data, and can be easily identified using dynamic steady-state data. The ability of the RDES model in predicting dynamic response is

also justified.

## 6.2 Elastomer Modeling

Modeling methods for elastomeric material behavior in simple shear were investigated. Most prior models introduced nonlinear terms into the conventional Kelvin model or Zener model. As filled elastomers are anelastic materials, friction damping mechanism has proven useful to model rate-independent damping. Nonlinearity in elastomeric materials was manifested in two ways. First, the forced response of an elastomer is nonlinear which means the response cannot be predicted by linear differential and integral equations. The other is that the stiffness and damping of elastomers are not constant with varying amplitudes and frequencies. While some models capture the amplitude dependent complex moduli very well using constant parameters, they cannot predict stress-strain hysteresis accurately. On the other hand, existing hysteresis models that can predict stress time histories well require parameters that are usually amplitude and frequency dependent, that is, these models require amplitude and frequency as prior information when these models are implemented.

Developed from a hysteresis modeling method, a distributed rate-dependent elasto-slide elastomeric model was used to describe the amplitude dependent characteristics of an elastomer. This physically motivated damper model resembles the behavior of filler structures in an elastomer under loading. The method to determine the model parameters was presented. It was found that a unique exponential function can be used to describe the yield force distribution for elastomers. Numerical algorithms were developed for model applications. Dynamic

tests conducted on an elastomeric specimen and an elastomeric lag damper were used to evaluate the modeling method. The fidelity of the model was verified by the good correlation between predicted force-deflection hysteresis and the experimental results except that the damping over lower amplitude range can not be fully predicted by the model. Since the proposed model is a time domain model, the adaptability of the model in predicting damper response under complex loading was evaluated. The predicted force response for slowly varying amplitude loading correlated quite well with the corresponding experimental data. Finally, a single degree of freedom system was used to study the influence of the elastomeric damper on the blade lag motion. The transient response and limit cycle oscillations were simulated by the model.

In conclusion, the distribute rate-dependent elasto-slide elastomeric damper model is a time-domain modeling approach to capture nonlinear behavior of the elastomer. The damper model can easily be implemented into the dynamic systems. Since the model is physically motivated, the flexibility in determining the distribution function provides a potential to improve the model performance especially in small amplitude range.

### **6.3 MRFE Damper Design and Analysis**

To develop an MRFE damper, equivalent damping analysis was conducted based on MR fluid flow motion model and a quasi-steady damping analysis. The quasi-steady damping analysis was conducted for flow mode MR dampers with an approximate parallel plate assumption. Using idealized Bingham plastic model to characterize the MR fluid behavior, the damping control capacity un-

der different fields control can be predicted on any different sized dampers. The effect of the magnetic circuit and passive flow path on the quasi-steady damping was also evaluated. On the other hand, as a damping objective is required, design constraints for the MRFE damper were established based on the equivalent damping analysis, and three geometry constraints were developed as the directives for MRFE damper design.

## **6.4 MRFE Damper Development and Modeling**

A prototype linear stroke MRFE damper was developed. An MRFE damper setup was designed and tested on the MTS machine. Damper forces under sinusoidal displacement loading were measured with different amplitudes. The magnetic field applied to the MR component was varied with different currents. Complex modulus and equivalent viscous damping were used to evaluate the damper characteristics. As shown in the experimental result of the linear stroke MRFE damper, the MR component in the MRFE damper can provide substantial damping augmentation and control range while the geometry and loading conditions are compatible with the baseline damper. The Field-OFF MRFE damper behaves similarly to the baseline elastomeric damper. As the current is applied to the MR component, the damping of the MRFE damper can be varied dramatically (loss factor was increased from the baseline value of 0.3 to 0.5), and meanwhile the effective stiffness is not changed substantially by the application of field. Compared with the baseline damper, the MRFE damper demonstrates similar amplitude dependence and stronger frequency dependence.

An MRFE modeling method was described. Model parameters of both elastomeric and MR components in the MRFE damper were determined using force-displacement hysteresis data. The MRFE damper model hysteresis behavior was constructed by linear superposition of both components. The modeling results correlated well with experimental results.

## **6.5 Future Work**

### **6.5.1 Future MR and Elastomeric Model**

In this study, the rate-dependent elasto-slide element has shown great promise in terms of modeling elastomeric and MR damper behavior. Both rate-dependent elasto-slide MR model and distributed elasto-slide elastomer model can well capture the hysteresis behavior of the elastomeric and MR damper over a moderate amplitude range. However, the capability of the model over a broad frequency range, and for different scaled dampers, has not been studied. To further evaluate the model performance and then improve the model, three future tasks should be undertaken.

1. Since the MRFE damper model should be used to predict damper behavior from wind tunnel rotor speed condition to full scale rotor speed condition, the validity of the model over a broad frequency range should be evaluated. Thus, high frequency (i.e. 10-30 Hz) sinusoidal displacement loadings should be applied to the MR and elastomeric damper, and the experimental data should be compared with modeling results.
2. Since future MRFE dampers vary in size and performance according to

different rotor hub requirements, the variation of the model parameters with the damper scale should be studied such that the damper model can be used to predict the behavior of the damper at any scale or configuration. In addition, although only a one-dimensional elastomeric model is described in this thesis, the distributed elasto-slide model can also be extended into a three-dimensional form such that it can be implemented easily into a finite element analysis for a complex elastomeric damper formation.

3. Several MR modeling efforts have proven to be successful in describing nonlinear behavior of the MR damper. To assess inherent characteristics and performance of the rate-dependent elasto-slide MR model, this model could be compared with the hydro-mechanical model developed by Hong *et al* [47]. In this way, the model parameters of the RDES model could be correlated with the damper parameters of the hydro-mechanical model.

### 6.5.2 Future Development of the MRFE Damper

Though the preliminary semi-active MRFE damper has shown great promise for helicopter lag damping augmentation, significant challenges remain to implement the MagnetoRheological Fluid-Elastic (MRFE) system on a full-scale rotor system. A key element of the future work is to refine and ruggedize the damper for operation at high centrifugal loading conditions and wide operating temperature ranges ( $-40^{\circ}F$  to  $200^{\circ}F$ ). Additionally, the MRFE damper must be configured to operate in fail-safe mode by behaving as a passive element in the event of power loss or MRF failure. The passive damping of the elastomeric and magnetorheological damper components will be designed to meet a baseline

damping requirement to ensure rotor stability. The existing prototype damper design will be scaled up to meet the damping requirements of a full-scale rotor system (such as Boeing MD-500). Finally, to evaluate the performance of the MRFE damper for helicopter stability augmentation, the damper model need to be incorporated into the rotor dynamics analysis codes, and the effect of the adaptable MRFE damping on the helicopter stability need to be evaluated in the future. Lag damping control strategy is also required. In general, the future work of the MRFE damper can be summarized in three major efforts, i.e. damper refinement, full-scale damper development and ground/air resonance analysis using MRFE damper model.

### **Damper Refinement**

Based upon the databases and analyses of magnetorheological (MR) fluids and dampers, as well as the extensive database of elastomeric material properties, damper refinement together with a comprehensive design analysis needs to be conducted to meet the operating conditions for a helicopter lead-lag damper. Systems parameters such as magnetic field dependent MR fluid yield stress and post-yield viscosity, MRFE damper geometry, mechanical characteristics, and power and control electronics will be examined to the first order. Refinement will be made to the analysis in parallel as the MRFE damper is prototyped, tested, and refined. In detail, the damper refinement includes:

1. Formulate comprehensive MRFE design tool based on full-scale rotor requirements
2. Exploit commercial off-the-shelf MR fluids and elastomeric bearings

3. Develop MRFE damper current control and feedback control system
4. Maximize device efficiency through minimization of frictional losses
5. Improve reliability by utilizing few or no moving parts (no dynamic seal)
6. Prototype laboratory devices and control electronics for systems evaluation and validation
7. Conduct single and dual frequency sinusoidal excitation tests in vacuum chamber and wind tunnel to assess system performance/validate design tools
8. Assessment of long term behavior fatigue, erosion of internal parts, temperature dependence

### **Full-scale MRFE Lag Damper Development**

Based on the performance evaluation conducted on the prototype MRFE damper, full-scale MRFE lag damper can be further developed to be incorporated in a specific helicopter. Necessary refinements such as component replacement, part redesign, and possible ruggedization of high-wear components, must be undertaken to ensure that the MRFE damper can be integrated and fielded with an advanced bearingless rotor. The potential for single and dual frequency semi-active damping control of the MRFE damper can be investigated in hover stand. Additional empirical testing of the MRFE lag damper bearing will be conducted to establish the performance of the semi-active or controllable damper under single (lag/rev) and dual frequency (lag/rev plus 1/rev) excitation.

## **Full-scale Comprehensive Analysis for Ground Resonance utilizing MRFE damper**

The MRFE model has been used to model hysteretic behavior of the prototype MRFE damper with good success. Thus, it would be useful to include the MRFE model in a comprehensive rotor analysis and investigate the effects of the MRFE damper on the rotor dynamics. Ground/air resonance modeling needs to be examined utilizing refined damper model and semi-active damping control algorithms.

## BIBLIOGRAPHY

- [1] Major General Joseph Bergantz, "Improving Rotorcraft Acceptance Through Active Controls Technology," AHS International National Specialists' Meeting, Bridgeport, Connecticut, October 4-5, 2000.
- [2] McGuire D.P., "Fluidlastic Dampers and Isolators for Vibration Control in Helicopters," Lord Corporation, 2001.
- [3] Kamath, G.M., Wereley, N.M. and Jolly, M.R., "Characterization of Magnetorheological Helicopter Lag Dampers," *Journal of American Helicopter Society*, Vol. 44, No. 3, 1999, pp. 234-248.
- [4] Chopra, I., "Perspectives in Aeromechanical Stability of Helicopter Rotors," *Vertica*, Vol. 14, No. 4, 1990, pp. 457-508.
- [5] Johnson, W., *Helicopter Theory*, Dover Publications, Inc., New York, 1994.
- [6] Panda, B., Mychalowycz, E., Kothmann, B., and Blackwell, R., "Active Controller for Comanche Air Resonance Stability Augmentation," Proceedings of the 60th American Helicopter Society Annual Forum, Baltimore, MD, 2004.

- [7] Almeras, P., "Active Control of Aeromechanical Stability Applied by Eurocopter," Proceedings of the 23rd European Rotorcraft Forum, Germany, 1997.
- [8] Teves, D., Kloppel, V., and Richter, P., "Development of Active Control Technology in the Rotating System, Flight Testing and Theoretical Investigations," Proceedings of the 18th European Rotorcraft Forum, France, 1992.
- [9] Ham, N.D., Behal, B.L. and McKillip Jr., R.M., "Helicopter Rotor Lag Damping Augmentation Through Individual-Blade-Control," *Vertica*, Vol. 7, No. 4, 1983, pp. 361-371.
- [10] Hebert, C.A. and Lesieutre, G.A., "Rotorcraft blade Lag Damping Using Highly Distributed Tuned Vibration Absorbers," Proceedings of the 39th AIAA/ASME/ASCE/AHS/ASC Structures, Structural Dynamics, and Materials Conference and Exhibit and AIAA/ASME/AHS Adaptive Structures Forum, Long Beach, CA, 1998.
- [11] Kim S.J. and Yun, C.Y., "Performance Comparison between Piezoelectric and Elastomeric Lag Dampers on Ground Resonance Stability of Helicopter," *Journal of Intelligent Material Systems and Structures*, Vol. 12, No. 4, 2000, pp. 215-222.
- [12] Felker, F., Lau, B., McLaughlin, S. and Johnson, W., "Nonlinear Behavior of an Elastomeric Lag Damper undergoing Dual-Frequency Motion and its Effect on Rotor Dynamics," *Journal of the American Helicopter Society*, Vol. 32, No. 1, 1987, pp. 45-53.

- [13] Ginder, J.M., Davis, L.C. and Elie, L.D., "Rheology of Magnetorheological Fluids: Models and Measurements," *International Journal of Modern Physics B*, Vol. 10, No. 23 and 24, 1996, pp. 3293-3303.
- [14] Carlson, J.D. and Chrazn, M.J., "Magnetorheological Fluid Dampers," US Patent 5,277,281, 1992.
- [15] Jolly, M.R., Bender, J.W. and Carlson, J.D., "Properties and Applications of Commercial Magnetorheological Fluids," *Journal of Intelligent Material Systems and Structures*, Vol. 10, No. 1, 1999, pp. 5-13.
- [16] Ahmadian, M., Poynor, J.C., and Gooch, J.M., "Application of Magnetorheological Dampers for Controlling Shock Loading," Proceedings of the ASME DSC 67, 1999, pp. 731-735.
- [17] Choi, S.B., Nam, M.H. and Lee, B.K., "Vibration Control of a MR Seat Damper for Commercial Vehicles," *Journal of Intelligent Material Systems and Structures*, Vol. 11, No.12, 2000, pp. 936-944.
- [18] Choi, Y.T. and Wereley, N.M., "Semi-active Vibration Isolation Using Magnetorheological Isolators," Proceedings of SPIE 2697, 2002, pp.284-291. AIAA J. Aircraft, at press.
- [19] McManus, S.J., Clair, K.A.St., Boileau, P.E., Boutin, J., and Rakheja, S., "Evaluation of Vibration and Shock Attenuation Performance of a Suspension Seat with a Semi-Active Magnetorheological Fluid Damper," *Journal of Sound and Vibration*, Vol. 253, No. 1, 2002, pp. 313-327.

- [20] Namuduri, C.S., Golden, M.A., and Praeckel, J., "Concurrent Research and Development of a Magnetic Ride Control System," IECON Proceedings (Industrial Electronics Conference), Vol. 3, 2003, p.p. 2853-2858.
- [21] Panda, B. and Mychalowycz, E., "Aeroelastic Stability Wind Tunnel Testing with Analytical Correlation of the Comanche Bearingless Main Rotor," *Journal of the American Helicopter Society*, Vol. 42, No. 3, 1997, pp. 207-217.
- [22] McGuire, D.P., "Fluidlastic Dampers and Isolators for Vibration Control in Helicopters," 50th Annual Forum of the American Helicopter Society, Washington, D.C., 1994.
- [23] Jones, P.J., "Fluid Damper including Flexible Damping Plate," US Patent Number 6,045,328, 2000.
- [24] Panda, B., Mychalowycz, E. and Tarzanin, F.J., "Application of Passive Dampers to Modern Helicopters," *Smart Materials and Structures*, Vol. 5, No. 5, 1996, pp. 509-516.
- [25] Hu, W. and Wereley, N.M., "Hybrid Magnetorheological Elastomeric Lag Dampers for Helicopter Stability Augmentation," 59th Annual Forum of the American Helicopter Society, Phoenix, Arizona, May 6-8, 2003.
- [26] Wang, K.W., Kim, Y.S. and Shea, D.B., "Structural Vibration Control via Electrorheological-Fluid Based Actuators with Adaptive Viscous and Frictional Damping," *Journal of Sound and Vibration*, Vol. 177, No. 2, pp. 227-237.

- [27] Sims, N.D., Stanway, R., Peel, D.J., Bullough, W.A. and Johnson, A.R., "Controllable Viscous Damping: An Experimental Study of An Electrorheological Long-Stroke Damper Under Proportional Feedback Control," *Smart Materials and Structures*, Vol. 8, No. 5, pp.601-615.
- [28] Dyke, S.J., Spencer Jr., B.F., Sain, M.K. and Carlson, J.D., "Modeling and Control of Magnetorheological Dampers for Seismic Response Reduction," *Smart Materials and Structures*, Vol. 5, pp. 565-575.
- [29] Marathe, S., Gandhi, F. and Wang, K.W., "Helicopter Blade Response and Aeromechanical Stability with a Magnetorheological Fluid Based Lag Damper," *Journal of Intelligent Material Systems and Structures*, Vol. 9, No. 4, 1998, pp. 272-282.
- [30] Gandhi, F., Wang, K.W. and Xia, L., "Magnetorheological Fluid Damper Feedback Linearization Control for Helicopter Rotor Application," *Smart Materials and Structures*, Vol. 10, No. 1, pp. 96-103.
- [31] Zhao, Y.S., Choi, Y.T. and Wereley, N.M., "Semi-active Damping of Ground Resonance in Helicopters Using Magnetorheological Dampers," *Journal of American Helicopter Society* Vol. 49, No. 4, 2004, pp. 468-482.
- [32] Wang, W. and Xia, P.Q., "Ground Resonance Analysis of Helicopter with Magnetorheological Lag Damper," *Journal of Nanjing University of Aeronautics and Astronautics*, Vol. 35, No. 3, 2003, pp. 264-267.
- [33] Phillips, R.W., *Engineering Application of Fluids with a Variable Yield Stress*, Ph.D. Thesis, Mechanical Engineering, University of California at Berkeley, 1969.

- [34] Kamath, G.M., Hurt, M.K., and Wereley, N.M., "Analysis and Testing of Bingham Plastic Behavior in Semi-Active Electrorheological Fluid Dampers," *Smart Materials and Structures*, Vol. 5, No. 5, 1996, pp. 576-590.
- [35] Wereley, N.M., and Pang, L., "Nondimensional Analysis of Semi-active Electrorheological and Magnetorheological Dampers Using Approximate Parallel Plate Models," *Smart Materials and Structures*, Vol. 7, No. 5, 1998, pp. 732-743.
- [36] Pang, L., Kamath, G.M., and Wereley, N.M., "Analysis and Testing of A Linear Stroke Magnetorheological Damper," AIAA/ASME Adaptive Structures Forum, Long Beach, CA, April, 1997.
- [37] Snyder, R.A., Kamath, G.M., and Wereley, N.M., "Characterization and Analysis of Magnetorheological Damper Behavior Under Sinusoidal Loading," *AIAA Journal*, Vol. 39, No. 7, July 2001, pp. 1240-1253.
- [38] Williams, S., Rigby, S.G., Sproston, J.L. and Stanway, R., "Electrorheological Fluids Applied to an Automotive Engine Mount," *Journal of Non-Newtonian Fluid Mechanics*, Vol. 47, 1993, pp. 221-238.
- [39] Stanway, R., Sproston, J.L., and El-Wahed, A.K., "Application of Electrorheological Fluids in Vibration Control: A Survey," *Smart Materials and Structures*, Vol. 6, No. 3, 1997, pp. 351-358.
- [40] Lionel, B., Choi, Y.T., and Wereley, N.M., "Electrorheological Damper Analysis Using an Eyring-plastic Model," Proceedings of the 2002 SPIE-The International Society for Optical Engineering, Vol. 4697, 2002, pp. 324-335.

- [41] Wereley, N.M., Pang, Li, and Kamath, G.M., "Idealized Hysteresis Modeling of Electrorheological and Magnetorheological Dampers," *Journal of Intelligent Material Systems and Structures*, Vol. 9, No. 8, 1998, pp.642-649.
- [42] Kamath, G.M. and Wereley, N.M., "Nonlinear Viscoelastic-Plastic Mechanisms-Based Model of an Electrorheological Damper," *AIAA Journal of Guidance, Control and Dynamics*, Vol. 20, No. 6, 1997, pp. 1225-1332.
- [43] Choi, S.B., Lee, S.K. and Park, Y.P., "A Hysteresis Model for the Field-Dependent Damping Force of a Magnetorheological Damper," *Journal of Sound and Vibration*, Vol. 245, No. 2, 2001, pp. 375-383.
- [44] Gamota, D.R. and Filisko, F.E., "Dynamic Mechanical Studies of Electrorheological Materials: Moderate Frequencies," *Journal of Rheology*, Vol.35, No. 3, 1991, pp. 399-425.
- [45] Wen, Y.K., "Method for Random Vibration of Hysteretic Systems," *Journal of the Engineering Mechanics Division*, Vol. 102, No. EM2, 1976, pp. 249-263.
- [46] Spencer(Jr.), B.F., Dyke, S.J., Sain, M.K. and Carlson, J.D., "Phenomenological Model of a Magnetorheological Damper," *Journal of Engineering Mechanics*, Vol. 123, No. 3, 1997, pp. 230-238.
- [47] Hong, S.R., Choi, S.B., Choi, Y.T. and Wereley, N.M., "Comparison of Damping Force Models for An Electrorheological Fluid Damper," *International Journal of Vehicle Design*, Vol. 33, No. 1A, 2003, pp. 17-35.

- [48] Coveney, V.A., Johnson D.E., and Turner D.M., "A Triboelastic Model for The Cyclic Mechanical Behavior of Filled Vulcanizates," *Rubber Chemistry and Technology*, Vol. 68, 1995, pp. 660-670.
- [49] Zener, C.M., *Elasticity and Anelasticity of Metals*, University of Chicago Press, Chicago, IL., 1948.
- [50] Gandhi, F., and Chopra, I., "A Time-domain Non-linear Viscoelastic Damper Model," *Smart Materials and Structures*, Vol. 5, No. 5, 1996, pp. 517-528.
- [51] Kunz, D.L., "Influency of Elastomeric Lag Damper Modeling on the Predicted Dynamics Response of Helicopter Rotor Systems," AIAA/ASME/ASCE/AHS/ASC 38th Structures, Structural Dynamics and Materials Conference, Kissimmee, Florida, April 1997, AIAA paper No.97-1179.
- [52] Tarzanin F.J., and Panda, B., "Development and Application of Nonlinear Elastomeric and Hydraulic Lag Damper Models," Proceedings of the 36th AIAA/ASME/ASCE/AHS/ASC Structures, Structural Dynamics, and Materials Conference, New Orleans, Louisiana, April 1995.
- [53] Krishnan, R., "Mechanisms-based Analysis and Modeling of Elastomeric Lag Damper Behavior," *Master of Science*, University of Maryland, Aerospace Engineering, 2000.
- [54] Snyder, R.A., "Mechanisms-based Modeling of Filled Elastomeric Lag Damper Behavior," *Master of Science*, University of Maryland, Aerospace Engineering, 2001.

- [55] Strganac, T.W., “An Experiment and Analytical Methodology to Characterize Nonlinear Elastomeric Lag Dampers,” Proceeding of the 38th AIAA/ASME/ASCE/AHS/ASC Structures, Structural Dynamics, and Material Conference, Orlando, Florida, April 1997.
- [56] Lesieutre, G.A., and Bianchini, E., “Time Domain Modeling of Linear Viscoelasticity Using Augmenting Thermodynamic Fields,” Proceedings of the 34th AIAA/ASME/ASCE/AHS/ASC Structures, Structural Dynamics and Materials Conference, La Jolla, CA, April 1993.
- [57] Lesieutre, G.A., and Mingori, D.L., “Finite Element Modeling of Frequency-Dependent Material Damping Using Augmenting Thermodynamic Fields,” *Journal of Guidance, Control and Dynamics*, Vol. 13, No. 8, 1990, pp. 1040-1050.
- [58] Govindswamy, K., Lesieutre, G.A., Smith, E.C., and Beale, M.R., “Characterization and Modeling of Strain-Dependent Dynamics Behavior of Viscoelastic Elastomers in Simple Shear,” Proceedings of the 36th AIAA/ASME/ASCE/AHS/ASC Structures, Structural Dynamics, and Materials Conference, New Orleans, LA, April 1995.
- [59] Brackbill, C.R., Lesieutre, G.A., Smith, E.C., and Govindswamy, K., “Thermomechanical Modeling of Elastomeric Materials,” *Smart Materials and Structures*, Vol. 5, No. 5, 1996, pp. 529-539.
- [60] Ramrakhyani, D.S., Lesieutre, G.A., and Smith, E.C., “Efficient Modeling of Elastomeric Materials Using Fractional Derivatives and Plastic Yielding,”

Proceedings of the 43rd AIAA/ASME/ASCE/AHS/ASC Structures, Structural Dynamics, and Materials Conference, Denver, CO, April 2002.

- [61] Payne, A.R. and Whittaker, R.E., "Strain Dynamic Properties of Filled Rubbers," *Rubber Chemistry and Technology*, Vol. 44, 1971, pp. 440-478.
- [62] Timoshenko, S.P., *Strength of Materials*, Part 2, D. Van Nostrand Company, New York, N.Y., 1933, pp. 679-680.
- [63] Iwan, W.D., "Distributed-Element Model for Hysteresis and Its Steady-State Dynamic Response," *Journal of Applied Mechanics*, Vol. 33, 1966, pp. 893-900.
- [64] Iwan, W.D., "A Class of Models for the Yielding Behavior of Continuous and Composite Systems," *Journal of Applied Mechanics*, Vol. 34, 1967, pp. 612-617.
- [65] Turner, D.M., "A Triboelastic Model for the Mechanical Behavior of Rubber," *Plastics and Rubber, Processing and Applications*, No.9, 1988, pp. 197-201.
- [66] Hu, W., Chen, P. and Wereley, N.M., "Helicopter Snubber Lag Damper Employing Passive Elastomeric and Semi-Active Magnetorheological Materials," 15th International Conference on Adaptive Structures and Technologies, October 25-27, 2004.
- [67] Gavin, H.P., Hanson, R.D. and Filisko, F.E., "Electrorheological Dampers, Part I: Analysis and Design," *Journal of Applied Mechanics*, Vol. 63, No. 3, 1996, pp. 669-675.

- [68] Gavin, H.P., "The Effect of Particle Concentration Inhomogeneities on the Steady Flow of Electro- and Magneto-Rheological Materials," *Journal of Non-Newtonian Fluid Mechanics*, Vol. 71, No. 3, 1997, pp. 165-182.
- [69] Carlson, J.D., "MR Fluids and Devices in the Real World," *International Journal of Modern Physics B*, Vol. 19, No. 7-9, 2005, pp. 1463-1470.
- [70] Lord Corporation, [www.lord.com](http://www.lord.com).
- [71] Barry Controls Aerospace, [www.barrycontrols.com](http://www.barrycontrols.com).
- [72] Lee, D.Y. and Wereley, N.M., "Quasi-steady Herschel-Bulkley Analysis of Electro- and Magneto-Rheological Flow Mode Dampers," *Journal of Intelligent Material Systems and Structures*, Vol. 10, No. 10, 1999, pp. 761-769.
- [73] Lee, D.Y., Choi, Y.T. and Wereley, N.M., "Performance Analysis of ER/MR Impact Damper Systems Using Herschel-Bulkley Model," *Journal of Intelligent Material Systems and Structures*, Vol. 13, No. 7-8, 2002, pp. 525-531.
- [74] Aklonis, J.J., and McKnight, W.J., *Introduction to Polymer Viscosity*, John Wiley and Sons, New York, 1983.
- [75] Constantinou, M., Mokha, A., and Reinhorn, A., "Teflon Behavior in Base Isolation, Part 2:Modeling," *Journal of Structural Engineering*, Vol. 116, No. 2, February, 1990, pp. 455-474.
- [76] Berger, E.J., "Friction Modeling of Dynamic System Simulation," *Appl. Mech. Rev.*, Vol. 55, No. 6, November 2002, pp. 535-577

- [77] Li, W.H., Yao, G.Z., Chen, G., Yeo, S.H. and Yap, F.F., "Testing and Steady State Modeling of a Linear MR Damper under Sinusoidal Loading," *Smart Materials and Structures*, Vol. 9, No. 1, 2000, pp. 95-102.
- [78] Nashif, A.D., Jones, D.I.G. and Henderson, J.P., *Vibration Damping*, John Wiley and Sons, Inc., 1985.
- [79] Faires, J.D. and Burden, R., *Numerical Methods*, Brooks/Cole Publishing Company, Pacific Grove, California, 1998.
- [80] Hausmann, G. and Gergely, P., "Approximation Method for Thermoviscoelastic Characterization and Analysis of Elastomeric Lead-Lag Dampers," Proceedings of 18th European Rotorcraft Forum, paper No. 88, France, 1992.
- [81] Hausmann, G., "Elastomeric Components in the Helicopter Industry - Advances in Design and Performance Prediction," 55th Annual Forum of the American Helicopter Society, Montreal, Canada, 1999.
- [82] Tongue, B.H., "Limit Cycle Oscillations of a Nonlinear Rotorcraft Model," *AIAA Journal*, Vol. 22, No. 7, 1984, pp. 967-974.
- [83] Pohit, G., Venkatesan, C. and Malik, A.K., "Elastomeric Damper Model and Limit Cycle Oscillation in Bearingless Helicopter Rotor Blade," *Journal of Aircraft*, Vol. 37, No. 5, 2000, pp. 923-926.
- [84] Sanliturk, K.Y. and Ewins, D.J., "Modeling Two-Dimensional Friction Contact and Its Application Using Harmonic Balance Method," *Journal of Sound and Vibration*, Vol. 193, No. 2, 1996, pp. 511-523.

- [85] Wang, X.J. and Gordaninejad, F., "Dynamic Modeling of Semi-Active ER/MR Fluid Dampers," Proceedings of SPIE Conference on Smart Materials and Structures, Vol. 4331, 2001, pp. 82-91.
- [86] Singh, R., Kim, R. and Ravindra, P.V., "Linear Analysis of Automotive Hydro-mechanical Mount with Emphasis on Decoupler Characteristics," *Journal of Sound and Vibration*, Vol. 158, No. 2, 1992, pp. 219-243.
- [87] Nishiyama, H., Fushimi, S. and Nakano, M., "Numerical Simulation of MR Fluid Damping Characteristics Using a Modified Bingham Model," *Journal of Intelligent Material Systems and Structures*, Vol. 13, No. 10, 2002, pp. 647-653.
- [88] Choi, Y.T. and Wereley, N.M., "Vibration Control of a Landing Gear System Featuring Electrorheological/Magnetorheological Fluids," *Journal of Aircraft*, Vol. 40, No. 3, 2003, pp. 432-439.
- [89] Kordonski, W., Gorodkin, S. and Zhuravski, N., "Static Yield Stress in Magnetorheological Fluid," *International Journal of Modern Physics B*, Vol. 15, No. 6-7, 2001, pp. 1078-1084.
- [90] Tang, X., Zhang, X. and Tao, R., "Flexible Fixture Device with Magnetorheological Fluids," *Journal of Intelligent Material Systems and Structures*, Vol. 10, No.9, 1999, pp. 690-694.